CFD simulation of forced convection heat transfer of laminar phase-change non-Newtonian fluids in rectangular straight micro-channels

Thesis

Master of Science in Mechatronics

BY

Adi Corrales Magallanes

Querétaro, Qro. México, Septiembre de 2010

A Bet, por todo tu amor y paciencia.

Fue duro, pero lo logramos.

CFD simulation of forced convection heat transfer of laminar phase-change non-Newtonian fluids in rectangular straight micro-channels

Acknowledgments

I want to thanks some persons that were important part of this work. I will permit myself to thanks some of them in my first language, Spanish.

A mi amada esposa, que padeció tanto o más que yo durante la realización de este trabajo. Espero que tanto tiempo que estuvimos separados haya valido la pena y sientas por mí la admiración y orgullo que siento yo por ti.

A mi madre y mi hermana. Gracias por todo el apoyo de siempre y por alentarme a continuar en este difícil camino. Las quiero mucho a ambas.

A mi familia que ha crecido mucho recientemente, familia Torres Magallanes, familia Pérez Corrales, y a mis queridos suegros y familia De la Mora Morales.

I want to thanks to the all the personal of CIDESI, especially to Dr. Felipe Rubio and to M. Sc. Vicente Bringas, for this great opportunity. I hope that I'll be able to return some of the acquired knowledge to the center. To my supervisor, Dr. René Estrada: thanks for the advices and recommendations for generating this work. I also want to thanks my friends and colleges, for their support along all this years.

Thanks to all my professors in CIDESI, Queretaro and in FH, Aachen, Germany. The knowledge and new way in which I see the world now is thanks to you. To all the personal of PICyT, thanks for your support, and to all the wonderful people I have the opportunity to known in the Fachhochshule.

Thanks to the personal in Texas A&M University in College Station, USA, especially to Dr. Jorge Alvarado, for proposing and supervising this work.

To all my friends from now and the past, thank you.

Page intentionally left blank

CFD simulation of forced convection heat transfer of laminar phase-change non-Newtonian fluids in rectangular straight micro-channels

Abstract

The department of Engineering Technology and Industrial Distribution (ETID) at the University of Texas A&M, in College Station, Texas is at the vanguard of modeling fluids to evaluate their heat transfer performance under various conditions. Until now, they have been working with Newtonian flows, single phase and with a phase change material, but their work will now include non-Newtonian fluids, also in single phase and with a phase change material. This work presents the first studies of non-Newtonian flows with phase change materials done in this department as an introduction for further investigation.

Several analyses were done in this work to compare the heat transfer performance of various rectangular micro-channels with different aspect ratios and non-Newtonian power law fluids as a single phase fluid and with a phase change material (PCM). The performance was compared by calculating the Nusselt number (Nu) and the Fanning friction factor (*f*) and then, with the thermal performance factor.

The cases were tested under a constant heat flux with constant peripheral temperature (H1) and constant wall temperature (CWT) boundary conditions. Only the fully developed region where analyzed, and the entry region was set as combined, allowing the hydrodynamic and the thermal development simultaneously. The phase change effects were simulated using a specific heat model.

The rectangular tubes with a lower aspect ratio height/width were found to have higher values of Nu for the same fluid. In terms of viscosity, the fluids with lower power law indexes were found to have the highest values.

Comparing single phase fluids with the slurry formed by a non-Newtonian carrier and a PCM, the slurry presented a notable increment of the value of Nu during the phase change of the fluids under H1 condition, while the fluids under CWT presented only an increment of the value during the entry region.

The case that presented the higher values of Nu was with PCM slurry in a rectangular micro-channel with low aspect ratio, and a fluid with low power index, but only during the phase

CFD simulation of forced convection heat transfer of laminar phase-change non-Newtonian
fluids in rectangular straight micro-channels

change region, as the values in the sub-cooled and liquid region converges to the values of the
single phase fluid.

Keywords: CFD, non-Newtonian fluid, PCM, phase change material, Nusselt number, heat
transfer, rectangular micro-channel.

CFD simulation of forced convection heat transfer of laminar phase-change non-Newtonian fluids in rectangular straight micro-channels

Contents

CFD simulation of forced convection heat transfer of laminar phase-change non-Newtonian fluids in rectangular straight micro-channels

CFD simulation of forced convection heat transfer of laminar phase-change non-Newtonian fluids in rectangular straight micro-channels

CFD simulation of forced convection heat transfer of laminar phase-change non-Newtonian fluids in rectangular straight micro-channels

Table of figures

CFD simulation of forced convection heat transfer of laminar phase-change non-Newtonian fluids in rectangular straight micro-channels

CFD simulation of forced convection heat transfer of laminar phase-change non-Newtonian fluids in rectangular straight micro-channels

x

CFD simulation of forced convection heat transfer of laminar phase-change non-Newtonian fluids in rectangular straight micro-channels

CFD simulation of forced convection heat transfer of laminar phase-change non-Newtonian fluids in rectangular straight micro-channels

Tables

CFD simulation of forced convection heat transfer of laminar phase-change non-Newtonian fluids in rectangular straight micro-channels

Symbols

A_c: cross section area

BC: Boundary condition

c: volumetric concentration of PCM

c_p: specific heat

CWT: constant wall temperature BC

D_h: hydraulic diameter

f: Fanning friction factor

F_b: Body force

G: mass flux

h: overall convection coefficient

H1: Constant heat flux and constant peripheral temperature BC

H2: : Constant heat flux and variable peripheral temperature BC

i: enthalpy

k: conduction coefficient

K_c: consistency index

L: Length of the tube

L_h: Latent heat of PCM particles

m: mass

n: power law index

Nu: Nusselt number

P: pressure

PCM: Phase change material

Pe: Peclet number

Per: perimeter

Pr: Prandtl number

q'': heat flux

r: radial coordinate in cylindrical system

Re: Reynolds number

Re_{NN}: Reynolds number for non-Newtonian fluids

S: surface

So: source function

St: Stanton number

S_w: surface area where the BC is applied

t: temperature

t_∞: free stream temperature

t_d: dimensionless temperature

t_i: Inlet temperature

t_m: bulk temperatrure

t_o: Outlet temperature

t_w: temperature at the wall

u: velocity in x direction

u_∞: free stream velocity in x direction

V: mean velocity

v: velocity in y direction

w: velocity in z direction

x^+: dimensionless x

y^+: dimensionless y

z^+ : dimensionless length

α: aspect ratio of rectangular tubes (height/width)

$\dot{\gamma}$: shear rate

δ: differential measure

η: apparent viscosity

η_p: thermal performance factor

θ: time

μ: dynamic viscosity

ρ: density

σ: normal stress

τ: shear stress

x, y, z: Cartesian coordinates

Bold symbol represents a vector or a matrix.

Page intentionally
left blank

CHAPTER 1   Introduction

1.1   Introduction

Mechatronics is the field of engineering that deals with problems related to electronics, control, mechanics and computer science. The interrelations of these engineering areas are very important for today's industry, because almost any technical problem can be treated as a combination of these disciplines. From the design of electronic or electromechanical devices, their fabrication process and tests, the design of the machines to build them, etc. requires an interdisciplinary team that can deal with the several aspects of the product life.

In the area of mechanics and computer science it is possible to find computational analysis. The numerical methods to solve complex simulations of real devices is, nowadays, an almost obligatory step in the design stages to avoid errors or failures in the final design of products. Simulation allows to have an overview of the product behavior before build any prototype, and then, it allows a cost and time reduction.

Many kinds of simulations methods can be use in the analysis of products, being one of the most important the numerical simulations such the finite element method (*FEM*). This method is widely spread in industry and investigation centers and it is used for diverse kind of analyses, from structural to magnetic and electric. To simulate flow of fluids and transfer of heat, a method called computational fluid dynamics (*CFD*) is widely used, and that method allows to study many fluid problems, like control surfaces in airplanes, hydrodynamics of ships, or flow in channels and pipes, and at the same time, the ability of the fluids to transfer energy between the several elements of the system.

This work deals principally with heat transfer by convection, which involves heat transfer and fluids dynamics, and tries to demonstrate that CFD is a valuable tool for solving this kind of problems, especially in heat transfer between surfaces and the fluid in cooling systems, where the fluid transports the heat to out of the system.

CFD simulation of forced convection heat transfer of laminar phase-change non-Newtonian fluids in rectangular straight micro-channels

1.2   Objective

Simulate phase-change non-Newtonian fluids (shear-thinning power-law fluids) in straight rectangular micro-channels, under laminar regime, to determine their heat transfer properties for comparing their thermal performance with single phase fluids and to obtain a better understand of the phenomenon and it's simulation with CFD for further investigations.

1.3   Justification

The department of Engineering Technology and Industrial Distribution at the University of Texas A&M, in College Station, Texas, is at the vanguard of the heat transfer analysis in micro channels. They are developing numerical analyses for various cases that could lead to an increment in the performance of new micro cooling systems and micro heat exchangers for multiple micro systems such as electronic devices. Their actual work deals with single phase Newtonian flows, phase change materials and Newtonian fluids slurries in finned channels and tubes with staggered pins. Now they have the interest of working with phase change nanofluids, which are non-Newtonian fluids and thus, the necessity of a work like this that allows to known if the actual CFD software can deliver reliable data and to understand how that phase change non-Newtonian fluids behaves is an important step for further investigations.

The first step is to model simple geometric figures as rectangular micro channels to known if the software has the capacity of deliver reliable data for these fluids. It is necessary to realize a previous verification and replication of known data such as non-Newtonian single phase fluids and phase change material added to a Newtonian fluid working with the power law model to understand how the diverse parameters affects the results. If it is possible to replicate this known data under certain accuracy, then it is possible to start modeling phase change material in non-Newtonian fluids with certain degree of confidence in the power law model and the selected parameters. The phase change non-Newtonian fluids will be compared with the results of the verification section to evaluate the thermal performance of the former as the equation to do this comparison include the Fanning friction (that will be defined in section 4.3) which is a function of the pressure drop between the input and the outflow.

After this work, more complex geometries can be tested and evaluated knowing that the proposed models are delivering results that are in agreement with what is known about the phenomenon.

Newtonian fluids have been the standard model for the fluid mechanics for a long time. But although the theory for this fluids is more or less developed, there still phenomena that cannot be predicted by exact solutions. The use of numerical methods had helped to solve these problems with confidence and it is an invaluable tool for acquiring approximate solutions for many complex systems.

Non-Newtonian fluids behavior, on the other hand, where the viscosity varies with the shear ratios are more complex that Newtonian fluids; the fluid react in a very different way as the Newtonian fluids does. As an example, the velocity profiles of the non-Newtonian fluids are totally unfamiliar in Newtonian fluid mechanics. But this is just the beginning; non-Newtonian fluid mechanics differs from classic Newtonian fluid in many important aspects (1), many of which this work will not deal with.

Solving non-Newtonian problems in analytical way is sometimes just not possible as far as the exact solution for the governing equations is not known. It is fair to say that the problems found in fitting constitutive equations to such fluids is an extremely difficult one, and a one-size-fits-all solution is unlikely to be found. The best hope appears to be to fit a given constitutive relationship to a specialized set of circumstances and applications (2). Then, the use of numerical methods is the only viable alternative tool that exists today to solve complex non-Newtonian fluid problems, and because of this, it is very important to have reliable numerical models for this kind of materials.

Many new technologies may involve micro scale internal flows, for example, as a heat exchanger for micro-electronic devices. As it will be see in posterior chapters, the heat transfer increases when used micro fluid (3), which, combined with non-Newtonian fluids, could lead to new and more efficient heat transfer.

Chandrupatla (4) in 1977, investigated the behavior of non-Newtonian fluids in square ducts, giving as a result of its work a relation of various Nusselt numbers for a $\alpha=1.0$ rectangular

CFD simulation of forced convection heat transfer of laminar phase-change non-Newtonian fluids in rectangular straight micro-channels

cross-sectional area for index $n = 0.5…1.0$. In 1994, Chung (5) worked with non-Newtonian flows, with index $n=0, 0.2, 0.25, 0.5, 1.0$ in rectangular cross-sectional areas of 0.5 and 0.2 ratios. In 1996, Syrjälä (6) realized an extensive work with rectangular cross-sectional areas with ratios of 1.0, 0.5, 0.2 and 0.1 and several power law indexes; all these works with single phase fluids. Garimella (7) presented a work dealing with heat transfer in rectangular micro-channels using Newtonian and single phase flows in 2006. More recent works such the one realized by Muzycha (8) deals with micro channels and non-Newtonian flows single phase flows, and Kondle (9), in 2009 worked with micro channels and phase change materials, but only with Newtonian flows.

The phase change model was simulated using the model proposed by Yamagishi (10) in 1999, which produces results that are comparable with experimental findings.

As the research with non-Newtonian fluids is still very limited, the importance of this kind of works, which allow the understanding of these complex fluids, is enormous. These simulations will help in the comprehension of the behavior of non-Newtonian fluids in straight micro-channels, from which more advanced studies such convective heat and mass transfer could be developed in the future.

1.4   Organization of the thesis

This thesis is organized in chapters that cover all the aspects of the work done.

The first one is this introduction and basic information about the generalities of the work. Chapter two presents a brief introduction to the basic concepts and governing equations of fluid mechanics and heat transfer that will be used to compare results and verification.

Two chapters dedicated to the methodology of the numerical method and the simulation follows the theory documentation. The first chapter includes some validation of the use of the software by modeling Newtonian fluids in circular and rectangular cross sections with a constant viscosity, and the second deals with the methodology for simulating power law fluids. The subsequent chapter shows the results, divided in a section for verification of the power law model and the presentation of the new data with which this work is contributing to

understand the non-Newtonian flows with PCM. It follows one chapter discussion dedicated to discuss some aspects of the results, then, one chapter dedicated to conclude. The final one presents the future work proposed and recommendations for future researchers that want to continue or go deeper into the development of the subject.

Page intentionally
left blank

CHAPTER 2   Governing equations and physical principles

2.1   Introduction convective heat transfer

Convection is the heat transfer mode that involves two mechanisms for the transfer of energy. The first mechanism is called advection. In advection, the energy is transferred by the bulk movement of the fluid, in which a group of molecules moving as a single package or as aggregates and the thermal energy moves if there are temperature gradients in the fluid. The second mechanism is called diffusion and in this one, the heat is transferred by the random motion of single molecules as it is done by conduction. Convection is the cumulative transport of these two mechanisms.

It is of special interest the convection heat transfer between a surface and the fluid. If the temperature of the surface t_w is different than the temperature of the fluid at the free stream t_∞ a heat flow is developed between both elements[1]. It is important to define certain characteristics of this heat exchange, because the fluid in contact with the surface generates certain conditions that affect directly to the amounts of energy that can flow from the surface to the fluid.

Convection can be caused by two mechanisms called *forced convection* and *natural convection*. In forced convection, an external force induces the flow, with the help of, as an example, pumps and fans. In natural convection, the fluid moves thanks to buoyancy forces, caused by differences in density which are due to differences in temperature on different areas of the fluid. A mixture of both mechanisms can be found, where a natural and forced movement of the fluid acts in the system.

As it has been said, the convection involves advection and diffusion, and this becomes especially important in an area of the fluid where certain gradients are generated due the difference of velocity, temperature and mass concentration of species. These areas, called *thermal boundary layers*, are the areas where heat can move away from the surface.

---

[1] In case that $t_w > t_\infty$ there is a positive heat flow from the surface to the fluid, and if $t_w < t_\infty$ then the positive heat flows from the fluid to the surface. In this work, it will be typically assumed that $t_w > t_\infty$.

CFD simulation of forced convection heat transfer of laminar phase-change non-Newtonian fluids in rectangular straight micro-channels
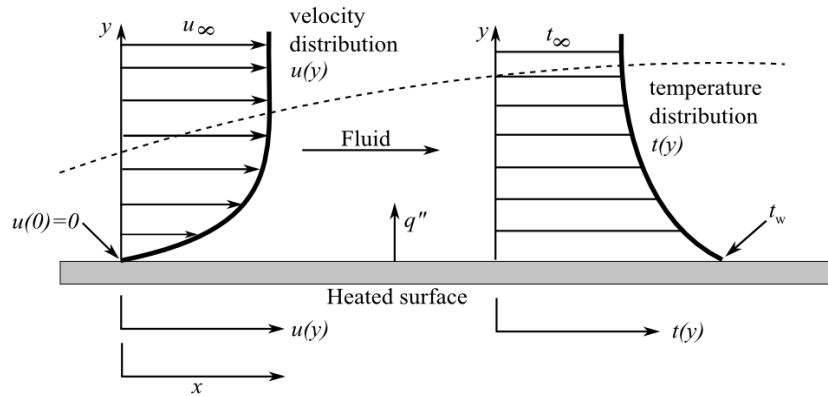
Figure 2-1, thermal boundary layers development

Although the thermal energy that is transfer by convection is typically the sensible or the internal energy, when a change of phase is involved in the process there is in addition, latent energy involved.

But regardless of the nature of the convection process, it is always possible to express the heat transfer as

$$q'' = h\,(t_{\mathrm{w}} - t_{\infty})$$ 2.1

Where q'' is the heat flux and h is a constant called convection heat transfer coefficient and depends on many characteristics and properties of the surface and the fluid. The equation above is known as the Newton's law of cooling (3).

When using this equation, this work assumes that $t_w > t_\infty$ and that the positive heat flux goes from the surface to the fluid.

2.1.1 Convection boundary layers

The concept of boundary layers has been briefly explained in the paragraphs above, and now a more detailed description will be done.

2.1.1.1 Velocity boundary layer

The *velocity layer* is caused by the gradients in the fluid velocity from the surface to the free stream fluid. When the fluid is in contact with the surface, it has a velocity of $u = 0$ (*no slip*

condition) and it will be larger as the distance in *y* increases. When there is no a sensible change in the magnitude of the speed between two adjacent layers, then the fluid reach a limit called the boundary limit thickness that is the distance *δ* from the surface when the gradient approaches to 0. The higher gradients are located near to the surface.
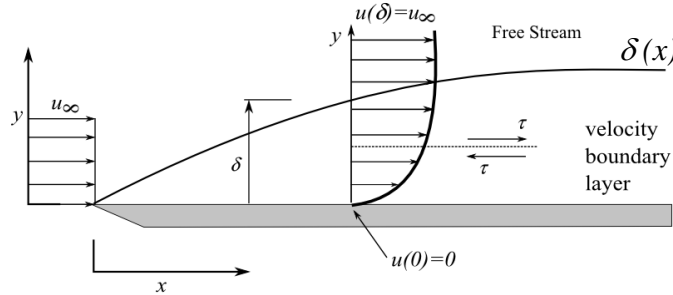
Figure 2-2, velocity boundary layer on a flat plate

The gradient in the velocities is generated due the shear stress that affects every parallel layer to the flux. When *y=0* the velocity of the fluid is 0. This layer of fluid acts to retard the motion of the next layer of particles and this new layer acts to slow down the next one, until a distance *δ* is reached. At this point, the velocity of the layers is almost the same. The boundary limit thickness *δ* is usually defined as the length in *y* for which *u = 0.99 u∞.*

The value of *δ* is a function of *x*, so, the value of the thickness increases as the fluid flows over the plate. This value delimits the fluid in two regions: one in which the gradients of the shear stress and velocity are big enough to be considered, and a second region where the gradients are so small that are negligible.

As an example of the behavior of the fluid inside this layer, for a Newtonian fluid, the shear stress *τ* between the parallel layers is (3)

$$\tau = \mu \frac{\partial u}{\partial y}\bigg|_{y=0} \qquad\qquad \textbf{2.2}$$

In last equation, μ is a property known as *dynamic viscosity* of the fluid. As the velocity on the fluid *u* is a function of *x*, then *τ* is also a function of *x*. The stress for a non-Newtonian fluid will be defined in section 2.4.

The parameters of the last equation can be observed in the next figure.

9

CFD simulation of forced convection heat transfer of laminar phase-change non-Newtonian fluids in rectangular straight micro-channels
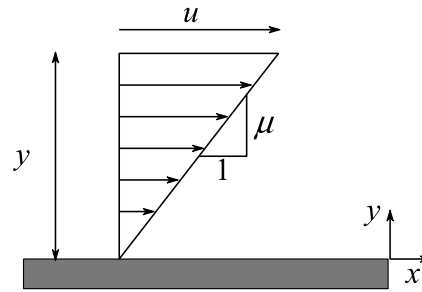
Figure 2-3, schematic representation of the unidirectional shearing flow

The general case of equation 2.2 will be presented in section 2.6.

2.1.1.2 Temperature boundary layer

For this layer, a temperature gradient is generated between the stream fluid and the surface. The heat flows from the surface to the fluid stream (assuming $t_w > t_\infty$) until it reaches a region where the gradient can be neglected. As in the velocity boundary layer, the higher gradients are located near to the surface.
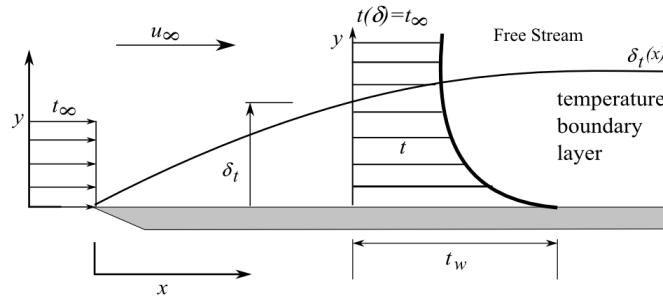
Figure 2-4, temperature boundary layer on a flat plate

In this case, δ_t is defined as the distance in y for which $(t_w - t)/(t_w - t_\infty) = 0.99$, where t is the temperature as a function of y.

As the velocity of the fluid is $u(y = 0) = 0$, the mechanism of energy transfer in this layer is done only by conduction and not due bulk movement. For conduction heat transfer, the Fourier's law (3) can be used:

$$q'' = -k\left.\frac{\partial t}{\partial y}\right|_{y=0} \qquad\qquad 2.3$$

10

In last equation, k represents the conduction coefficient. For convection, the Newton's law of cooling can be recalled:

$$q'' = h \left(t_w - t_\infty \right) \qquad \textbf{2.4}$$

And combining both equations, it is possible to find the *convection transfer coefficient*

$$h = \frac{-k \left. \dfrac{\partial t}{\partial y} \right|_{y=0}}{\left(t_w - t_\infty \right)} \qquad \textbf{2.5}$$

It is possible to see that the temperature layer depends strongly in the temperature gradient between the fluid and the surface. As $(t_w - t_\infty)$ is a constant depending on x, and the value of δ_t increases when x increases, then, the value of the temperature gradients decreases when x increases, and the value of h and the heat flux q'' decreases too.

The convection coefficient h is a very important parameter as it represents the behavior of the heat flux in the flow in a simple and compact way. It can be hard to determine by theoretical methods and because of that CFD and experiments are widely used to characterize the coefficient for fluid problems.

2.1.1.3 *Concentration boundary layer

The concentration phenomenon will not be of interest of this work, but it is mentioned here for the sake of completeness. This concentration boundary layer is formed for a gradient in the level of saturation of two different species in the fluid (i.e. a mixture of liquid water and vapor). A mass transfer is done within this layer if these gradients exist.

More generally, a binary mixture of two species will be considered, calling these species A and B. The molar concentration is designated as $C_{A,S}$ at the surface, and $C_{A,\infty}$ at the free stream. If these both molar concentrations are not equal, then the gradient is formed.

CFD simulation of forced convection heat transfer of laminar phase-change non-Newtonian fluids in rectangular straight micro-channels
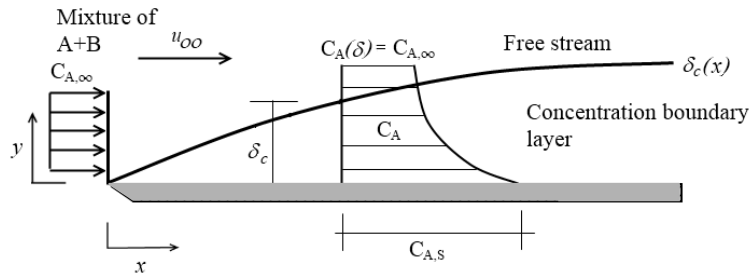
Figure 2-5, concentration boundary layer on a flat plate

As in the temperature layer, the value of δ_c is the distance of y for which $(C_{A,s} - C_A)/(C_{A,s} - C_{A,\infty}) = 0.99$.

2.1.2 Laminar and turbulent flow

Laminar and *turbulent* flow are two characteristics of the flow related to the order in the movement of the particles. In laminar flow, the boundary layers keep a relative order from one to another, in a way in which it is possible to identify streamlines along which fluid particles move. This ordered movement continues until a point in which certain conditions break this order and the fluid starts to move in a chaotic way, with high variations in velocity and pressure. This point is in a zone called transition zone, and after the fluid crosses it, it will develop a highly chaotic behavior and a new region called turbulent zone is created.

The turbulent behavior of the flow is triggered by certain conditions in the fluid or in the structure such as the roughness, and can be summarized in a dimensionless parameter known as the Reynolds number Re:

$$Re = \frac{\rho V D_0}{\mu}$$

2.6

Where D_0 is the reference length of parallel flow from the entry point, ρ is the density, and V is the mean velocity of the stream in the x direction. Actually, the Reynolds number represents the ratio of inertia to viscous forces and while the number is small, the inertia forces are insignificant relative to the viscous forces and the flow remains laminar.

2.2   Fully developed flow

For internal flows, there are two considerations to take in account with the laminar or turbulent behavior in a flat plate, and these are if the flow is in the entrance or in the fully developed region.

If the flow enters in a pipe at a constant velocity, the viscid effects will keep the fluid that is in contact with the wall at zero velocity. As the fluid moves down the tube a low velocity layer will grow up from the surface, and a particular and simplified feature of this growing, is that the boundary layer must meet itself at the centerline of the tube. The velocity profile generated at that point is invariant with the length of the tube. This is valid for fluids whose properties do not change with the distance.
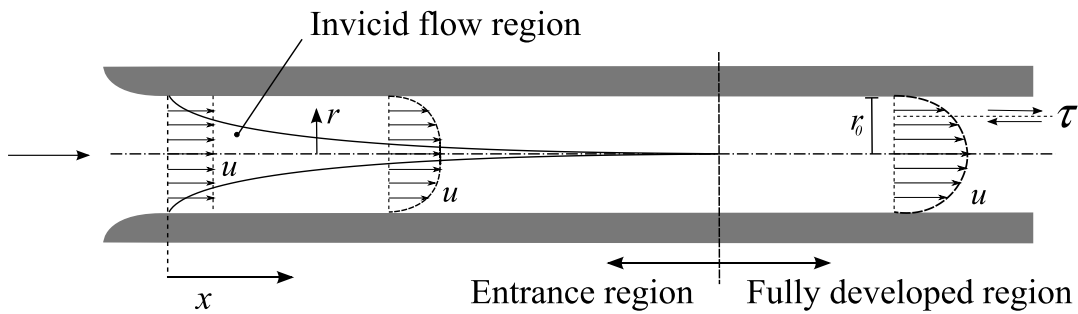
Figure 2-6, development of the velocity *u(r,x)* for laminar fluid

For a circular tube, the profile generated by *u* is parabolic and defined by (3)

$$u(r) = -\frac{1}{4\mu}\left(\frac{dP}{dx}\right)r_0^2\left[1 - \frac{r^2}{r_0^2}\right] \qquad \text{2.7}$$

This equation comes from a pressure and shear stress in a control volume. The velocity components *v* and the gradient of *u* with respect to the flow direction must be zero everywhere

$$v = 0 \; ; \frac{\partial u}{\partial x} = 0 \qquad \text{2.8}$$

As the velocity *u* varies over the cross section in *r* direction, it is usually convenient to work with a mean value, which is defined as (11)

CFD simulation of forced convection heat transfer of laminar phase-change non-Newtonian fluids in rectangular straight micro-channels

$$V = \frac{1}{A_c \rho} \int_{A_c} u\rho \, dA_c \qquad \text{2.9}$$

The pressure gradient $\frac{dP}{dx}$ for equation 2.7 can be determined from

$$V = -\frac{r_0^2}{8\mu} \frac{dP}{dx} \qquad \text{2.10}$$

For temperature, the fully developed profile implies that under certain conditions, exists a generalized temperature profile that is invariant with the tube length.

For convenience, a term denominated bulk temperature t_m is used, and it represents the average thermal energy state of a fluid. (11)

$$t_m = \frac{1}{A_c V} \int_{A_c} ut \, dA_c \qquad \text{2.11}$$

The fully developed thermal profile is when a dimensionless temperature factor t_d, based on t_m, the temperature of the wall t_w, and the local temperature t is invariant with the length. If the length is defined to go in the positive x direction, then

$$t_d = \frac{\partial}{\partial x}\left(\frac{t_w - t}{t_w - t_m}\right) = 0 \qquad \text{2.12}$$

A similar plot as for the velocity (Figure 2-6) can be observed for the temperature profile.
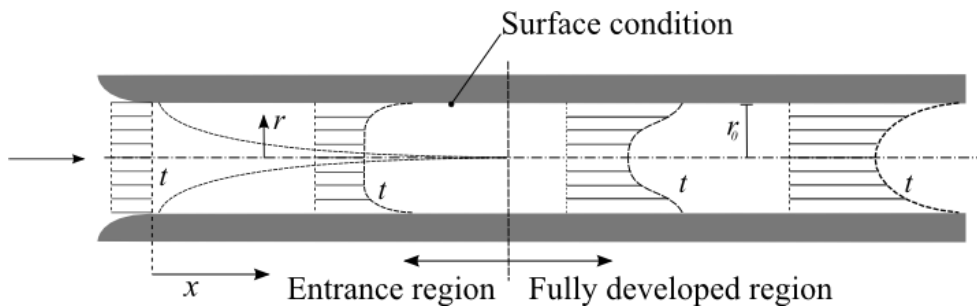
Figure 2-7, thermally developed fluid

For the case of the Figure 2-7, $t_w > t(r,x)$.

14

It is possible to observe from the last figure, that as the boundary layers get into a contact in the middle of the tube, at $r = 0$, the temperature at the center is the equivalent to the free stream temperature (although the numerical values are not necessarily the same).

2.3   Nusselt Number

An important parameter for the convection heat transfer is the dimensionless number called Nusselt number, Nu. This number is the ratio of conductive to convective heat transfer across the surface boundary and it remains constant for a fully developed fluid.

For laminar flow, the Nusselt number is based on the solution of the differential momentum and energy equations 2.45 and 2.47, but for this work, that procedure is of no interest.

For tubes, the Nusselt number is defined as (3)

$$Nu = \frac{h\,D_h}{k}$$

2.13

Where D_h is the hydraulic diameter defined as

$$D_h = \frac{4A_c}{Per}$$

2.14

By using equation 2.1 to calculate h, it follows,

$$Nu = \frac{q''\,D_h}{(t_w - t_m)k}$$

2.15

There are three main boundary conditions (BC) considered for the calculation of the Nusselt number. One is to consider a constant heat flux in the boundaries with a constant peripheral temperature (H1), the second is a constant heat flux but with a variable peripheral temperature (H2) and the third one is a constant temperature in the boundary (CWT). The values are not the same, and it must be defined the kind of boundary condition will be used for the calculation or selection of the number.

For many known geometries, theses values have been calculated. Kays ((11) page 117) or Incropera ((3) page 519, reproduced from Kays) have tables were Nusselt numbers for circular and rectangular cross sections are shown, as well as a detailed explanation of how they were calculated. Many other researchers have found values for Nu in various works ((4),(5), (6)).

15

CFD simulation of forced convection heat transfer of laminar phase-change non-Newtonian fluids in rectangular straight micro-channels

Cross Section	$\frac{b}{a}$	$Nu_D \equiv \frac{hD_h}{k}$ (Uniform q_s'')	(Uniform T_s)	$f\,Re_{D_h}$
○	—	4.36	3.66	64
□	1.0	3.61	2.98	57
▭	1.43	3.73	3.08	59
▭	2.0	4.12	3.39	62
▭	3.0	4.79	3.96	69
▭	4.0	5.33	4.44	73
▭	8.0	6.49	5.60	82
▭	∞	8.23	7.54	96
Heated / Insulated	∞	5.39	4.86	96
△	—	3.11	2.49	53

Used with permission from W. M. Kays and M. E. Crawford, *Convection Heat and Mass Transfer*, 3rd ed. McGraw-Hill, New York, 1993.

Figure 2-8, Theoretical Nusselt numbers

(Reproduced under "fair use" from (3))

The Nusselt number can be expressed as a function of other known parameters such as (11)

$$Nu = \text{St}\,\text{Pr}\,\text{Re} = \frac{h\,D_h}{k} \qquad \textbf{2.16}$$

Where
- St: The Stanton number $h/(V\,\rho\,c_p)$ or $h/(G\,c_p)$
- Pr: The Prandtl number $\mu\,c_p/k$
- Re: The Reynolds number $D_h\,V\,\rho\,/\mu$ or $D_h\,G\,/\,\mu$

As it has been said, the Nusselt number is one of the most important parameters in the convection problems. It describes the heat transfer between the boundary and the fluid and thus the capacity of the fluid to extract heat from a solid surface, as instance.

2.3.1 Microflow considerations

From the definition of the Nusselt number (eq. 2.13), it is possible to see that the convective heat transfer coefficient are inversely proportional to the hydraulic diameter. Therefore, if the size of the flow is decreased significantly, the heat transfer coefficients will increase dramatically (3). This is an important property of the fluids to consider when developing, as instance, cooling systems; small transport channels leads to a more efficient heat transfer.

16

2.4 Non-Newtonian fluids

It has been seen that the shear stress τ for a Newtonian fluid is proportional to the gradient of the velocity of the fluid in y direction:

$$\tau = \mu \frac{\partial u}{\partial y}$$

2.17

More precisely, it is proportional to the shear rate $\dot{\gamma}$ that is defined just as the rate at which a shear is applied (1)

$$\dot{\gamma} = \frac{\partial u}{\partial y}$$

2.18

For Newtonian fluids, then, the shear stress can be expressed as

$$\tau = \mu \dot{\gamma}$$

2.19

In the last equation μ is constant.

If this relation is plotted in a diagram (called rheogram) the linear relation for Newtonian fluids will behave as in the next figure
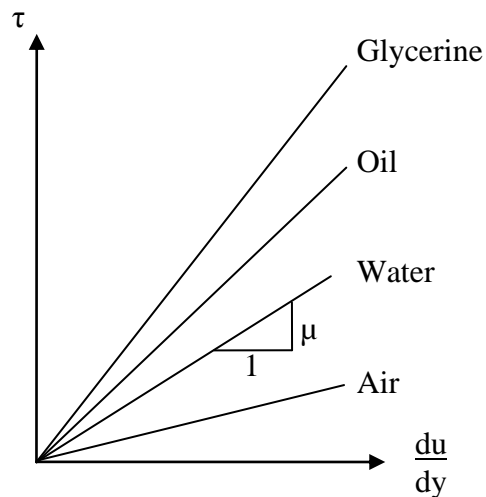
Figure 2-9, rheogram for Newtonian fluids

CFD simulation of forced convection heat transfer of laminar phase-change non-Newtonian fluids in rectangular straight micro-channels

The simplest deviation that causes a non-Newtonian behavior occurs when the stress has not a linear relation with the stress rate or when the line does not cross the zero. There are other conditions, but they are out of the scope of this work.

These materials can be classified, for example, as follows (1)

1. Systems for which the value of $\dot{\gamma}$ at a point within the fluid is determined only by the current value of σ and τ at that point; these substances are variously known as *purely viscous, inelastic, time-independent* or *generalized Newtonian fluids(GNF)*,
2. Systems for which the relation between σ, τ and $\dot{\gamma}$ shows further dependence on the duration of shearing and kinematic history; these are called *time-dependent fluids*, and finally,
3. Systems which exhibit a blend of viscous fluid behavior and of elastic solid-like behavior. For instance, this class of materials shows partial elastic recovery, recoil, creep, etc. Accordingly, these are called *visco-elastic* or *elastico-viscous fluids*.

This classification is arbitrary, but convenient, as stated by Chhabra(1). Generally, most real materials will display a behavior that can be classified in more than one of these categories, but they resume in a very convenient way the characteristics of non-Newtonian fluids by identifying its dominant aspect and use it for subsequent calculations.

Some known non-Newtonian fluids are, for example, Bingham plastics, yield pseudo-plastics, yield dilatants, pseudo-plastics or dilatants; these last two are classified as power law fluids and this is the model that will be used for this work. . In the following sections, a reference to a non-Newtonian fluid must be assumed to be a reference to a power-law fluid.

2.4.1   Power Law or Ostwald - de Waele equation

Shear-thinning is perhaps the most common type of time-independent non-Newtonian fluids in engineering. They are characterized by an apparent viscosity η which gradually decreases with increasing shear rate, or in other words, it is not constant.

The apparent or non-Newtonian viscosity η is defined as

$$\eta = \frac{\tau_{xy}}{\dot{\gamma}_{xy}}$$ 2.20

However, although the apparent viscosity of a pseudo-plastic substance decrease with the shear rate, the rate of decrease in viscosity varies from system to system depending on many factors such as concentration if the fluid is a solution, the nature of the fluid, if it is a polymer, for instance, etc. Thus, it is impossible to suggest a valid generalization in the behavior of these fluids.

The next figure show how, for three different polymers, the values for η decrease as the shear rate increases, but it also shown how the rate of decrease in apparent viscosity is different for the same range of share rate interval. This rate is influenced by many factors such the concentration of the polymer, the nature of the solvent, etc.
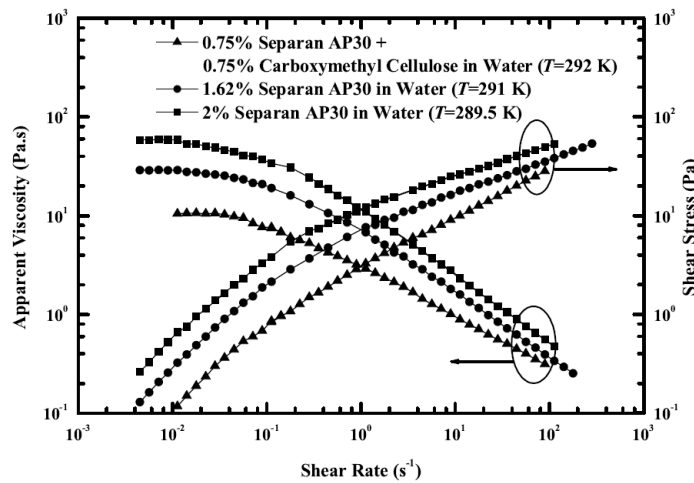
Figure 2-10, representative shear stress and *AV* for three pseudo-plastics

(Reproduced under "fair use" from (1))

To approximate this type of behavior, many mathematical equations varying in complexity have been developed (1). Some are based in straight curve fitting from experimental data; others used some theoretical base mixed with empirical statistical information as an extension of the kinetic theory. The list is extensive, but one of the simplest representations is the power law fluids.

CFD simulation of forced convection heat transfer of laminar phase-change non-Newtonian fluids in rectangular straight micro-channels

If the relationship between the shear rate and the shear stress is plotted on a log-log coordinates, this relation can be approximated by a straight line over an interval of shear rate (1):

$$\tau = K_c \, (\dot{\gamma})^n \qquad \textbf{2.21}$$

Or in terms of the apparent viscosity

$$\eta = \frac{\tau_{xy}}{\dot{\gamma}_{xy}} = K_c \, (\dot{\gamma})^{n-1} \qquad \textbf{2.22}$$

In these equations K_c is the consistency index and n is the power law index. These values are obtained with empirical curve fitting methods.

The power law fluid behavior is then described by

$$\tau = K_c \left(\frac{\partial u}{\partial y}\right)^n \qquad \textbf{2.23}$$

It is obvious that if $n = 1$, the fluid behaves as a Newtonian fluid (with $K_c = \mu$). The other possibilities are:

- $n < 1$: shear-thinning (pseudo-plastic behavior)
- $n > 1$: shear-thickening (dilatants behavior)

The rheogram for power law fluids is as follows:
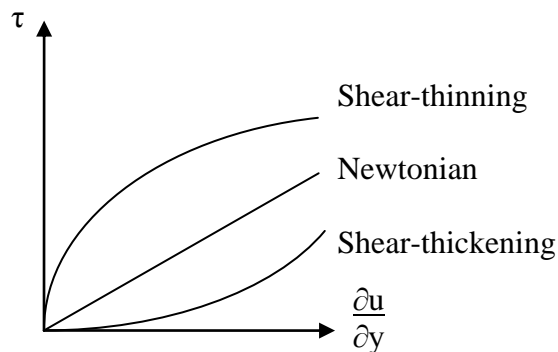
Figure 2-11, rheogram for power law fluids

Although these equations offer a simple approximation of the shear-thinning behavior, they predict neither the upper or lower limits when $\dot{\gamma} \to 0$ or $\dot{\gamma} \to \infty$, and the values of n and K_c are constant only over a narrow interval of shear range, so the working range of shear rate needs to be known *a priori*.

The velocity profiles of non-Newtonian flows are different from the Newtonian flows as well. The next figure shows an example of these profiles. Some works has been done to obtain an equation that describes these profiles, like the work of Marco and Han, cited by Garimella (7), but as this work will deal with developing flows, those equations will not be used, allowing the flow to develop naturally.

Newtonian, parabolic profile

Power law, n = 0.5

Power law, n >> 1
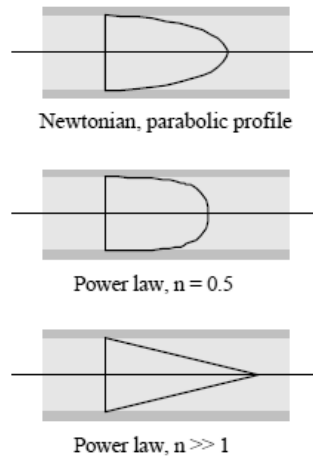
Figure 2-12, typical non-Newtonian velocity profiles

(Reproduced under "fair use" from (12))

2.4.2 Dimensionless correlations for non-Newtonian fluids

The Reynolds number for non-Newtonian fluids is not the same as for Newtonian, as consequence of the variable viscosity. The generalized Reynolds number for non-Newtonian fluids Re_{NN} is given by (13):

$$Re_{NN} = \frac{\rho D_h^n V^{2-n}}{K_c} \qquad \textbf{2.24}$$

The Nusselt number definition is the same than for the Newtonian fluids, and it is given in equation 2.13.

CFD simulation of forced convection heat transfer of laminar phase-change non-Newtonian fluids in rectangular straight micro-channels

2.5   Phase change materials

The use of phase change material as heat exchange fluid has been extensively studied recently due its great properties to transfer heat.

Major phase changes of a substance are their melting/freezing point (solid to liquid phase change) and the boiling/condensation point (liquid to gas change).   The changes have in common the highest values in enthalpy during the phase change, and the enthalpy that is stored during the phase change is called latent heat, in contrast to the direct heat storage in a substance during heating due its heat capacity (14).

The use of melting microcapsules has been widely extended due its capacities to upgrade a transfer fluid. Microcapsules are micro containers which pack the core material individually with a hard shell. The microcapsules are dispersed in a transport fluid and the phase change of these solid microcapsules to liquid allows a high heat transfer from the boundaries to the fluid domain.

But for micro-channels, microcapsules can be large compared with the dimension of the duct (typical microcapsules diameters goes from 1-100[µm](14)). The use of Nanofluids, where the PCM particles are even smaller is an advance in heat transfer with phase change technologies (15).

An advantage of using PCM is that the ability to store energy is not affected by the temperature, as it stays almost constant during the process. Three regions can be recognized during the melting process and can be observed in the next figure:
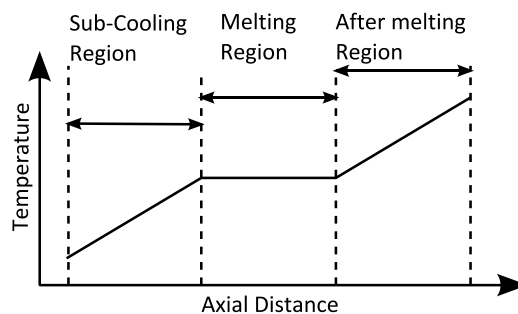
Figure 2-13, phase change regions with the temperature dependence

Many attempts to numerically model a phase change have been done, like the one of Charunyakorn (16) where a source was used to model the amount of heat absorbed or released during the phase change process, but this source term is a function of the radius of the PCM particles. To obtain this radius, a fourth order equation must be solved. It was found that this method was computationally expensive and complicated.

Avanic (17) found that comparable results can be achieved by using a simple specific heat approach. It was found that the shape of the specific heat function (i.e. triangular, rectangular or sinusoidal) was not a parameter in determining the heat transfer performance of the PCM slurry.

In this method, the pipe is divided in the three regions of the phase change process, where the location of the regions depends on radial distance because of the laminar flow velocity profile, as depicted in the next figure (18):
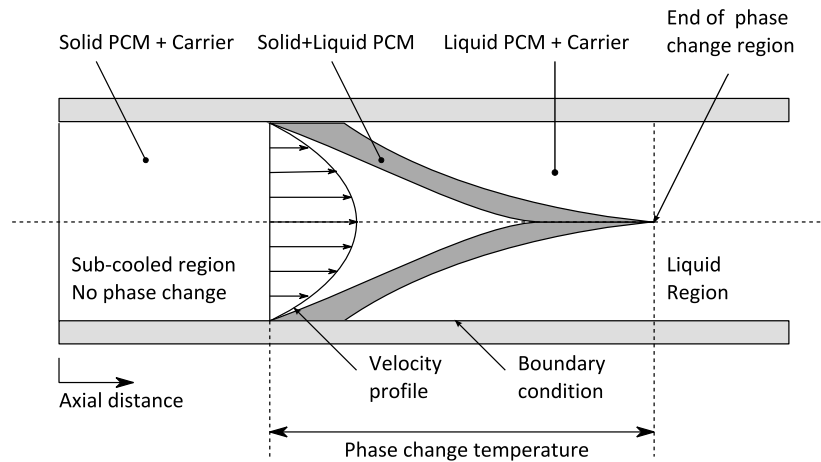
Figure 2-14, melting process in a circular tube

The specific heat of the PCM takes into account the specific heat of the carrier fluid in the first and in the third region (from Figure 2-13) as well as the latent heat capacity and the temperature range of the PCM during the melting region.

CFD simulation of forced convection heat transfer of laminar phase-change non-Newtonian fluids in rectangular straight micro-channels
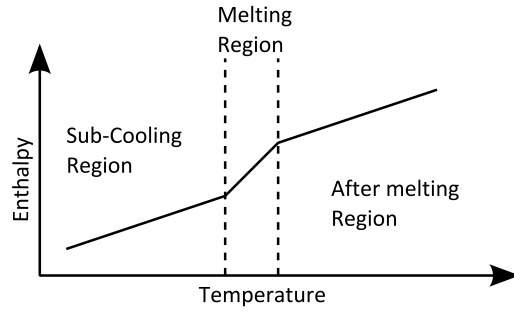
Figure 2-15, variation of the specific heat with temperature

The relation between enthalpy and specific heat is given by

$$(i_2 - i_1) = L_h = c_p(t_2 - t_1) \qquad \text{2.25}$$

The model does not consider particle behavior and assume that the phase change material is a completely homogeneous single phase fluid. The phase change is approximated with a change in the specific heat of the fluid, within the melting temperature range of the phase change material.

Yamagishi (10) found that this model gives results that are comparable with experimental data, and this method is easy to implement in commercial software like Fluent.

The following equations are used to define the specific heats (10):

For $t < t_1$ or $t > t_2$:

$$c_{p,b} = c \ c_{p,p} + (1 - c) \ c_{p,f} \qquad \text{2.26}$$

For $t_1 < t < t_2$:

$$c_{p,b} = (1 - c) \ c_{p,f} + \frac{c \ L_h}{(t_2 - t_1)} \qquad \text{2.27}$$

Where t_1 is the temperature where the phase change starts, t_2 is the temperature where the phase change ends, $c_{p,x}$ where f is the specific heat of the carrier, b is for the bulk fluid (PCM + carrier) and p is for the PCM particles; L_h is the latent heat of the PCM particles, and c is the volumetric concentration of PCM.

24

As it has been said, the profile of the specific heat of the slurry seems to have no effect on the heat transfer, thus, a rectangular profile were selected for simulate the phase change. The next figure depicted the specific heat change for the bulk fluid:
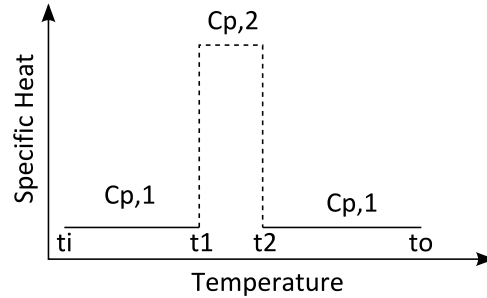
Figure 2-16, specific heat profile to simulate phase change ($c_p = c_{p,b}$)

The properties of the slurry like viscosity and density also changes from the single fluid. The equations that define these properties are (9):

Viscosity:

$$\frac{\mu_b}{\mu_f} = (1 - c - 1.16\ c^2)^{-2.5} \qquad\qquad \textbf{2.28}$$

Density:

$$\rho_b = c\ \rho_p + (1 - c)\rho_f \qquad\qquad \textbf{2.29}$$

Thermal conductivity:

$$k_b = k_f \frac{2 + \frac{k_p}{k_f} + 2c\left(\frac{k_p}{k_f} - 1\right)}{2 + \frac{k_p}{k_f} - c\left(\frac{k_p}{k_f} - 1\right)} \qquad\qquad \textbf{2.30}$$

2.6   Governing equations

This section deals with the equations that government the mechanics of fluids and heat transfer. It is intend as a brief introduction, to allow the understanding of what the CFD software is solving and not as a complete explanation of how to do it. The solution of his equations is complex, and very often just not possible up to date, and thus, the CFD is a

CFD simulation of forced convection heat transfer of laminar phase-change non-Newtonian fluids in rectangular straight micro-channels

valuable tool for this kind of problems. To use a CFD program, it is not necessary to know these equations, but if it is the case, it will be very hard for the user to judge the accuracy of the results.

2.6.1 Conservation principles

If *creation* is defined as the outflow minus the inflow quantities, plus the internal generation in a control volume, then the conservation principles that rule the fluids flow can be enlisted as follow: (11)

- The rate of creation of matter $=0$
- The rate of creation of momentum $=g_c\vec{F}$
- The rate of creation of energy $=0$

Where g_c is a proportionality factor and $\vec{F}$ is the resultant of all external forces acting on the surface of a control surface or volume.

With this first approach, it is possible to obtain the differential equations that rule the behavior of the fluid in the boundary layers.

If the boundary layer thickness is very small in relation with all the other flow dimensions, then the following conditions must prevail within the layers: (11)

$$u \gg v \qquad \text{2.31}$$

$$\frac{\partial u}{\partial y} \gg \frac{\partial u}{\partial x}, \frac{\partial v}{\partial x}, \frac{\partial v}{\partial y} \qquad \text{2.32}$$

$$\frac{\partial t}{\partial y} \gg \frac{\partial t}{\partial x} \qquad \text{2.33}$$

$$\sigma_x \approx -P, \quad \frac{\partial P}{\partial y} \approx 0 \qquad \text{2.34}$$

Because the boundary layer is so thin, the pressure gradient in the x direction can be approximated to the free stream pressure gradient (3).

$$\frac{\partial P}{\partial x} \approx \frac{dP_\infty}{dx} \qquad\qquad \textbf{2.35}$$

In these equations, v is the velocity in y direction, P is the pressure and σ_x is the normal stress. These assumptions allow neglecting certain terms when deducing governing equations, such as the velocity of the fluid in the y direction.

2.6.1.1 The continuity equations

For an infinitesimal two-dimensional control volume, the continuity equations can be obtained by the principle of conservation of mass.

If $\vec{G}$ represents the mass flux (mass flow rate per unit of normal area) and G_x and G_y the x and y components. Note that $G_x = \rho u$ and $G_y = \rho v$, that is the mass flux is the density of the fluid times the velocity in the appropriate direction. Then, the fluxes acting in a control volume of dimensions δ_x x δ_y x 1unit are:

- Inflow: $G_x \delta y + G_y \delta x$ (mass flux component times face area)
- Outflow: $\left(G_y + \frac{\partial G_y}{\partial y} \delta y\right) \delta x + \left(G_x + \frac{\partial G_x}{\partial x} \delta x\right) \delta y$
- Increase of storage: $\frac{\partial \rho}{\partial \theta} \delta y \delta x$ where θ is the time.

Then

$$\frac{\partial G_x}{\partial x} + \frac{\partial G_y}{\partial y} + \frac{\partial \rho}{\partial \theta} = 0 \qquad\qquad \textbf{2.36}$$
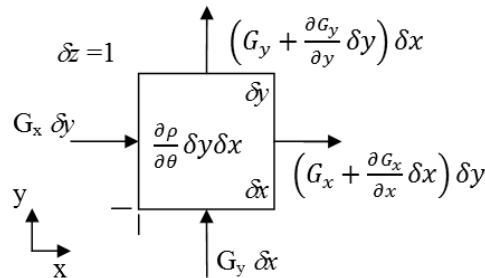
Figure 2-17, control volume for development of the continuity equation

CFD simulation of forced convection heat transfer of laminar phase-change non-Newtonian fluids in rectangular straight micro-channels

And the equivalent for three-dimensional flow

$$\frac{\partial G_x}{\partial x} + \frac{\partial G_y}{\partial y} + \frac{\partial G_z}{\partial z} + \frac{\partial \rho}{\partial \theta} = 0 \qquad \text{2.37}$$

Or in vectorial format

$$\nabla \cdot \vec{G} + \frac{\partial \rho}{\partial \theta} = 0 \qquad \text{2.38}$$

If the flow is steady, it means that there are no time dependencies, and then the equation reduces to

$$\nabla \cdot \vec{G} = 0 \qquad \text{2.39}$$

2.6.1.2   The steady-flow momentum equations

In similar way, it is possible to develop the momentum equations. If an infinitesimal control volume is taken from the velocity boundary layer and let the flux goes into the positive x direction. The fluxes and the velocities in the y directions are negligible.

The momentum is defined as $m\,\vec{V}$ or the mass m times the velocity (referred to an inertial coordinate system).

Assuming that there are not body forces such as gravity, and that the flow is in the laminar region, since a turbulent fluid is, by its nature, unsteady, the inputs and outputs of momentum in the control volume (for $\delta_z = 1$) can be defined as follows:

- Inflow of momentum: $(G_x\,u)\delta y + (G_y\,u)\delta x$
- Outflow of momentum: $\left[G_x\,u + \frac{\partial(G_x)u}{\partial x}\,\delta x\right]\delta y + \left[G_y\,u + \frac{\partial(G_y)u}{\partial y}\,\delta y\right]\delta x$
- External forces: $-\sigma_x\,\delta y - \tau_{xy}\,\delta x + \left(\sigma_x + \frac{\partial \sigma_x}{\partial x}\,\delta x\right)\delta y + \left(\tau_{xy} + \frac{\partial \tau_{xy}}{\partial x}\,\delta y\right)\delta x$
- Increase of momentum storage $= 0$

28
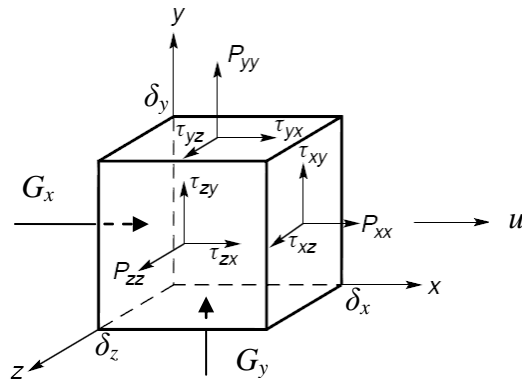
Figure 2-18, three dimensional flow stress state

As it has been seen when explaining the velocity boundary layer, the fluids are subject to stresses too. The stresses that act over a control volume are a normal and a shear stress. By now, only the stresses for Newtonian fluids will be discussed; stresses for non-Newtonian will be explained on the following chapters. The normal stresses are defined (2) as

$$\sigma_i = \frac{2}{3}\mu \left(\frac{\partial u_i}{\partial x_i} + \frac{\partial u_j}{\partial x_j} + \frac{\partial u_k}{\partial x_k} \right) - 2\mu \frac{\partial u_i}{\partial x_i} \qquad \text{2.40}$$

The shear stress is defined by

$$\tau_{ij} = \tau_{ji} = -\mu \left(\frac{\partial u_j}{\partial x_i} + \frac{\partial u_i}{\partial x_j} \right) \qquad \text{2.41}$$

Where σ_i is the normal stress in the ith face and direction of a fluid element, τ_{ij} is the shear stress on the ith face in the jth direction, u_i is the velocity in the ith direction, x_j is the jth direction coordinate, and μ' is the second viscosity coefficient.

The normal stress can be expressed as the combination of two components: isotropic pressure and a contribution due to flow. It could be expressed as

$$P_{ii} = -P + \sigma_i \qquad \text{2.42}$$

For an incompressible Newtonian fluid, P is given by

CFD simulation of forced convection heat transfer of laminar phase-change non-Newtonian fluids in rectangular straight micro-channels

$$P = \frac{1}{3}(P_{xx} + P_{yy} + P_{zz})$$

<div align="right">2.43</div>

From equations 2.42 and 2.43, it follows that

$$\sigma_x + \sigma_y + \sigma_z = 0$$

Then, if the fluid is in simple shearing motion, the deviatoric normal stress components are identically zero: $\sigma_x = \sigma_y = \sigma_z = 0$

By combining these equations with the rate of creation of momentum $= g_c \vec{F}$ and simplifying it is possible to obtain (11)(19)

$$\rho u \frac{\partial u}{\partial x} + \rho v \frac{\partial u}{\partial y} + g_c \frac{\partial P}{\partial x} = \frac{\partial}{\partial y}\left(\mu \frac{\partial u}{\partial y}\right)$$

<div align="right">2.44</div>

2.6.1.3 The Navier-Stokes equations

For a three-dimensional control volume, the equation of momentum must include the terms in the z direction. A general form of the momentum equation, without simplifications and including body loads can be obtained. Applying the momentum equation for the x direction it is possible to obtain

$$\rho\left(\frac{\partial u}{\partial \theta} + u\frac{\partial u}{\partial x} + v\frac{\partial u}{\partial y} + w\frac{\partial u}{\partial z}\right) + g_c\frac{\partial y}{\partial x} = \frac{\partial}{\partial x}\left(\mu\left[2\frac{\partial u}{\partial x} - \frac{2}{3}\left(\frac{\partial u}{\partial x} + \frac{\partial v}{\partial y} + \frac{\partial w}{\partial z}\right)\right]\right) +$$

$$\frac{\partial}{\partial y}\left(\mu\left(\frac{\partial u}{\partial y} + \frac{\partial v}{\partial x}\right)\right) + \frac{\partial}{\partial z}\left(\mu\left(\frac{\partial w}{\partial x} + \frac{\partial u}{\partial z}\right)\right) + g_c F_{bx}$$

<div align="right">2.45</div>

Similar equations can be set up for y and z directions. F_{bx} is the body force in the x direction.

Equation 2.45, with the equivalents for y and z, are the general form of the Navier-Stokes equations. These equations can be particularized to a simplified form for different flow cases.

2.6.1.4 The steady-flow energy equations

The deduction of the energy equation follows the same methodology of the past equations. Defining enthalpy i as $i = e + PV$ or $i = e + P/\rho$, that is the sum of the flow work and the internal energy per unit of mass, then the energy transfer terms for a two-dimensional fluid, assuming steady flow, with no internal energy generation and no work done by external fields are by definition: (11)

- $\dot{E}_{conv,x} = G_x \delta y \left(i + \frac{u^2}{2g_cJ} \right)$

- $\dot{E}_{conv,x+\delta x} = \delta y \left\{ G_x \left(i + \frac{u^2}{2g_cJ} \right) + \frac{\partial}{\partial x} \left[G_x \left(i + \frac{u^2}{2g_cJ} \right) \right] \delta x \right\}$

- $\dot{E}_{conv,y} = G_y \delta y \left(i + \frac{u^2}{2g_cJ} \right)$

- $\dot{E}_{conv,y+\delta y} = \delta x \left\{ G_y \left(i + \frac{u^2}{2g_cJ} \right) + \frac{\partial}{\partial y} \left[G_y \left(i + \frac{u^2}{2g_cJ} \right) \right] \delta y \right\}$

- $\dot{E}_{diff,y} = - \left(\sum_j \gamma_j \frac{\partial m_j}{\partial y} i_j \right) \delta x$

- $\dot{E}_{diff,y+\delta y} = - \left[\sum_j \gamma_j \frac{\partial m_j}{\partial y} i_j + \frac{\partial}{\partial y} \left(\sum_j \gamma_j \frac{\partial m_j}{\partial y} i_j \right) \delta y \right] \delta x$

- $\dot{q}_y = -k \left(\frac{\partial t}{\partial y} \right) \delta x$

- $\dot{q}_{y+\delta y} = - \left[k \left(\frac{\partial t}{\partial y} \right) + \frac{\partial}{\partial y} \left(k \frac{\partial t}{\partial y} \right) \delta y \right] \delta x$

- $\dot{W}_{shear,y} = \left(\frac{\tau_{xy} u}{J} \right) \delta x$

- $\dot{W}_{shear,y+\delta y} = \frac{1}{J} \left[\tau_{xy} u + \frac{\partial (\tau_{xy} u)}{\partial x} \delta y \right] \delta x$

In last equations J is a conversion factor from mechanical to thermal units (11).

The input and output energies are combined with the "The rate of creation of energy = 0" equation and with the use of the boundary layer simplifications and the momentum equation it is possible to obtain the general energy equation for a viscous fluid (11)

$$\left(\rho u \frac{\partial i}{\partial x} + \rho v \frac{\partial i}{\partial y} + \rho w \frac{\partial i}{\partial z} + \rho \frac{\partial i}{\partial \theta} \right) - \left[\frac{\partial}{\partial x} \left(k \frac{\partial t}{\partial x} \right) + \frac{\partial}{\partial y} \left(k \frac{\partial t}{\partial y} \right) + \frac{\partial}{\partial z} \left(k \frac{\partial t}{\partial z} \right) \right] -$$

$$\left[\frac{\partial}{\partial x} \left(\sum_j \gamma_j \frac{\partial m_j}{\partial x} i_j \right) + \frac{\partial}{\partial y} \left(\sum_j \gamma_j \frac{\partial m_j}{\partial y} i_j \right) + \frac{\partial}{\partial z} \left(\sum_j \gamma_j \frac{\partial m_j}{\partial z} i_j \right) \right] - \frac{\mu}{g_cJ} \Phi -$$

2.46

31

CFD simulation of forced convection heat transfer of laminar phase-change non-Newtonian fluids in rectangular straight micro-channels

$$\frac{1}{J}\left(u\frac{\partial P}{\partial x} + v\frac{\partial P}{\partial y}w\frac{\partial P}{\partial z} + \frac{\partial P}{\partial \theta}\right) - So = 0$$

In last equation, *So* is the source function that represents the internal creation of heat in the control volume mostly due a chemical reaction and Φ is the viscous dissipation function that is the transformation of mechanical energy to heat by the flow working against the viscous stresses.

In vectorial form, the equation can be written in a more elegant and compact form:

$$\rho\frac{Di}{D\theta} - \nabla \cdot k\,\nabla t - \nabla \cdot \left(\sum_j \gamma_j i_j\,\nabla m_j\right) - \frac{\mu}{g_c J}\Phi - \frac{1}{J}\frac{DP}{D\theta} - So = 0 \qquad \text{2.47}$$

For steady flow, with no source function and neglecting the dissipation function and with no mass concentration gradients the energy equation reduces to

$$\vec{G}\,\nabla i - \nabla \cdot k\,\nabla t = 0 \qquad \text{2.48}$$

2.6.2 Non-Newtonian fluid governing equations

To consider a fluid as Newtonian, that fluid must satisfy certain criteria, that, based on experiments and experience could be stated as (2):

1. Stress is dependant only of pressure and rate of deformation. Temperature can affect only indirectly through coefficients as viscosity.
2. If the rate of deformation goes to zero, all shear stresses disappear and the normal stresses are each equal to –P
3. The fluid is *isotropic*.
4. The stress depends of the rate of deformation in a linear manner.

These statements lead to equations 2.40 and 2.41 and to the Navier-Stokes equations.

But as it has been seen, statement number 4 is not valid for non-Newtonian fluids, as the relation between the stress and the shear ratio is not linear. If the Newtonian fluids can be considered as a particular case of the non-Newtonian fluids (with $n = 1$, for a power law fluid

for instance) then this relation can be extended to include quadratic terms in the rate of deformation (2).

The most general form of constitutive equation for flows that are described only by stress and shear ratio is given by

$$\tau_{ij} = -(P + \mu' \nabla \cdot v)\delta_{ij} + \mu \, d_{ij} + \mu'' \, d_{ik} \, d_{kj}$$

<div align="right">2.49</div>

Where μ'' is an additional viscosity coefficient and

$$\nabla \cdot v = \frac{\partial u_i}{\partial x_i} + \frac{\partial u_j}{\partial x_j} + \frac{\partial u_k}{\partial x_k} = \frac{\partial u}{\partial x} + \frac{\partial v}{\partial y} + \frac{\partial w}{\partial z}$$

<div align="right">2.50</div>

This constitutive law (2.49) describes what are called *Stokesian fluids*, after George Stokes. The introduction of the second power term increase the difficulty in solving the equation, but fortunately, there has not been found so far fluids that obey this law better than the first power law (2).

2.6.3   CFD and the governing equations

When using a numeric method to approximate flux problems, the solver actually uses the equations discussed in past section to generate a balance in mass, momentum and energy and to calculate the values of the variables in each node of the finite model. The various existing methods for solving the equations are out of the scope of this work, but it is important to known these equations to understand what the numeric method is doing in each of the elements of the model.

It is of fundamental importance to understand that the solvers are not getting an exact solution for these equations, but a numerical approximation, thus, as in every numerical method, there are implicit errors and it is responsibility of the user to known how large these errors could be allowed. Normally, trying to reduce the error results in an increment of computing power, then, it is necessary to find a balance between accuracy and economy of resources.

More of this and the principles of the CFD will be discussed in section 2.7.

CFD simulation of forced convection heat transfer of laminar phase-change non-Newtonian fluids in rectangular straight micro-channels

2.7   Principles of computational fluid dynamics

Although an extensive description of the numeric methods used in CFD is out of the scope of this work, a brief introduction is presented here.

First of all, it is important to remember that, as every numeric method, CFD will never give an exact solution of a problem. Every result obtained from the simulations is subject to many causes of error (that will be discussed later in this section) and it is responsibility of the user to determine the validity of such results.

A numerical calculation never investigates the real system. To find a simple model that includes all the important effects is, maybe, the hardest part of the analysis. Many effects are often neglected form the model, thus, the results will never be exact as the results of an experimental setting, but just an approximation. Of course, the approximations may be close enough to consider the results as valid for predicting behaviors of the system.

There are four models that can be constructed for solving the governing equations of the CFD (19):

- Finite control volume fixed in space
- Finite control volume moving in space
- Differential fluid element fixed in space
- Differential fluid element moving in space

Every model will lead to a set of equations that must be solved to obtain a solution, but in the end, the equations generated by these models are really different representations of the governing equations.

If a fixed finite volume is used, the model will lead directly to a set of integral equations known as the *conservation* form of the governing equations. These equations can be manipulated to obtain a differential form but they are still in the *conservation* form. If the volume is moving with the fluid, the equations obtained are called *non-conservation*, in either integral or differential form. The same applied for the differential element, but in this case, the

34

model leads directly to a set of partial differential equations that can be manipulated to obtain an integral form.

As the CFD software used in this work uses the conservation equations, this section will focus in describing this form. More information about the models can be found in, i.e., (19). Detailed information about the parameters used in this work could be found in CHAPTER 4 Power law fluids simulation methodology.

2.7.1   The governing equations for CFD

Considering a differential element fixed in space and from section 2.6 that the balance of mass flow defined by ρu_i entering and leaving the element is equal to the rate of change in density (20).

$$\frac{\partial \rho}{\partial \theta} + \frac{\partial(\rho u_i)}{\partial x_i} \equiv \frac{\partial \rho}{\partial \theta} + \nabla(\rho \, \mathbf{u}) = 0 \qquad \text{2.51}$$

The balance of momentum is given by

$$\frac{\partial(\rho u_j)}{\partial \theta} + \frac{\partial(\rho u_j)u_i}{\partial x_i} - \frac{\partial \tau_{ij}}{\partial x_i} + \frac{\partial P}{\partial x_j} - \rho F_{bi} = 0 \qquad \text{2.52}$$

And the balance of energy is

$$\frac{\partial(\rho E)}{\partial \theta} + \frac{\partial(\rho u_i I)}{\partial x_i} - \frac{\partial}{\partial x_i}\left(k\frac{\partial t}{\partial x_i}\right) + \frac{\partial(\tau_{ij}u_j)}{\partial x_i} - \rho F_{bi}u_i - So = 0 \qquad \text{2.53}$$

Where

$$I = i + \frac{u_i u_i}{2} = E + \frac{P}{\rho} \qquad \text{2.54}$$

These governing equations can be written in conservation form as (20)

CFD simulation of forced convection heat transfer of laminar phase-change non-Newtonian fluids in rectangular straight micro-channels

$$\frac{\partial \mathbf{\Phi}}{\partial \theta} + \nabla \mathbf{F} + \nabla \mathbf{G} + \mathbf{Q} = 0 \qquad \text{2.55}$$

Or in Cartesian notation:

$$\frac{\partial \mathbf{\Phi}}{\partial \theta} + \frac{\partial \mathbf{F}_i}{\partial x_i} + \frac{\partial \mathbf{G}_i}{\partial x_i} + \mathbf{Q} = 0 \qquad \text{2.56}$$

Where

$$\mathbf{\Phi} = \begin{pmatrix} \rho \\ \rho u \\ \rho v \\ \rho w \\ \rho E \end{pmatrix}, \mathbf{F}_x = \begin{pmatrix} \rho u \\ \rho u^2 + P \\ \rho u v \\ \rho u w \\ \rho I u \end{pmatrix}, etc.; \mathbf{G}_x = \begin{pmatrix} 0 \\ -\sigma_x \\ -\tau_{xy} \\ -\tau_{xz} \\ -(\sigma_x u + \tau_{xy} v + \tau_{xz} w) - k\frac{\partial t}{\partial x} \end{pmatrix}, etc. \qquad \text{2.57}$$

$$\mathbf{Q} = \begin{pmatrix} 0 \\ -\rho F_{bx} \\ -\rho F_{by} \\ -\rho F_{bz} \\ -\rho(F_{bx} u + F_{by} v + F_{bz} w) - S \end{pmatrix}, etc.$$

With

$$\tau_{ij} = \tau_{ji} = -\mu \left[\left(\frac{\partial u_j}{\partial x_i} + \frac{\partial u_i}{\partial x_j} \right) - \delta_{ij} \frac{2}{3} \frac{\partial u_k}{\partial x_k} \right] \qquad \text{2.58}$$

Equation 2.55 is the complete set of the Navier-Stokes equations in vectorial notation. As a particular case, if viscosity can be assumed as zero and there is no heat transfer, the set is known as the Euler Equation ($\tau_{ij} = k = 0$).

The numerical method solves these equations by approximations. There are many methods such as the Petrov-Galerkin or the standard Galerkin to get an approximate solution to the equation. The explanation of these methods is out of the scope of this work, but there are well documented works from, e.g. Anderson (19) or Zienkiewicz (20) that go deeper in the explanation.

2.7.2 The CFD Strategy

In a simple way, the CFD strategy to solve fluid problems is to replace the continuous domain with a discrete domain by the generation of a grid. The advantage of this is that the flow variables are not defined in every point in the domain, but only in certain defined points, generated by the grid. The difference of both scenarios, considering, for example, the velocity v, can be expressed as (21):

$$Continouus: v = v(x), 0 < x < 1$$
$$Discrete: v = v(x_i), i = 1,2, \dots, N$$

2.59

It is possible to see that the advantage of dealing with a discrete domain is that the value of the variable must be defined only in a finite number of points, and the values for the other locations are determined by interpolating the values at those points.

The governing equations are defined in term of continuous variables, i.e. u. These variables can be approximated in the domain in terms of the variables at each point, for example u_N. The discrete system turns to a large set of algebraic equations in those discrete variables that can be solved with the help of a computer.

For the finite volume method, the domain is divided in a grid in which commonly every element is called a *cell* and the points in the grid a *node*. As it has been said, for this method, the equations used are in the integral form, then, for example, if the continuity equation for steady, incompressible flow is defined as

$$\int_S \boldsymbol{V} \, \boldsymbol{\hat{n}} \, ds = 0$$

2.60

This equation is the integration over the surface S and $\boldsymbol{\hat{n}}$ is the outward normal at the surface. Physically, this equation means that the net volume flow into the control volume is zero.

Consider the rectangular cell shown below.

CFD simulation of forced convection heat transfer of laminar phase-change non-Newtonian fluids in rectangular straight micro-channels
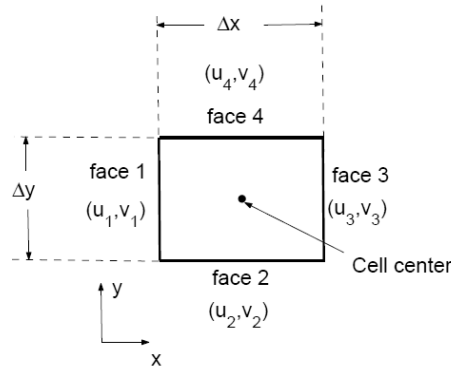
Figure 2-19, control volume in the CFD method

(Reproduced under "fair use" from (21))

The velocity at face i is given by

$$V_i = u_i i + v_i j \qquad \text{2.61}$$

By applying the continuity equation 2.60, it is possible to obtain the discrete form of the continuity equation for the cell.

$$-u_1 \Delta y - v_2 \Delta x + u_3 \Delta y + v_4 \Delta x = 0 \qquad \text{2.62}$$

It is equivalent to summing up the net mass flow into the control volume and set it to zero, so, for example, it ensures that the net mass flow into the cell is zero: the mass is conserved for the cell.

It is usual to solve the values for the center of the cell by inverting the discrete system, and the values at the faces are obtained by a suitable interpolation. Similar equations can be obtained for the conservation of momentum and energy of the cell.

2.7.3   CFD work flow

In the CFD method there are basically by three principal steps:

1. Pre-processing
2. Solving
3. Post-processing

An explanation of these steps is developed next. As the methods to follow these steps depend on the software used, only a brief description will be done. Usually the documentation provided by the developer will cover these aspects in detail.

2.7.3.1   Pre-Processing

This step deals with the preparation of the model for the solver. The first step is to model the geometries. Many packages exist that allows creating up to 3d models, but is not uncommon to find 2d or 1d models, depending of the complexity of the system. Usually, for CFD, the model represents the fluid domain and not the structure, as should be in a structural analysis.

Next in the pre-processing stage is to mesh the model. The calculation domain is split in finite volumes. The use of these volumes will be evident in the solving stage, when the unknown quantities in the center of the finite volumes are approximated and iteratively calculated by the flow terms between neighboring volumes (22).

There are two principal control volumes for a 3d model: tetrahedral and hexahedral. Both of them could lead to same levels of accuracy in the solution, depending of the system and the nature of the problem, but tetrahedral elements use more computer resources, because the algorithm can't keep the volumes as a regular matrix and need to store the position and relation of every neighbor node, as can be done with the hexahedral. Also, the tetrahedral requires a larger number of volumes to mesh the domain. However, for complex geometries, tetrahedral elements may create a better approximation of the model than the hexahedral.

The boundary conditions are a very delicate part of the pre-processing stage. Wrong or incomplete definition could lead to error in the solution. To assign BC, it is important to understand the problem and the system. In many occasions, some conditions could be neglected, but it is not a rule of thumb and as every problem is different, the analysis of the BC is fundamental.

Boundary conditions are applied to the boundaries, usually a wall or a surface. The conditions consist in assign a heat flux or a temperature to a wall, for instance. It is possible to assign

velocities or pressures to the fluid, for example, in zones defined as inlet or outlet for the flow entering and leaving the domain.

Assigning properties to the materials involved in the system is part of the pre-processing too. The characteristics of the fluid such as density, specific heat, viscosity, etc. must be assigned. It is important to notice that most of the solvers does not take into account the units or magnitude of the numerical quantities, thus, it is important to verify that the quantities are in agreement with the units' system used. A mistake in these values will not be detected by the solver and it is usually very hard to find it after the solution is done.

2.7.3.2 Solving

In CFD software, the governing equations are solved with the help of some algorithms. Most of the times, these algorithms are proprietary code from the developer. For this work, the software used was FLUENT 12, thus, the solver theory presented in the following paragraphs is valid only for this software.

The first step is to select the precision method. Fluent has two versions to select: single-precision and double-precision. For most cases, the single-precision solver will be sufficiently accurate, but certain types of problems may benefit from the use of a double-precision version. Several examples are listed below:

• If your geometry has features of very disparate length scales (e.g., a very long, thin pipe), single-precision calculations may not be adequate to represent the node coordinates.

• If your geometry involves multiple enclosures connected via small-diameter pipes (e.g., automotive manifolds), mean pressure levels in all but one of the zones can be quite large (since you can set only one global reference pressure location). Double-precision calculations may therefore be necessary to resolve the pressure differences that drive the flow, since these will typically be much smaller than the pressure levels.

• For conjugate problems involving high thermal-conductivity ratios and/or high aspect- ratio meshes, convergence and/or accuracy may be impaired with the single-precision solver, due to inefficient transfer of boundary information.

• For multiphase problems where the population balance model is used to resolve particle size distributions, which could have statistical moments whose values span many orders of magnitude.

Next is necessary to select the numerical method. The software presents two methods:

- Pressure-based solver and,
- Density-based solver.

Historically speaking, the pressure-based solver was developed for low-speed incompressible flow, while the density-based approach was mainly used for high-speed compressible flows. However, these methods have been reformulated to solve and operate for a wide range of flow conditions beyond their original intent (23).

Using either method, the solution of the equations will be obtained from the integral equations for conservation of mass and momentum, and if needed, the energy and other scalars such as turbulence and chemical species. In both cases, a control volume technique is used, that consist in:

- Division of the domain into discrete volumes using a computational grid (handled by the pre-processor)
- Integration of the governing equations on the individual control volumes to construct algebraic equations for the discrete dependant variables such as velocities, pressure, temperature, etc.
- Linearization of the discretized equations and solution of the resultant linear equation system to yield updated values of the dependent variables.

To select the solver algorithm, it is necessary to consider many aspects of the system such the regime of the flow or the number of control volumes. Some algorithms can converge to a steady state solution faster than others, but at a cost of using more computational resources.

To obtain detailed information about the solvers and in which kind of problems could be applied, refer to the well documented ANSYS FLUENT 12.0 guides such (23) and (24).

CFD simulation of forced convection heat transfer of laminar phase-change non-Newtonian fluids in rectangular straight micro-channels

The time domain of the system is important too. If the parameters that are function of the time (i.e. *p(t)*) can be neglected, the system is the operating in a steady state. If these parameters are important and should be consider, the system must be solved under a transient state.

The accuracy is other important factor to select. FLUENT 12.0 have first-order accuracy and second-order accuracy among others that will not be discussed here. If the flow is aligned with the mesh, as in laminar flow in a rectangular duct as instance, the first-order discretization may be acceptable. However, this discretization increases the numerical error. In general, the first-order discretization yields better convergence, and the second-order scheme will lead, in general, to a better accuracy.

The accuracy of the solution is determined in part for the *residuals* of the result. Loosely speaking, the residuals are the error that remains after each iteration and can be used as a criteria if the exact solution of the equations are not known. If the residual is small, the accuracy is better, but asking for smaller residuals will lead to a larger computational expenses.

The full governing equations used by Fluent to solve the simulations are enlisted next:

- Mass conservation equation:

$$\frac{\partial \rho}{\partial \theta} + \nabla \cdot (\rho \vec{u}) = S_m \qquad \text{2.63}$$

This equation is valid for compressible and incompressible flows. The source S_m is the mass added to the continuous phase from the second phase disperse in the fluid (i.e. due vaporization) and user defined sources.

- Momentum conservation equations

$$\frac{\partial (\rho \vec{u})}{\partial \theta} + \nabla \cdot (\rho \vec{u}\vec{u}) = -\nabla P + \nabla \cdot (\bar{\bar{\tau}}) + \rho \vec{g} + \vec{F_b} \qquad \text{2.64}$$

The stress tensor is given by

$$\bar{\bar{\tau}} = \mu\left[(\nabla\vec{u} + \nabla\vec{u}^T) - \frac{2}{3}\nabla\cdot\vec{u}I\right]$$ 2.65

Where I is the unit tensor and the second term of the right hand side is the effect of the volume dilation.

- Energy conservation equation

$$\frac{\partial(\rho E)}{\partial\theta} + \nabla\cdot(\vec{u}(\rho E + P)) = \nabla\cdot\left(k_{eff}\nabla t - \sum_j i_j\vec{J}_{j+(\bar{\bar{\tau}}_{eff}\cdot\vec{u})}\right) + So_h$$ 2.66

Where k_{eff} is the effective conductivity and $\vec{J}$ is the diffusion flux of the species j.

2.7.3.3 Post-processing

To review the results after the solver has finished, it is necessary a post-processor. This module basically displays, in form of plots, graphs or lists, the results that the solver obtains. There are many types of post-processors, each with their strengths or limitation, so the use of the post-processors will not be discussed here.

2.7.4 Causes of errors in CFD

In CFD, there are many causes of possible errors to take in into account. Although sometimes it is not possible to completely control these errors, by knowing them, it is possible to minimize the impact.

The two principal branches in which errors can be classified are:

- Acknowledged errors: Have procedures for identifying them and removing. Otherwise, they can remain in the code with their error estimated and listed.
- Unacknowledged errors: Have no procedures for finding them and may continue within the code o simulation.

CFD simulation of forced convection heat transfer of laminar phase-change non-Newtonian fluids in rectangular straight micro-channels

Another difference between the errors is if they are local or global. Local errors may affect only at grid point or cell level, while global errors may affect the whole domain.

The errors can be classified as follows (25):

Acknowledged Error

1. Physical approximation error: They are due uncertainty in the formulation of the model and deliberated simplification of the model. They appear when the phenomenon is not well understood or, e.g. experimental verification of the model is not possible.
   a. Physical modeling error
   b. Geometry modeling error
2. Computer round-off error: This error develops with the representation of the floating point numbers on the computer and the accuracy at which the numbers are stored.
3. Iterative convergence error: The iterative procedures used for the simulation must stop at a point eventually. This error appears depending of the selection of such point.
4. Discretization error: those errors occur from the representation of the governing flow equations and other physical models as algebraic expressions in a discrete domain of space (finite-difference, finite-volume, or finite-element) and time.
   a. Spatial discretization error
   b. Temporal discretization error

Unacknowledged Error

1. Computer programming error: Bugs and mistakes made in programming the code. They depend mostly in the developers of the code.
2. Usage error: They are due to the application of the code in a less-than-accurate or improper manner. These errors depend mostly on the user of the software.

2.7.5 Viscosity for non-Newtonian fluids in the CFD software

It has been seen, the shear stress is proportional to the velocity gradient as shown in the next equation:

$$\tau = \mu \frac{\partial u}{\partial y}$$

<div align="right">2.67</div>

Fluent works with the deformation tensor $\bar{\bar{D}}$ and the shear stress is proportional to this as

$$\tau = \mu \bar{\bar{D}}$$

<div align="right">2.68</div>

Where $\bar{\bar{D}}$ is defined by

$$\bar{\bar{D}} = \left(\frac{\partial u_j}{\partial x_i} + \frac{\partial u_i}{\partial x_j} \right)$$

<div align="right">2.69</div>

For some non-Newtonian fluids, the shear stress can be similarly written as

$$\tau = \eta(\bar{\bar{D}})\bar{\bar{D}}$$

<div align="right">2.70</div>

In general, η is a function of all three invariants of the rate-of-deformation tensor $\bar{\bar{D}}$, however, in the models available in Fluent, the non-Newtonian viscosity is consider function of the shear rate only, which is related to the second invariant $\bar{\bar{D}}$ and defined as

$$\dot{\gamma} = \sqrt{\frac{1}{2} \bar{\bar{D}} : \bar{\bar{D}}}$$

<div align="right">2.71</div>

The non-Newtonian viscosity modeled in Fluent obeys the next equation:

$$\eta = K_c \, \dot{\gamma}^{n-1} H(t)$$

<div align="right">2.72</div>

Where *H(t)* is the temperature dependant component, which, for this work, will be neglected and used as 1, as the effects of the temperature in the viscosity will not be considered.

The values for the non-Newtonian viscosity must be defined to be as shown in the next figure:
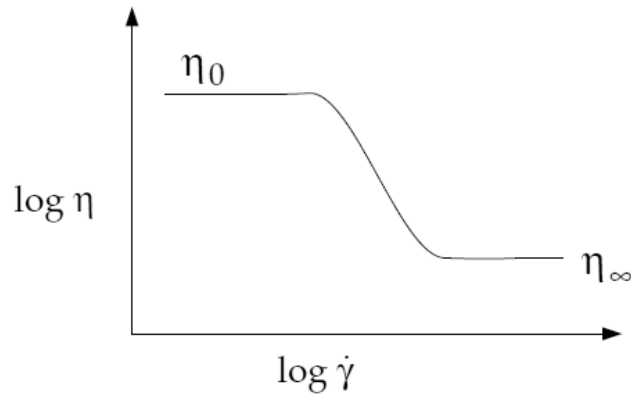
Figure 2-20, limits for the non-Newtonian viscosity under the power law model in fluent

(Reproduced under "fair use" from (24))

The selection of these rheological properties is very important for successful simulations. For this work, the values used were selected after various failed simulations were an incorrect setting of the limits could result in wrong values in the Nusselt numbers; as an example, for this work, when the inferior limit of the non-Newtonian viscosity was not set lower enough (e.g. 0.0001) the value during the simulation reached this point and the results showed the same value of Nu for every fluid with $n<0.5$. When the value was set extremely low (1×10^{-8}) the solution diverged.

2.8   Conclusions for the chapter

The theoretical background for fluid dynamics and heat transfer analysis is complex and the difficulty that involves to solve these equations analytically make it not practical to try to found an exact solution, and because of that, the use of CFD is a valuable tool to solve approximations to these problems. Although the governing equations such as the balance of energy and momentum or the Navier-Stokes equations are rarely directly used in solving complex non-Newtonian fluids problems, they are the heart of the CFD and the method takes care of finding an approximated solution to these equations. So, it is important to know those expressions to understand what the method is doing in each of the elements, and to know what to expect from the results of the analyses.

The importance of knowing concepts such as the boundary layers and what the Nusselt number is will be evident in next chapters when the use of numerical models for the CFD

requires the creation of a mesh, for example. The quality of the meshing is very important in the accuracy of the results, and if the governing principles of the heat transfer between the boundary and the fluid is not clear, it can lead to errors in the construction of such models.

It is important to recognize the differences between Newtonian and non-Newtonian fluids to understand why numerical methods are not only a valid option in finding an approximate solution for these problems, but a very convenient one. As the relation between the shear stress and the shear ratio is an extra non-linearity that the non-Newtonian fluids introduce in the equations, trying to solve it analytically could be very difficult, in case that it was possible to find a solution at all. Then CFD methods help in the task to understand these kinds of fluids.

Page intentionally
left blank

CHAPTER 3   Numerical method pre-verification

These first analyses, presented in this section, were developed as preliminaries numerical runs to verify beforehand how the many parameters and options modify the results of the computation. To get familiar with the numerical software, the Nusselt number for known basic geometries of a Newtonian fluid were calculated and compared with their corresponding theoretical values. The theoretical values used for comparison are shown in Figure 2-8 for H1 BC.

3.1   Verification of the numerical method

As only the value for a fully developed flow is of interest, because if Nu is calculated in the entry region, where the velocity profile and the dimensionless temperature are not constant, Nu will not be constant, but a function of the longitudinal position. It is of more interest the value of Nu when the fluid is fully developed because it will represent the heat transfer capacity of the system for length beyond the entry length. The theoretical values of Nu consider a fully developed fluid for simplicity in the calculations, although it is possible to obtain values in the entry length (these demonstrations are out of the scope of this work).   The length of the pipes must be long enough to allow this develop, and as the entry length for the thermal development is larger than the one for hydrodynamic, this last one is the value used for the models as a first approximation. The dimensionless entry length is given by (3)

$$\left(\frac{x_e}{D_h}\right)_{lam} \approx 0.05 \; Re \; Pr \qquad\qquad \textbf{3.1}$$

Where x_e is the length of the thermal entrance region.

A dimensionless distance for Newtonian flows is used for some results, and is given by (9)

$$z^+ = \frac{z}{D_h \; Re \; Pr} \qquad\qquad \textbf{3.2}$$

In this equation, z^+ is the dimensionless length.

CFD simulation of forced convection heat transfer of laminar phase-change non-Newtonian fluids in rectangular straight micro-channels

To define the constant heat flux applied in the walls as a boundary condition for the H1 BC, the next equation is used (3)

$$q'' = \dot{m}\, c_p\, \Delta t = \rho\, A_c\, V\, c_p\, \Delta t \qquad\qquad \textbf{3.3}$$

Where Δt is the differential in temperature at the inlet and the outlet, c_p is the specific heat of the fluid and A_c is the cross section area.

The mean velocity V of the flow at the inlet can be calculated with (3)

$$\mathrm{Re} = \frac{\rho\, V\, D_h}{\mu} \qquad\qquad \textbf{3.4}$$

The hydraulic diameter D_h is defined as

$$D_h = \frac{4A_c}{Per} \qquad\qquad \textbf{3.5}$$

Where Per is the perimeter of A_c.

The heat flux boundary condition must be applied per unit of area, so it is obtained by

$$q''_s = \frac{q''}{S_w} \qquad\qquad \textbf{3.6}$$

Where S_w is the area of the walls where the heat flux is being applied.

The fluid used is water at 300 [K] with an arbitrary constant Re = 200 to keep the flow laminar and $\Delta t = 40$[K]. Their properties are (26)

- Prandtl number: Pr = 5.51,
- Density: $\rho = 9.96\mathrm{e}{+}2$ [kg/m^3],
- Dynamic viscosity: $\mu = 8.33\mathrm{e}{-}4$ [kg/m s],
- Conductivity: $k = 0.615$ [W/m K],
- Specific heat: $c_p = 4.07\mathrm{e}{+}3$ [J/kg K].

The tubes modeled are one circular of 0.01 [m] of diameter and two rectangular of 0.01x0.01 [m] and 0.01x0.02 [m]. The length is determined by the development of the temperature

profile and it is 2 [m] for the circular tube and the rectangular with an aspect ratio of $\alpha = 1.0$, and 3[m] for the rectangular tube with $\alpha = 0.5$.

As these are only verification analyses, some minor steps of the process are omitted and only the final results are presented with their respective observations. Further details of the numerical models such as number of elements are omitted as it will be reported *in extenso* in the next chapter.

The simulations are steady state with first order solvers to save computing time; the fluid is laminar and the energy equation is considered. Constant viscosity model (Newtonian flow) was used for the simulations.

With the equations on section 2.3, it is possible to calculate the next boundary conditions:

- Constant heat flux at the wall (H1 BC): q''_s ,
- Velocity of the fluid at the inlet (normal to face): *V,*
- Temperature of the fluid at the inlet: 300 [K],
- Outflow condition at the outlet,
- Shell conduction was applied to the wall to simulate H1 condition (7).

3.2 Nu for internal flow in circular cross section, H1 condition

The model for this verification is shown in the next figure:
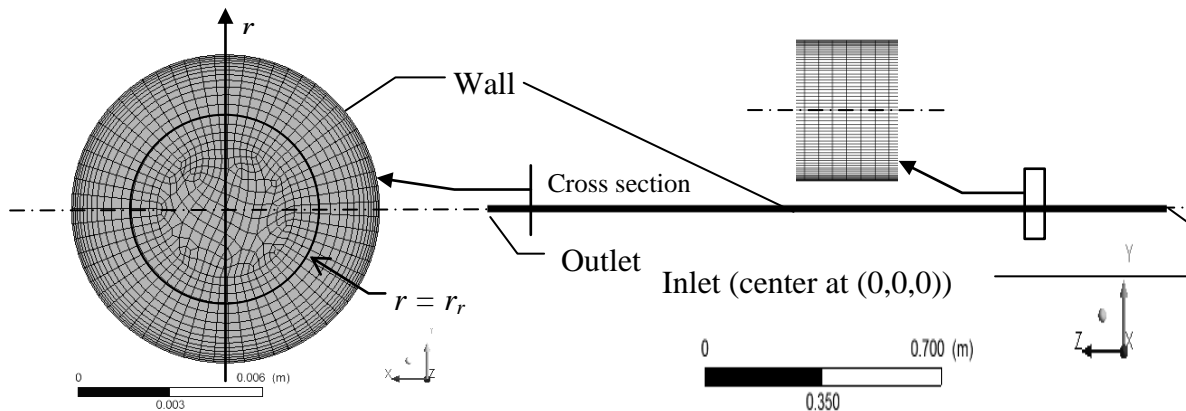
Figure 3-1, circular tube model for Nu calculation

(Right: cross-sectional area of the tube, left: length of the tube)

CFD simulation of forced convection heat transfer of laminar phase-change non-Newtonian fluids in rectangular straight micro-channels

The mesh is structured near the wall boundary and unstructured in the center. A structured mesh is characterized by regular connectivity that can be expressed as a two or three dimensional array. This restricts the element choices to quadrilaterals in 2D or hexahedra in 3D. An unstructured mesh is characterized by irregular connectivity that is not readily expressed as a two or three dimensional array in computer memory. This allows for any possible element that a solver might be able to use. Compared to structured meshes, the storage requirements for an unstructured mesh can be substantially larger since the neighborhood connectivity must be explicitly stored.

It is possible to see from Figure 3-1 that, near the wall boundary, the structured mesh starts with smaller elements in the radial direction, and start to grow as the elements get closer to the center. This is called inflation. It is important to use this inflation because, as it has been explained in the thermal layer definition, the critical gradients occur at a very short distance from the wall, thus, it is necessary to have smaller elements in this area in the radial direction r. The angular gradients (following the perimeter of the area) are not so important because they will be near to zero due the symmetry of the problem. The heat will flow from the wall to the center giving the same values of flow at every point of the respective layer to the fluid. This means that all the points in a circle with *radius* = r_r (see Figure 3-1) will have the same temperature, then, it is not necessary to have smaller elements in this direction. Near the center, the gradients are much smaller too (by the boundary layer definition), then, a free (unstructured) mesh is enough to capture the phenomena with a good certainty.

As stated at the beginning of this chapter, only the fully developed section of the fluid is of interest to compare the theoretical and the numerical values. In the next figure it is possible to observe that the velocity of the fluid w is invariant with z $\left(\frac{\partial w}{\partial z} = 0\right)$ after a short distance (the velocity entrance length) and this mean that the fluid is fully developed. It is used a dimensional length to allow a better visualization in how the fluid is developing along the tube.
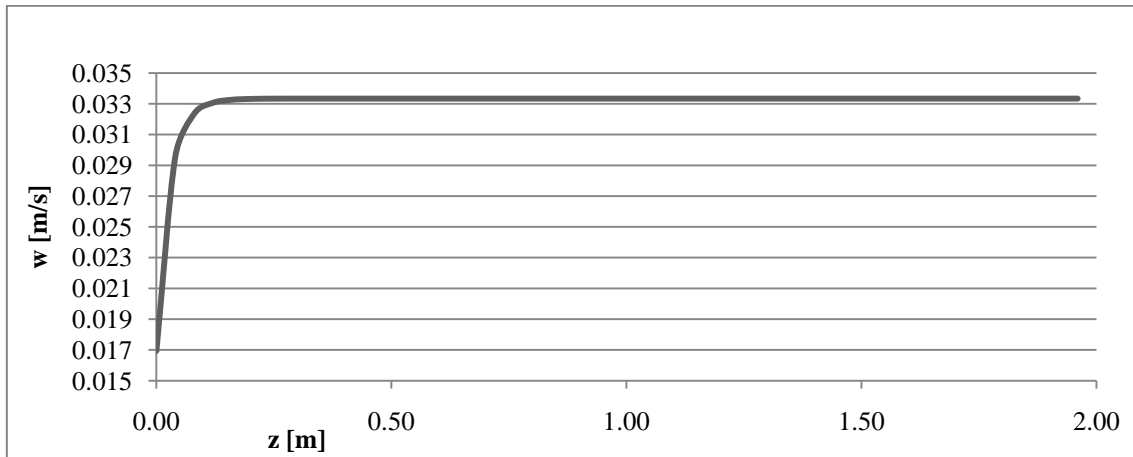
Figure 3-2, velocity profile (*w* at (0,0,z)) for a circular cross-sectional area tube

To go further in the fluid development verification, it has been seen from equation 2.7 that the fluid velocity profile is described by a parabolic equation when it is fully developed. The vectors in the next figure represent the magnitude of the velocity *w*. The larger vectors indicate the larger velocities magnitudes. It is possible to see that those vectors tend to zero when approaching the walls, as expected, because of the *no-slip* condition that generally prevail in the viscous fluids. The scale on the left in that Figure 3-3 shows the values of the magnitude according to each tone (large darker vectors correspond to the highest values).
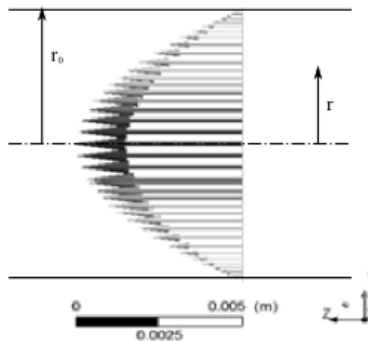
Figure 3-3, velocity vectors *w* at Z=1.96[m]

The theoretical value of the curve that describes the velocity *w* is defined by equations 2.7 and 2.10. For $r_0 = 0.005$, the pressure gradient is then

$$\frac{dP}{dz} = -\frac{8\,V\mu}{r_0^2} = -4.53[Pa/m]$$

CFD simulation of forced convection heat transfer of laminar phase-change non-Newtonian fluids in rectangular straight micro-channels

With equation 2.7, $u(r) = -\frac{1}{4\mu}\left(\frac{dP}{dx}\right)r_0^2\left[1 - \frac{r^2}{r_0^2}\right]$ for $r = $ -0.005 to 0.005 [m], the plot for velocity w is obtained as it follows:
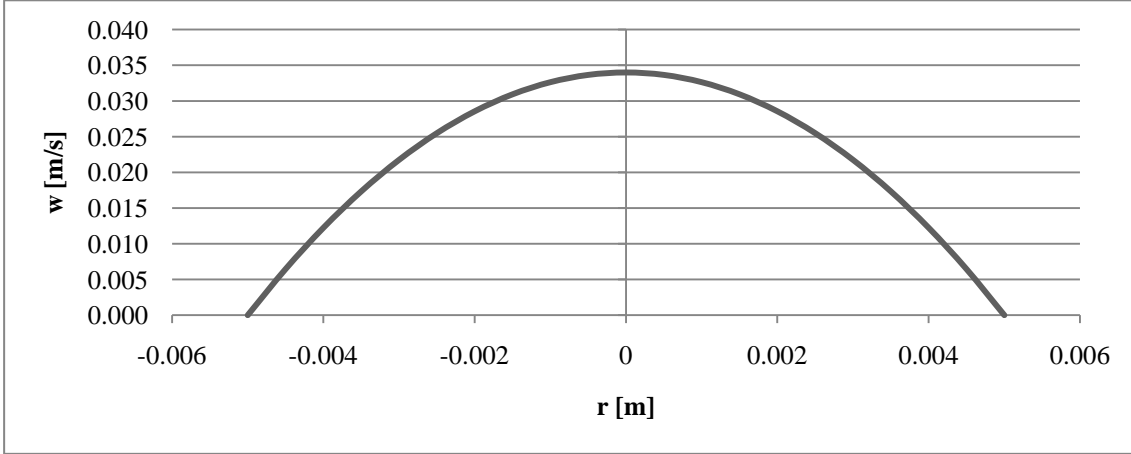
Figure 3-4, parabolic velocity w profile for fully developed flow

These values are in good agreement with the numerical results presented in Figure 3-3.

For the fully developed thermal conditions, it is possible to observe from the next figure, that the dimensionless temperature gets a nearly constant value for the length of the tube $\left(\frac{\partial}{\partial z}\left(\frac{t_w - t}{t_w - t_m}\right) = 0\right)$, showing that the fluid is thermally developed.
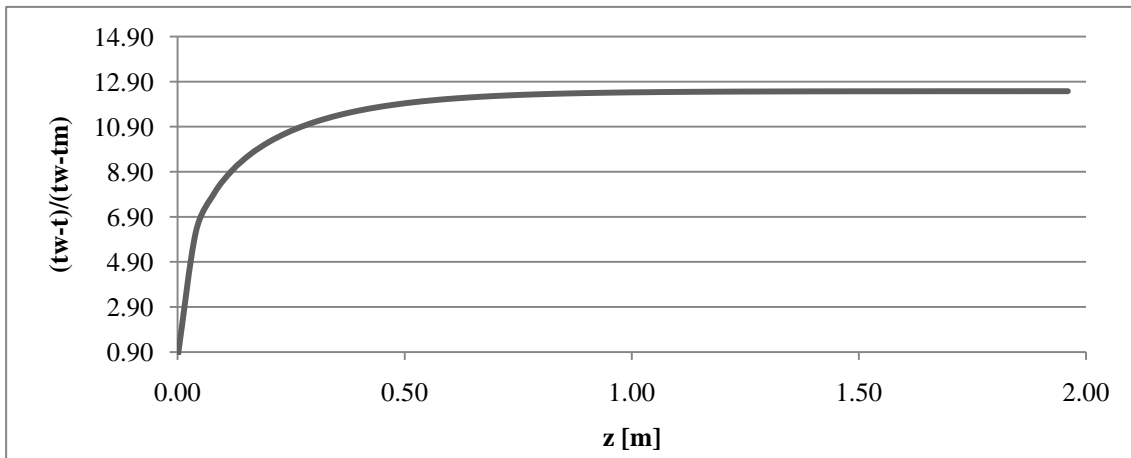
Figure 3-5, thermal profile with $t_d = $ constant for circular tube

After verifying the fluid is fully developed in terms of velocity and temperature, it is possible to calculate the Nusselt number. To do that with a constant heat flux in the wall (H1), it is necessary to get the convective heat transfer coefficient h from (11)

$$q''_{\text{s}} = h \left(t_{\text{w}} - t_m \right)$$

<div align="right">3.7</div>

The bulk and the wall temperature (t_m and t_w) are obtained directly from the CFD software and q'' is a boundary condition. Nu is calculated with

$$Nu = \frac{hD_h}{k}$$

<div align="right">3.8</div>

The next plot depicts the obtained values for Nu. The dimensionless length is used to generalize the results presented.
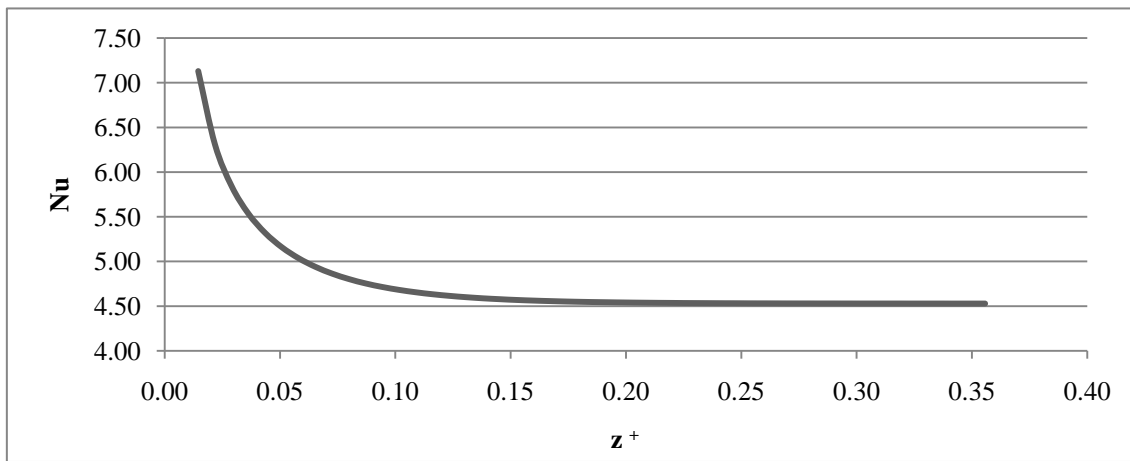
Figure 3-6, Nu for circular cross area section

The theoretical value of Nu for circular tubes has been extensively reported and can be found as Nu=4.36 (11). The value obtained from the simulation is 4.53, which represents a very good match with an error of just 3.9%.This is an acceptable agreement for this kind of simulations, being a common practice to work with errors up to 5%.

3.3 Nu for internal flow in a rectangular cross section, H1 condition

3.3.1 Rectangular 1.0 aspect ratio

The model for this simulation is located as it was done for the circular case, and the defined boundaries for modeling are also the same. This is the inlet, outflow and wall, were defined using the same considerations as those applied for the circular tube:

CFD simulation of forced convection heat transfer of laminar phase-change non-Newtonian fluids in rectangular straight micro-channels
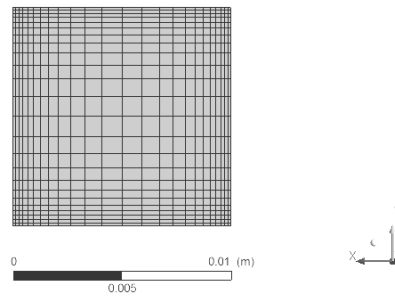
Figure 3-7, 1:1 rectangular tube model

The results are shown in the next figures. The parabolic velocity profile is not necessary to calculate the Nusselt number as all it is needed is a fully developed flow, so this verification is omitted.
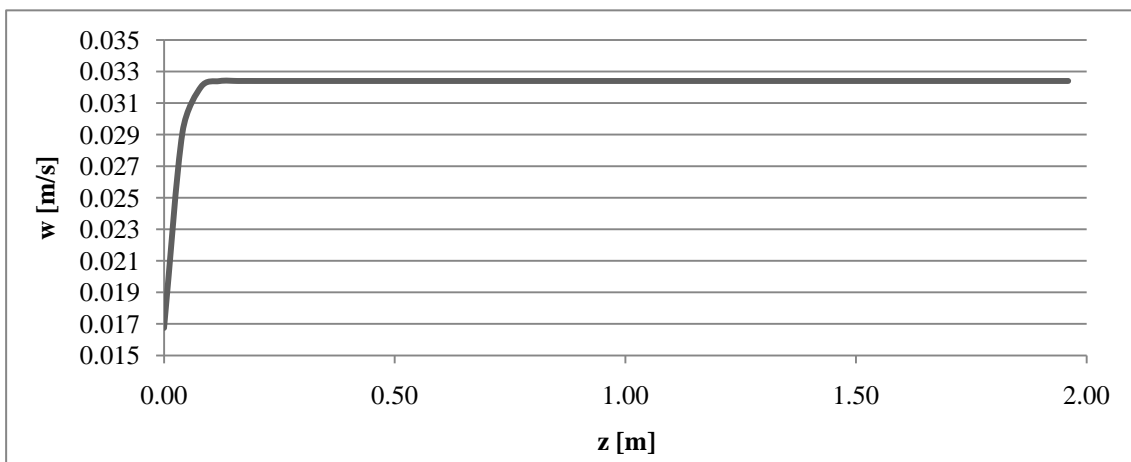
Figure 3-8, velocity profile (*w* at (0,0,Z)) for 1:1 rectangular tube.

Figure 3-8 shows that the velocity of the fluid w is invariant with z $\left(\frac{\partial w}{\partial z} = 0\right)$ beyond the velocity entrance length, meaning that the fluid is dynamically fully developed.
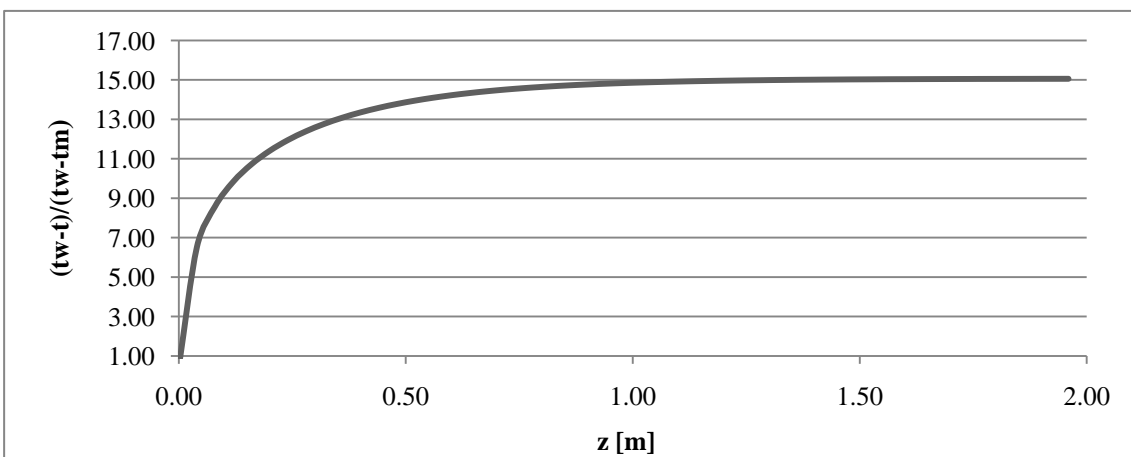
Figure 3-9, thermal profile with t_d = constant for 1:1 rectangular tube

From Figure 3-9, it is possible to observe that the dimensionless temperature gets a nearly constant value for the length of the tube $\left(\frac{\partial}{\partial z}\left(\frac{t_w-t}{t_w-t_m}\right)=0\right)$, showing that the fluid is thermally developed.
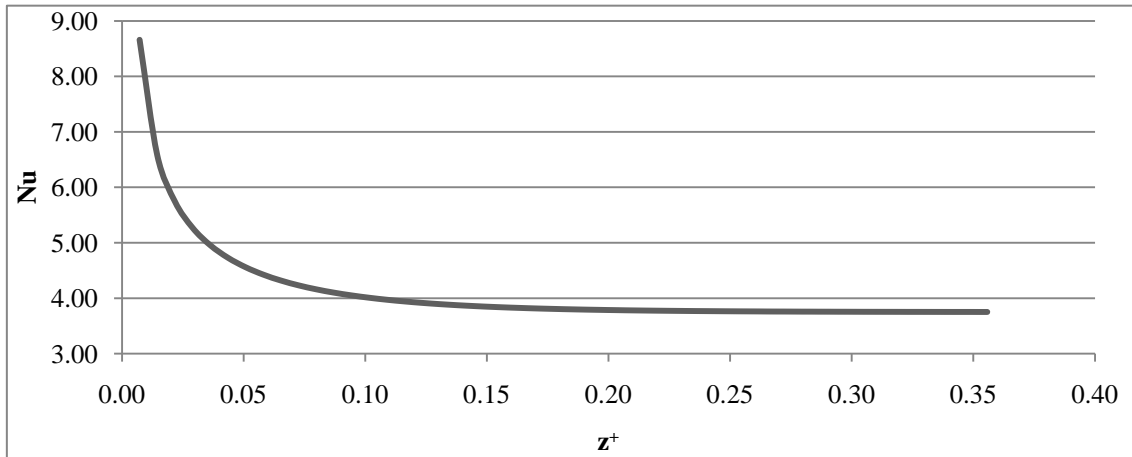
Figure 3-10, Nu for rectangular cross area section with α=1.0

For this case, the theoretical value of Nu is 3.61 (11) and the calculated value from the simulation is obtained as Nu=3.75, as it can be verified form Figure 3-10, these values represent an error of 3.9%. This result can be also deemed as acceptable.

Since square tube is more complex than the circular one, it is necessary to test the independence of the results from the tube length. To do this, the results of a second analysis with a 3 [m], α=1.0 square tube are presented. The model and considerations are exactly the same as for the 2[m] tube, just adapting the heat flux and wall surface area to the new dimensions. Next plot shows the value of Nu for the longer tube.

CFD simulation of forced convection heat transfer of laminar phase-change non-Newtonian fluids in rectangular straight micro-channels
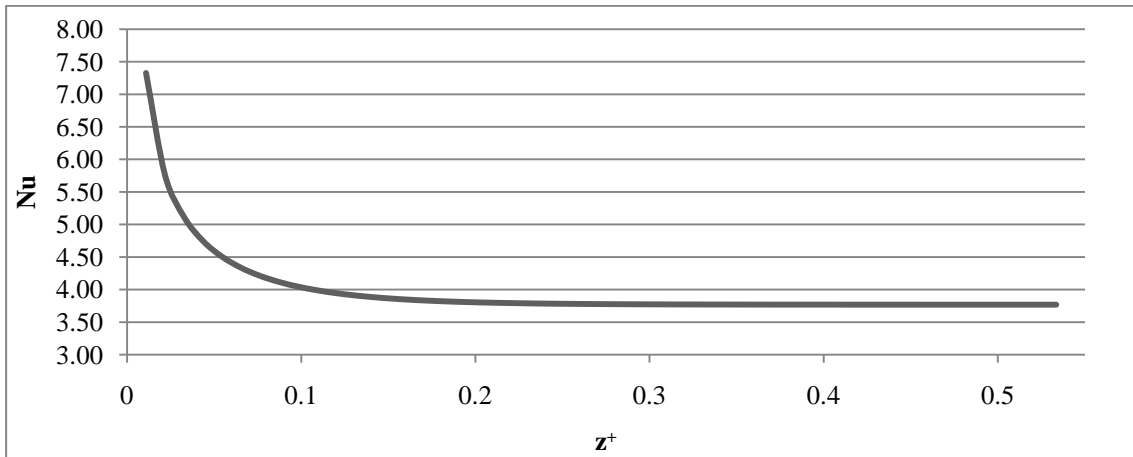
Figure 3-11, Nu for rectangular cross area section in a 3[m] tube with $\alpha=1.0$

As it can be observed in Figure 3-11, the value of Nu for this analysis is Nu=3.77 that represent an error of 4.4% and showing that the Nusselt number remains constant for larger tubes as expected. If needed, the error could be further minimized by using second order solvers although this could increase the calculation time.

3.3.2   Rectangular 0.5 aspect ratio

Following, the same procedure as for the 1:1 rectangular tube is now applied for a rectangular cross-sectional area with $\alpha=0.5$. In this case, the length of the tube was also changed to 3 [m] to allow a better thermal development of the fluid because 2 [m] seems not to be enough when applied to the new geometry. The variation of Nu for the 2[m] and 3[m] tubes can be recognized from Figure 3-16.

The used mesh is shown in the next figure.
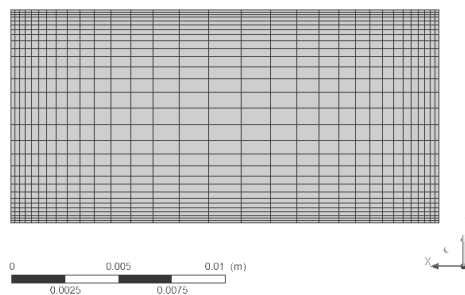
Figure 3-12, 1:2 rectangular tube model

Next figure shows that the velocity of the fluid w is invariant with z $\left(\frac{\partial w}{\partial z} = 0\right)$ beyond the velocity entrance length, meaning that the fluid is fully developed.
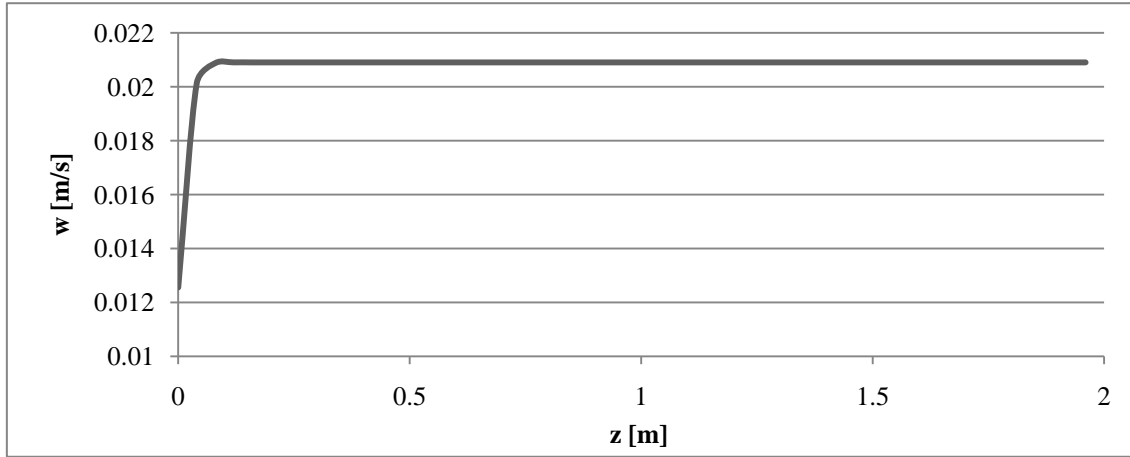
Figure 3-13, velocity profile (w at (0,0,Z)) for 1:2 rectangular tube.

For the thermal development, the temperature profile apparently develops different. This can be appreciated in the next plot, where the dimensionless temperature raises and then it gets lower before getting a stable value.
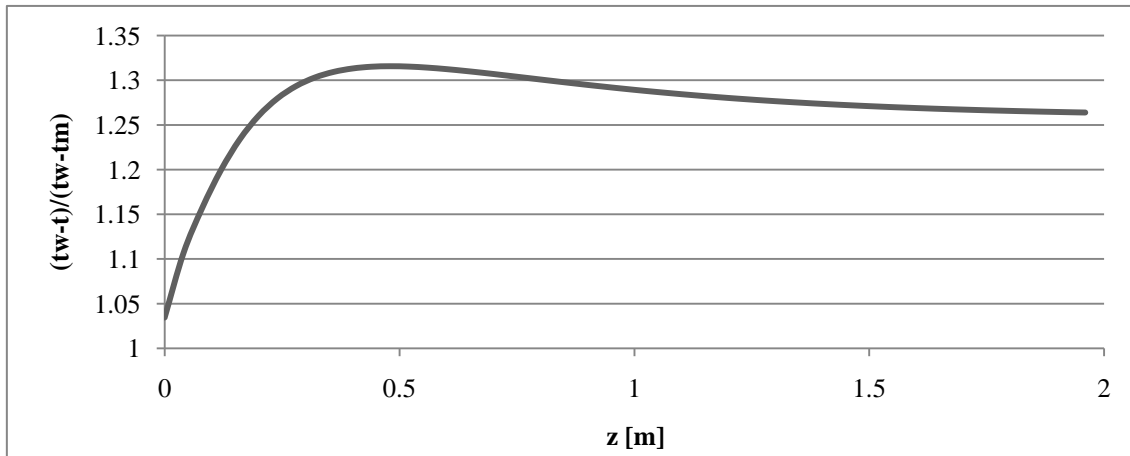
Figure 3-14, thermal profile with t_d = constant for a rectangular tube with α=0.5

The cause of the humpy variation of the curve before its horizontal trend was found to be due a very high value of the conductivity of the material of the wall of the tube, affecting the H1 BC in the entry region. For the fully developed region, the value behaves as expected.

H1 BC should not consider an axial conduction, thus, the results in the entry region for this simulation are not accurate, but as this verification does not require a high degree of exactness

CFD simulation of forced convection heat transfer of laminar phase-change non-Newtonian fluids in rectangular straight micro-channels

in the plots, and as the Nusselt number for the developed region is in agreement with the literature, no further analysis was done for this case. It was found that this behavior could be corrected by neglecting the axial heat conduction in the walls and allowing only the peripheral conduction. The values were corrected for the next chapter and the results are presented as this to demonstrate the effect of this parameter.

The results for the Nusselt number are shown in the next figure.
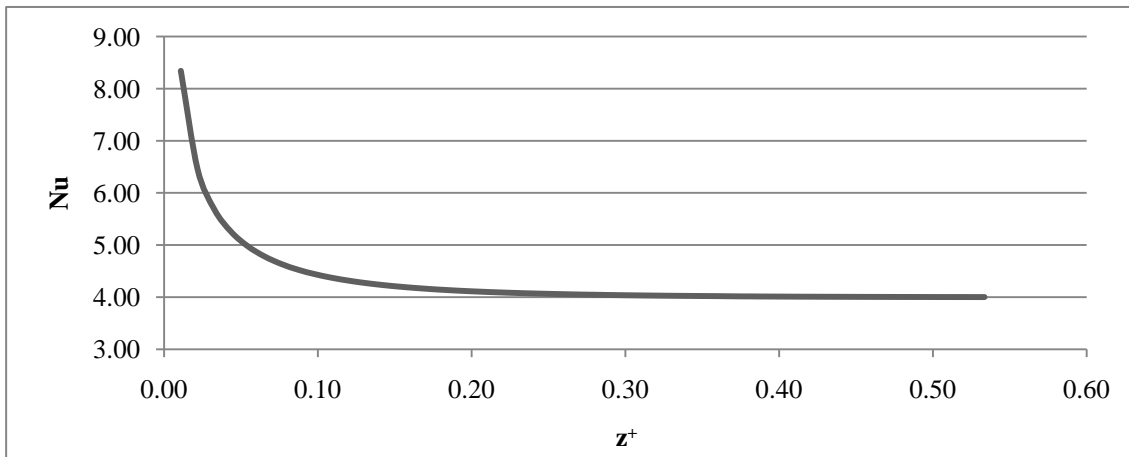
Figure 3-15, Nu for rectangular cross section area in a 3[m] tube with α=0.5

The simulation produces a Nu = 4.00. Comparing it with a theoretical value of 4.12, the error is 2.9% that can be deemed as acceptable. The entry region could not be reliable when compared with other works, due the error presented in Figure 3-14.

The next figure shows the results with a not fully developed flow (2 [m]) and the fully developed (3 [m]). It is clear from this that the 3[m] tubes have got a near constant value of Nu, while the 2[m] tube shows still a lot of variation in this value through the tube´s length. With 2[m] of length for the 0.5 aspect ratio tube, the maximum variation of Nu in the last 0.5 [m] is approximately 0.025, while in the rest of the simulations, this difference is roughly 0.01 or less. The 2[m] value seems to have a tendency to decrease even more. This is the reason why the length of the tube was purposely changed.
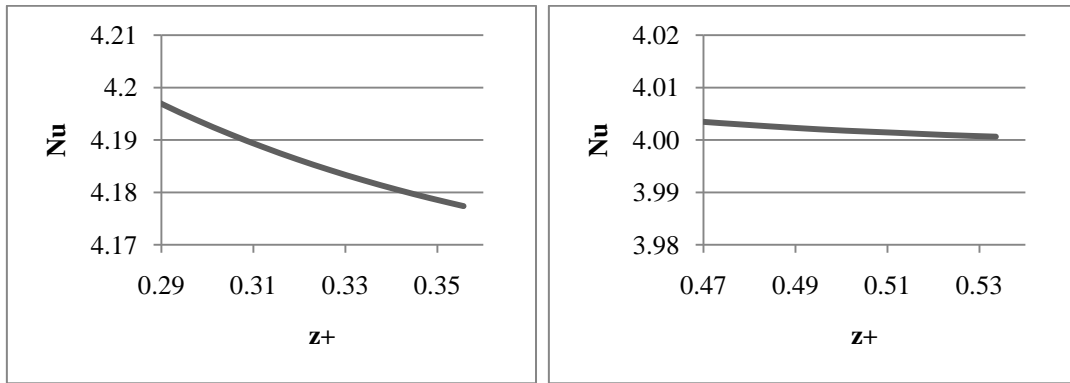
Figure 3-16, Nu values at the end of the rectangular tube, $\alpha=0.5$

2[m] (left) and 3[m] (right)

3.4 Conclusions for the chapter

Results from the verification analyses presented in this chapter showed that the simulations are highly sensitive to the quality of the mesh in the pipes cross section areas. It is necessary to use certain degree of inflation in the boundaries to get accurate results. It is important then to check result mesh independency by refining the mesh and verifying the variation in the results. When the variation is negligible within the levels required, then the mesh can be considered reliable.

As the theoretical value of the Nusselt number used to compare with the CFD outcomes were obtained under the H1 (constant heat flux and constant peripheral temperature) condition, it is required a constant temperature around the perimeter of the cross section area. For the rectangular cross section areas (and other non circular cross sections), it is important to consider the heat conduction across the walls (7) due the fact that the distance from the origin of the symmetry axes of these rectangular cross-sectional areas to their wall boundaries is not constant anymore as it is for the circular cross section areas (the distance from the center of the cross-sectional area to the wall is always the radio). If the conduction across the wall were not considered, the temperature will vary from the center of the wall to the corners. If the shell conduction is not considered, the result is Nu = 3.11 that is under the expected theoretical value for H1. However, wrong definition of the conductivity coefficient of the wall, *k,* could lead to large errors (see Figure 3-15), thus, it is important to limit the conduction of the wall to the perimeter only, neglecting the axial conduction.

CFD simulation of forced convection heat transfer of laminar phase-change non-Newtonian fluids in rectangular straight micro-channels
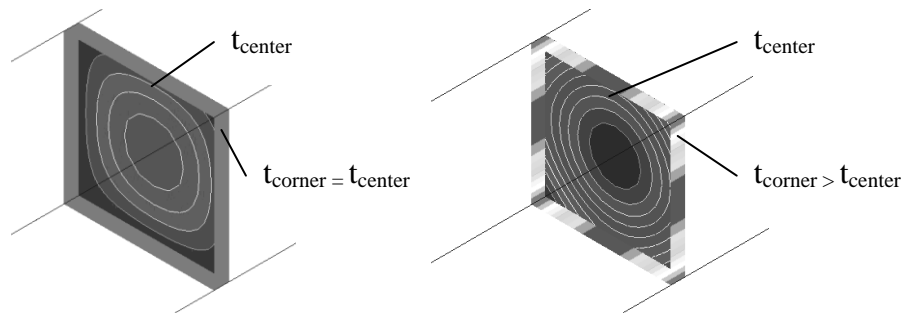
Figure 3-17, H1 BC, with shell conduction (left) and H2, without shell cond. (right)

Same hues represent same temperature. For the H2 (constant heat flux with variable temperature at the peripheral) case, the temperature goes from a lower value at the center of the face to higher in the corners. This situation makes complete sense considering that $t_w > t_\infty$, as it was initially stated. Therefore, the farther wall surfaces to the cross-section origin (the corners), would interchange less heat with the fluid compared to the heat interchanged with the centers of the wall, so the formers tending to remain hotter.

All these points must be taken into account for the development of the next chapter, to get a reliable simulation of the non-Newtonian power law fluids.

CHAPTER 4　　Power law fluids simulation methodology

After the pre-verification realized in last chapter, the simulation of power law fluids will be done in the present one. The chapter starts by describing the used models and its validation methods, as well as the fluid properties and boundary conditions applied.

The steps as followed in order to get the final results are presented in the next list.

Verification:

1. Newtonian fluids models (Power law with $n=1$,).
2. Non-Newtonian fluids models (Power law with $n=0.3, 0.5$).
3. PCM + power law fluid slurry models ($n=1.0$ rectangular cross sectional areas).

Contribution:

1. PCM + power law fluid slurry models ($n=0.5, 0.3$, rectangular cross sectional areas).

It is important to notice that , although at first glance the point 1of the verification section is repeating the analyses presented in CHAPTER 3, in this case, the power law model of viscosity with $n = 1$ and K_c is used, in contrast to the model with constant viscosity μ used in the last chapter (see section 2.4).

On the same way, the point 3 of the verification is similar to the work presented by Kondle (9); however, there is a very important difference: Kondle used a constant viscosity for their models, while in this work the fluids obey the power-law model, with a variable viscosity.

The results of the verification section will also be used as a reference fluid when evaluating the thermal performance of the PCM and non-Newtonian slurry.

Also, if the results are in good agreement with the values obtained for the models with constant viscosity, then it is possible to conclude that the power-law model is reliable and accurate.

CFD simulation of forced convection heat transfer of laminar phase-change non-Newtonian fluids in rectangular straight micro-channels

For point 2 and 3, only the rectangular ducts were analyzed, as the circular were intended only as a control for Newtonian flows.

4.1 Geometry and mesh

The models used in this works include one circular for Newtonian flows and three rectangular cross-sectional areas for the rest of the analyses. The aspect ratios for the rectangular areas were 1:1, 1:2 and 1:5 (α = 1.0, 0.5 and 0.2 respectively). The height and diameter of those sections were set fixed to a constant value of 150[μm] and the width was varied to get the desired aspect ratio. The wall thickness was set to an arbitrary value (1 [μm]) with a highly conductive material for the H1 condition.
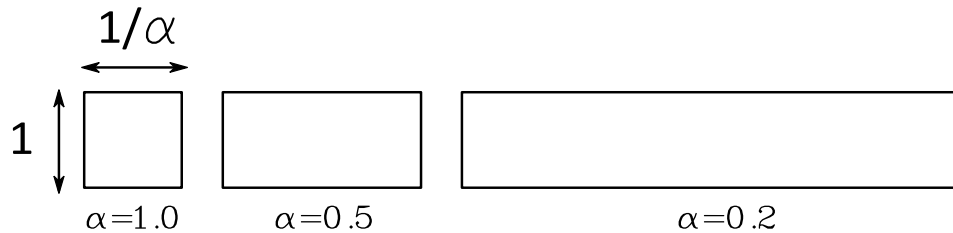
Figure 4-1, aspect ratios for rectangular tubes

According to the conclusions of the last section, the density of the mesh is larger near the walls, and the elements increase the size toward the innermost part of the section, to account for the large temperature gradients generated in the direction of the heat flow. In the entrance region, the mesh is also made finer, looking to have a better resolution of the entry length effects. The domain was meshed with hexahedral elements. Typical grids are shown for circular and rectangular tubes in the next figure.
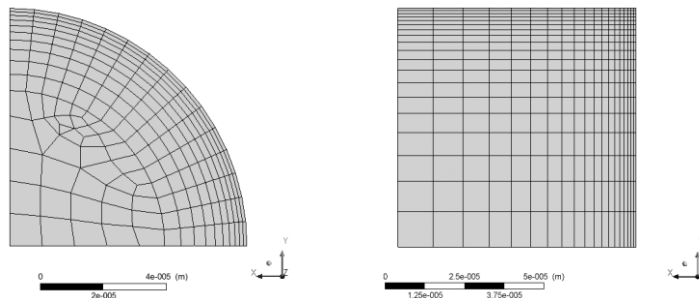
Figure 4-2, typical discretized domain for circular (left) and rectangular (right) tubes

As in the last chapter, only the value for a fully developed flow is of interest. The length of the pipes is assumed to be long enough to allow this develops.

64

A dimensionless distance is defined for the results in order to make them independent of the units. The distance is given by (5)

$$z^+ = \frac{z}{\text{Pe } D_h}$$

<div align="right">4.1</div>

In this equation, z^+ is the dimensionless length and Pe is the Peclet defined as

$$\text{Pe} = \frac{\rho \, c_p \, D_h \, V}{k} = Re \, Pr$$

<div align="right">4.2</div>

The dimensionless values for x^+ and y^+ in the cross sectional area, are calculated with

$$x^+ = \frac{x}{x_{max}}, y^+ = \frac{y}{x_{max}}$$

<div align="right">4.3</div>

The last equations assume that $x \geq y$.

For other dimensionless quantities used in this work the general equation to calculate them is

$$Dimensionless \; value = \frac{Variable}{Maximum \; value \; of \; the \; variable}$$

<div align="right">4.4</div>

4.2   Mesh independency

To test mesh independency in the models, three different grid resolutions were used. The comparison of the three models for each cross section is presented in the results section.

4.2.1   Grid resolution for circular tube

The next figure shows the grid resolutions for the circular tube case:
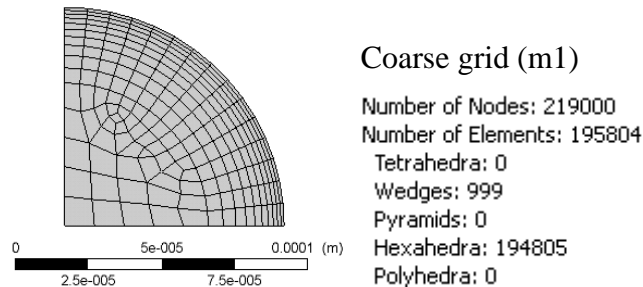
Coarse grid (m1)

Number of Nodes: 219000
Number of Elements: 195804
 Tetrahedra: 0
 Wedges: 999
 Pyramids: 0
 Hexahedra: 194805
 Polyhedra: 0

CFD simulation of forced convection heat transfer of laminar phase-change non-Newtonian fluids in rectangular straight micro-channels

Medium grid (m2)

Number of Nodes: 316316
Number of Elements: 288000
 Tetrahedra: 0
 Wedges: 0
 Pyramids: 0
 Hexahedra: 288000
 Polyhedra: 0

Fine grid (m3)

Number of Nodes: 632316
Number of Elements: 576000
 Tetrahedra: 0
 Wedges: 0
 Pyramids: 0
 Hexahedra: 576000
 Polyhedra: 0
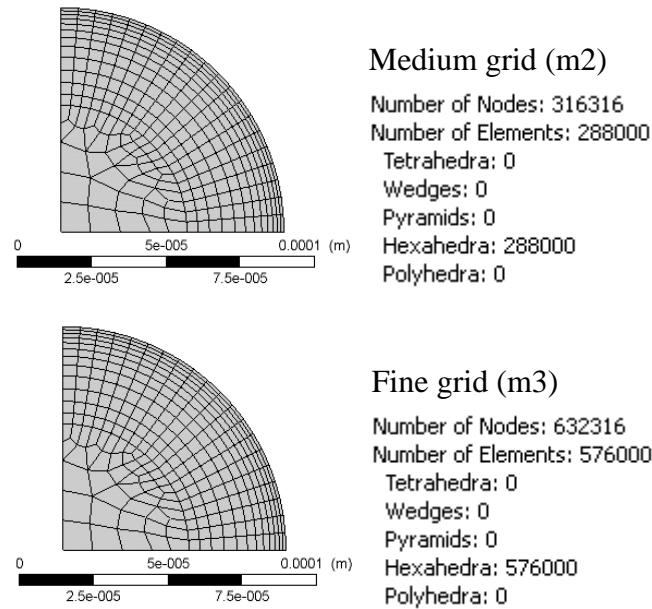
Figure 4-3, grid resolutions for circular tube (cross section area)

In the three cases, a size control was set in the outer wall to keep a regular number of divisions in the angular direction (see details in Table 4-1 in section 4.2.3). The minimum and maximum element size is of $5x10^{-6}$ and $1x10^{-5}$ respectively.

In z direction, the elements grow up gradually in the direction of the tube, as shown in the next figure:
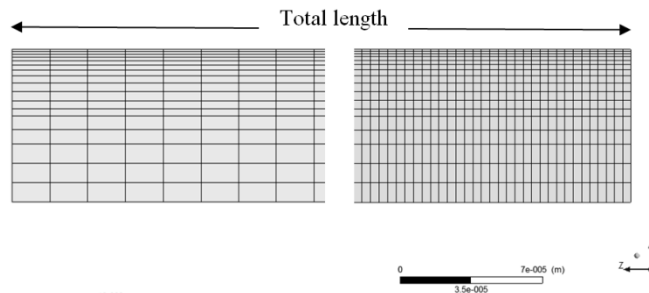
Figure 4-4, sketch of the discretized domain bias in z direction (not at scale)

In the case of m1 and m2 grid resolutions, the maximum element size (at the end of the tube) is $2x10^{-4}$ with a *sweep bias* (increment rate) of 50. For m3 grid resolution the maximum element size is $1x10^{-4}$ with a sweep bias of 50.

4.2.2 Grid resolution for rectangular tubes

The three different grid resolutions for the 1:1 rectangular tube are shown in the next figure:

Coarse grid (m1)

Number of Nodes: 256256
Number of Elements: 225000
Tetrahedra: 0
Wedges: 0
Pyramids: 0
Hexahedra: 225000
Polyhedra: 0

Medium grid (m2)

Number of Nodes: 400400
Number of Elements: 361000
Tetrahedra: 0
Wedges: 0
Pyramids: 0
Hexahedra: 361000
Polyhedra: 0

Fine grid (m3)

Number of Nodes: 800400
Number of Elements: 722000
Tetrahedra: 0
Wedges: 0
Pyramids: 0
Hexahedra: 722000
Polyhedra: 0
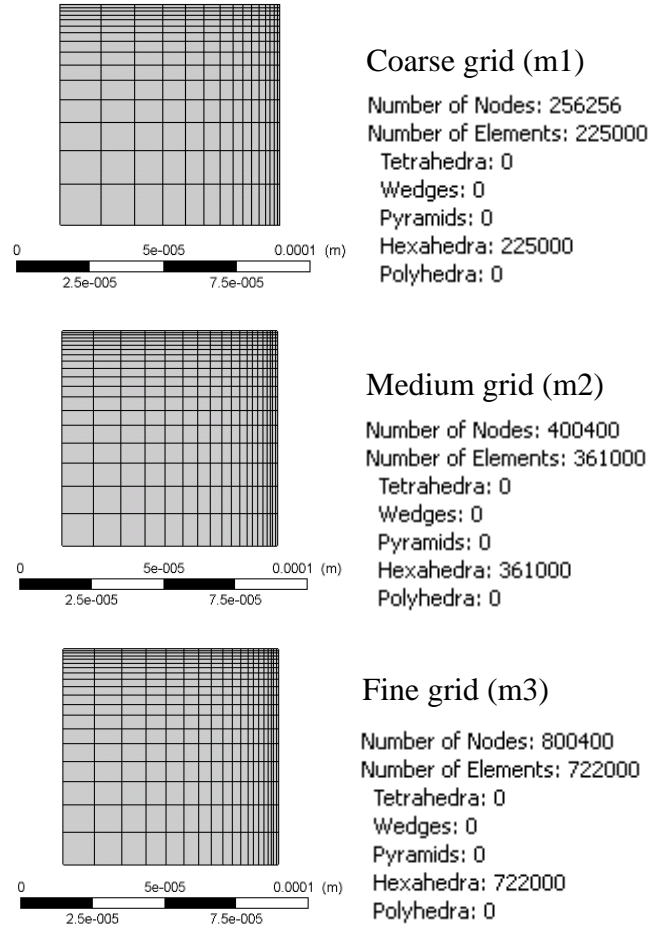
Figure 4-5, grid resolutions for rectangular tube

A size control was used to set the number of elements in the cross section area as shown in Table 4-1. For the grid in the z direction, the parameters used are the same as for the circular tube (see Figure 4-4).

4.2.3 Generalities

The resolutions are resumed in the next table.

CFD simulation of forced convection heat transfer of laminar phase-change non-Newtonian fluids in rectangular straight micro-channels

Table 4-1, grid resolutions for all cases

(Number of elements in cross section area, maximum element size in z direction)

α	m1	m2	m3
Circular	15x10, 2x10^{-4}	20x12, 2x10^{-4}	20x12, 1x10^{-4}
1.0	15x15, 2x10^{-4}	20x20, 2x10^{-4}	20x20, 1x10^{-4}
0.5	10x20, 2x10^{-4}	15x30, 2x10^{-4}	15x30, 1x10^{-4}
0.2	10x30, 2x10^{-4}	15x45, 2x10^{-4}	15x45, 1.5x10^{-4}

The distribution of the grid is very similar for the three rectangular cases (similar to grid shown in Figure 4-5).

For the circular tube, the first number represents the number of divisions in the wall boundary and the second the number of layers in depth to the center. As the rest of the surface is a free mesh, there is not an easy way to represent the density of the grid.

The number of elements was chosen in order to allow the meshing process to work with enough memory. Large number of elements could lead to a *"run out of memory"* kind of error. For example, for the fine grid of the rectangular cross sectional area with α=0.2, a grid of 15x45, 1x10^{-4} produces this error by the software on the workstation used for this work, thus, the resolution has to be kept to a reasonable size.

4.3 Governing equations

As Fluent was used to perform the simulations, the governing equations used by the software are the ones described next:

- Mass conservation equation

$$\nabla \cdot (\rho \vec{u}) = 0 \qquad\qquad \textbf{4.5}$$

- Momentum conservation equations

$$\nabla \cdot (\rho \vec{u}\vec{u}) = -\nabla P + \nabla \cdot (\bar{\bar{\tau}}) \qquad\qquad \textbf{4.6}$$

- Energy conservation equation

$$\nabla \cdot (\vec{\boldsymbol{u}}(\rho E + P)) = \nabla k \cdot \nabla t + \nabla(\bar{\bar{\boldsymbol{\tau}}} \cdot \vec{\boldsymbol{u}}) \qquad \text{4.7}$$

The Nusselt number is calculated with

$$Nu = \frac{hD_h}{k} \qquad \text{4.8}$$

For the last equation, the value of the convective coefficient is given by

$$h = \frac{q''/S_w}{(t_w - t_m)} \qquad \text{4.9}$$

To compare the performance of the different cases, the thermal performance factor (η_p) is used.

$$\eta_p = \frac{Nu/Nu_{reference}}{\left(f\,Re_{NN}/f\,Re_{NN\,reference}\right)^{1/3}} \qquad \text{4.10}$$

Where f is the Fanning friction factor, defined as:

$$f = \frac{D_h\,\Delta P}{2\,L\,\rho\,V^2} \qquad \text{4.11}$$

The reference Nusselt number and friction factor are the values for the fully developed single phase flow of every case.

4.4 Boundary conditions

Only one quarter of the fluid domain was modeled to save computational resources and time. A symmetry boundary condition was used for the models. The two internal sides of the modeled geometry were defined as a symmetry boundary condition having no heat flux or flow normal to the symmetry plane. The external sides were specified as no-slip walls (velocity =0) with no other boundary conditions considered, except for H1 and CWT.

CFD simulation of forced convection heat transfer of laminar phase-change non-Newtonian fluids in rectangular straight micro-channels
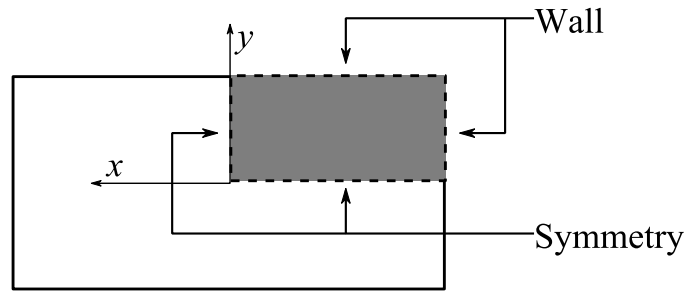
Figure 4-6, boundary conditions for the quarter cross section model

The boundary conditions are applied to the whole tube, meaning that it is a combined entry length, where the velocity profile and the thermal entry develop simultaneously. This condition raises the value of the Nusselt number in the entry region (3). As this work is interested in the values of Nu for the fully developed region, the effects in the entry length are proposed for future investigation.

The applied boundary conditions are depicted in the next figure. The explanation follows in the next sections.
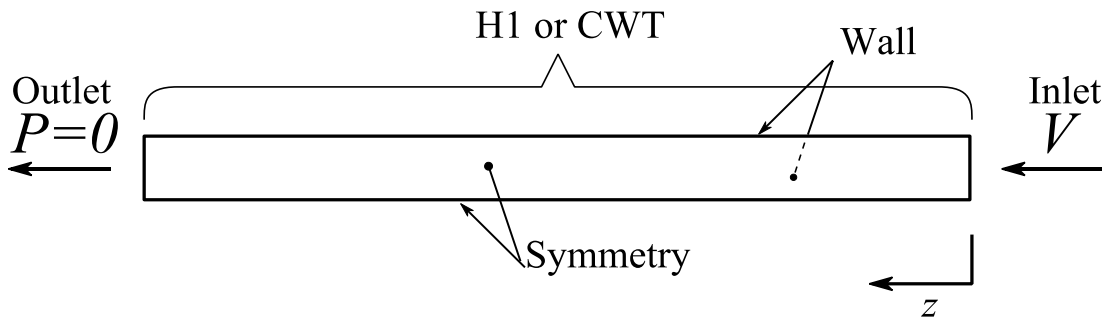
Figure 4-7, boundary conditions

4.4.1   H1 boundary conditions

The inlet fluid was defined with a velocity and an initial temperature. The outlet was an outflow with $P = 0$. A constant heat flux was applied to the wall, considering the shell conduction in the peripheral direction, but neglecting the axial conduction. The thickness of the wall was set to a very small arbitrary value and a high conductivity was used in the material of the wall (7). To achieve this boundary conduction, an orthotropic k was used, with a very high value for peripheral direction and setting a very low value for the axial conduction (24).

A mean velocity was calculated to keep a constant Re between the cases. The velocity V of the flow at the inlet can be calculated with (equation 2.24):

$$Re_{NN} = \frac{\rho D_h^n V^{2-n}}{K_c} \qquad \text{4.12}$$

The hydraulic diameter D_h has been defined as

$$D_h = \frac{4A_c}{Per} \qquad \text{4.13}$$

To define the constant heat flux applied in the walls as a boundary condition for the H1 BC, equation 3.3 is used:

$$q'' = \dot{m}\, c_p\, \Delta t = \rho\, A_c\, V\, c_p\, (t_o - t_i) \qquad \text{4.14}$$

Where t_o is the temperature of the fluid at the outlet, t_i is the temperature of the fluid at the inlet, cp is the specific heat of the fluid and A_c is the cross section area.

For the PCM simulations, to control the point at where the phase change starts, the next equation was used:

$$q'' = \dot{m}c_p(t_m - t_i) \qquad \text{4.15}$$

The heat flux boundary condition must be applied per unit of area and it is obtained by

$$q''_s = \frac{q''}{S_w} \qquad \text{4.16}$$

For single phase material, the surface area S_w is the area of the whole tube, while for PCM, is the area until the point where the bulk temperature reach the melting temperature $(Per \cdot z)$. This heat flux was used unless otherwise stated in the forthcoming sections.

4.4.2   CWT boundary condition

For the CWT BC a constant temperature was applied to the wall zone. The speed and temperature in the inlet and pressure in the outflow remains as in the H1 case. The wall thickness is neglected as well as the shell conduction.

CFD simulation of forced convection heat transfer of laminar phase-change non-Newtonian fluids in rectangular straight micro-channels

The velocity for PCM models could be changed from the single phase models depending on the output temperature. If the fluid does not reach the melting point, then the velocity could be lowered to reach that point.

4.5 Fluid properties

The selected fluid used for the simulations as single phase material, and as a carrier for PCM is water at 280 [K], with non-Newtonian power law characteristics:

- Density: $\rho = 998.2$ [kg/m^3],
- Conductivity: $k = 0.6$ [W/m K],
- Specific heat: $c_p = 4182$ [J/kg K],
- Consistency index $K_c = 0.01$ [Kg s^n / m s^2],

As the limits for the non-Newtonian viscosity are unknown, the consistency index was selected to be larger than the dynamic viscosity and a wide range was selected for this property and was defined as $1\text{x}10^{-7} < \eta < 10$. The selection was done after the considerations explained in section 2.7.5.

For the PCM, the selected fluid is N-Eicosane, a commonly used material for PCM heat transfer due its low phase change temperatures:

- Density: $\rho = 946.4$ [kg/m^3],
- Conductivity: $k = 0.15$ [W/m K],
- Specific heat: $c_p = 1973$ [J/kg K],
- Mass average dynamic viscosity: solid particles

For the bulk fluid (PCM + carrier) the properties are (after section 2.5):

- Density: $\rho = 990.43$ [kg/m^3],
- Conductivity: $k = 0.514$ [W/m K],
- Consistency index $K_c = 0.01$ [Kg s^n / m s^2],

4.6 Assumptions and simulation parameters

The fluid was kept under laminar regime with a constant Re = 50. To calculate the inlet velocity the equation 4.12 was used and the heat flux was calculated from equation 4.14 which derive in the initial simulation parameters presented in the next tables. The temperature for the CWT BC was set to 320 [K]. The values derived from the equations are not definitive and may need some tuning to get adequate flow conditions.

Table 4-2, initial values for simulations (*n=1.0)*

α	L [m]	Per [m]	A_c [m^2]	D_h [m]	V [m/s]	q'' [W] H1	q''/S_w [W/m^2] H1	t_w [K] CT	Pe
1.0	0.20	0.0006	2.25E-08	0.00015	3.3393	12.546	104550.00	320	3485
0.5	0.20	0.0009	4.5E-08	0.0002	2.5045	18.819	104550.00	320	3485
0.2	0.20	0.0018	1.125E-07	0.00025	2.0036	37.638	104550.00	320	3485
Circ	0.20	0.00047	1.767E-08	0.00015	3.3393	9.853605	104550.00	320	3485

Table 4-3, initial values for simulations (*n=0.5*)

α	V [m/s]	q'' [W] H1	q''/S_w [W/m^2] H1	t_w [K] CT	Pe
1.0	0.1187	0.44598	3716.50	320	123.8833
0.5	0.1079	0.810399	4502.22	320	150.0739
0.2	0.1001	1.88077	5224.36	320	174.1454

Table 4-4, initial values for simulations (*n=0.3*)

α	V [m/s]	q'' [W] H1	q''/S_w [W/m^2] H1	t_w [K] CT	Pe
1.0	0.0541	0.20339	1694.92	320	56.4972
0.5	0.0515	0.386644	2148.02	320	71.60076
0.2	0.0495	0.929287	2581.35	320	86.04505

For H1 BC, a $\Delta t = 40$ [K] was considered; the input temperature was set to 280 [K] and the length of the tube (*L*) were assumed to be long enough to allow the hydrodynamic and the thermal developments.

CFD simulation of forced convection heat transfer of laminar phase-change non-Newtonian fluids in rectangular straight micro-channels

A wall thickness of 1×10^{-6} [m] was used for the H1 conduction and a high value of k was set for the material of the wall. The value of k was set to an arbitrary value to 100000 [W / m K] for the peripheral direction and 0.0001[W / m K] for the axial conduction.

For the PCM simulations, the carrier fluid was water with a PCM volume concentration of 15%. The properties of the fluid are close to the properties of the N-Eicosane (9). The melting point of this material is 310 [K] but for the simulations is assumed to be 309-310 [K] for stability. The latent heat of the particles was assumed to be 230 [kJ/kg] (9). As the viscosity is not constant, the value of the consistency index used for non-Newtonian flows was kept.

The values of the specific heat used (from equations 2.26 and 2.27) are 3850.65 [J/kg K] for $t < t_1$ and $t > t_2$ and 38054.4 [J/kg K] for $t_1 < t < t_2$ with $t_1 = 309$ [K] and $t_2 = 310$ [K].
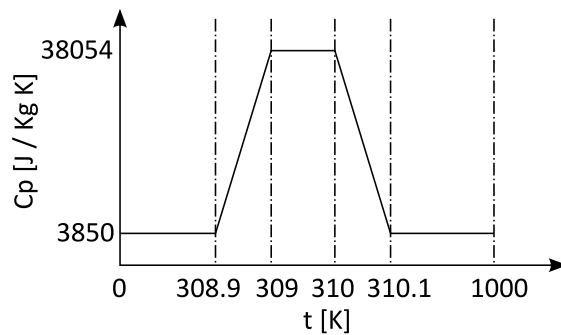
Figure 4-8, specific heat profile for PCM simulation

The final initial values for the PCM fluid simulations are listed in the next table. To allow a better development of the flow, the Reynolds number had been changed to 20, and the heat flow was set to allow the bulk temperature to reach the phase change temperature at a short distance from the inlet. The phase change will start before this point, when the temperature of the wall reaches the phase change temperature.

Table 4-5, initial values for PCM simulations

α	n	V [m/s]	q''/S_w [W/m^2] H1	t [K] CT	Pe
1.0	1.0	1.3462	75000.00	320	1497.475
0.5	1.0	1.0097	75000.00	320	1497.475
0.2	1.0	0.8077	75000.00	320	1497.475
1.0	0.5	0.0648	61911.14	320	72.05847
0.5	0.5	0.0589	75000.00	320	87.29262
0.2	0.5	0.0546	87029.79	320	101.2941
1.0	0.3	0.0317	59179.40	320	35.28937
0.5	0.3	0.0302	75000.00	320	44.72339
0.2	0.3	0.0290	90130.03	320	53.7456

The velocity for $\alpha = 0.5$, $n = 1.0$ for the CWT BC was set to 0.90 [m/s] to start the phase change at the same length than the other cases. The same modification was done with the case $\alpha=1.0$, $n = 0.5$ under CWT, with $V = 0.09$ [m/s].

In general, for all cases, the simulation follows the next assumptions:

1. Steady state, incompressible flow;
2. Constant thermo-physical properties of the fluid, except c_p for the PCM;
3. Negligibly small axial conduction and viscous dissipation;
4. Non-Newtonian fluids obeying the power law;
5. For PCM, single particle motion is not taken into account.

4.7   Simulation

The used software for the simulations was FLUENT 12 and all the models were created in the ANSYS Workbench environment; geometries in DesignModeler and grids in Workbench Meshing. Detailed information of how the geometry and grids were generated will not be presented in this work as they are very general processes.

In general, the solver was set to iterate until a residual of an order of 10^{-6} were reached. Second order solvers with double precision were used to minimize the round off errors.

CFD simulation of forced convection heat transfer of laminar phase-change non-Newtonian fluids in rectangular straight micro-channels

The post-processing was done in the CFX-Post module of Workbench. The value of Nu was calculated with a macro written in PERL language, specifically for this work. The macro can be read in the APPENDIX B.

For a more information of the parameters generally used for the solver in the simulations, consult the APPENDIX A.

4.8   Conclusions for the chapter

The verification section reported in this work is actually comparing the values obtained in the simulations with available data in literature, but without these important verifications, the results obtained from the contribution section cannot be deemed as reliable as for today, there is no available data to compare with.

It is necessary to state that even if the exactly the same data used in this works is used in trying to reproduce the results of this investigations, the results could be not exactly as the ones found in the next section, because, as it has been stated before, the numerical methods are not exact ones and the results depend on many factors. However, a good approximation could be expected.

CHAPTER 5 Results

5.1 Grid independency

The next plot shows the results of the simulation for the circular tube with $n = 1$ for the three different grid resolutions:
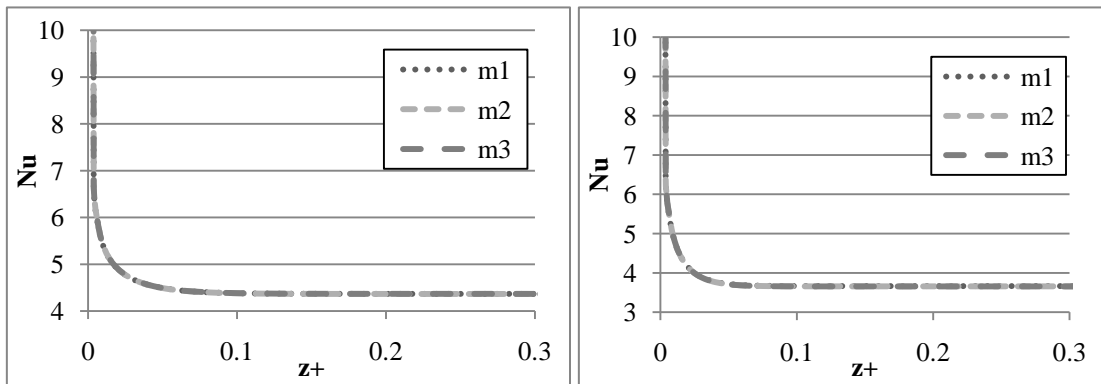
Figure 5-1, circular, $n=1$ fluid with H1 (left) and CWT (right) grid resolution comparison

As it can be observed, it is difficult to distinguish between the three grid curves as they have almost the same values and overlap each other, thus the results are independent of the mesh.

For the rectangular tubes, the solutions are also independent of the grid resolution. The next figure presents the results for the case $\alpha = 1.0$ with H1 and CWT BC.
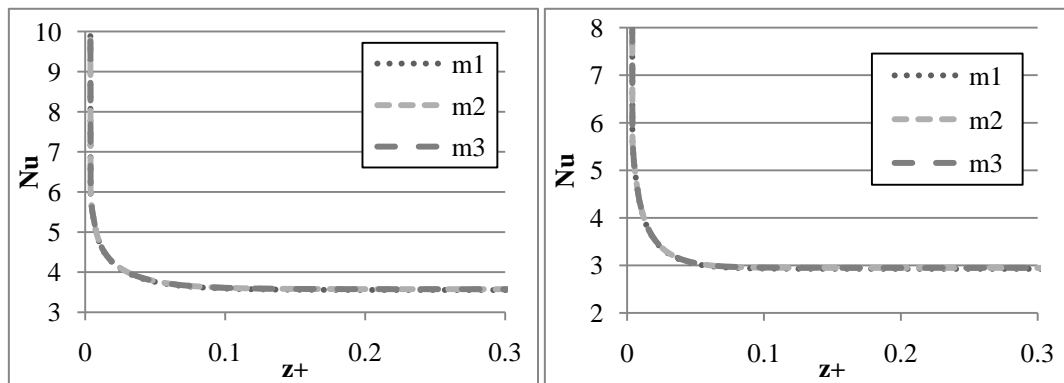
Figure 5-2, $\alpha = 1.0$, $n=1$ fluid with H1 (left) and CWT (right) grid resolution comparison

As in the circular tube case, it is hard to distinguish from one resolution to the other, meaning grid independent results are reliably achieved.

CFD simulation of forced convection heat transfer of laminar phase-change non-Newtonian fluids in rectangular straight micro-channels

The same comparison procedure was done for the Newtonian fluids showing the same behavior as the presented ones. The values of local Nu for the three resolutions a at constant distance z^+, where the fluid is fully developed (i.e. 0.2 for the circular tube), are shown in the next table as an example of the variations depending on the grid.

Table 5-1, local Nu for H1 and CWT at $n = 1$

α	m1 H1	m2 H1	m3 H1	m1 CWT	m2 CWT	m3 CWT
Circular	4.368	4.366	4.366	3.662	3.658	3.658
1.0	3.556	3.578	3.578	2.928	2.941	2.947
0.5	4.033	4.084	4.082	3.309	3.357	3,357
0.2	5.618	5.686	5.686	4.796	4.860	4.860

The variations between the three resolutions of the grid are very small, then, it is possible to conclude that the resolutions used are good enough to get results that are grid independent and because of this, the medium resolution grid (m2) was selected to present the results.

5.2 Verification of reference fluids

5.2.1 Single phase fluid

The importance of this section is evident when it is noted that there are no available data to compare with for the modeling of PCM non-Newtonian fluids presented in section 5.3. Without this verification, the new data presented cannot be deemed as reliable, as there are no sources to verify it. Also, the results obtained in this section were used as a reference fluid when evaluating the thermal performance of the non-Newtonian and PCM fluids in section 5.4.

This section is divided in Newtonian and non-Newtonian fluids, and a final comparison between all the cases is presented at the end of this section. The results cover H1 and CWT boundary conditions with n=1.0, 0.5, 0.3 for α=1.0, 0.5, 0.2, and the circular tube for the Newtonian case.

The theoretical and numerical values used for validation are reported by Kays (11) and others (Chung (5), Garimella (7), Syrjälä (6)).

5.2.1.1 Newtonian flow (*n*=1)

Next table shows the results for the fluid with *n*=1. For this case, the four geometries were analyzed, including the circular pipe.

Table 5-2, local Nu with H1 and CWT for fully developed Newtonian fluid

(Literature values from (4), (5), (6), (7))

α	CWT Nu Numerical	CWT Nu Literature	H1 Nu Numerical	H1 Nu Literature
Circular	3.66	3.66	4.37	4.36
1.0	2.94	2.98	3.58	3.61
0.5	3.36	3.39	4.08	4.12
0.2	4.84	4.83	5.69	5.73

Form the last table, it is possible to observe that the values are in a good agreement with the literature values, then, it can be conclude that the non-Newtonian power law model works as expected for the $n = 1$ case.

Plots for the Newtonian flows are presented in section 5.2.1.4.

5.2.1.2 Non-Newtonian velocity profiles

As a verification of the hydrodynamically developed power law fluid model, the generated velocity profiles for the various rectangular cases are presented in the next figures.
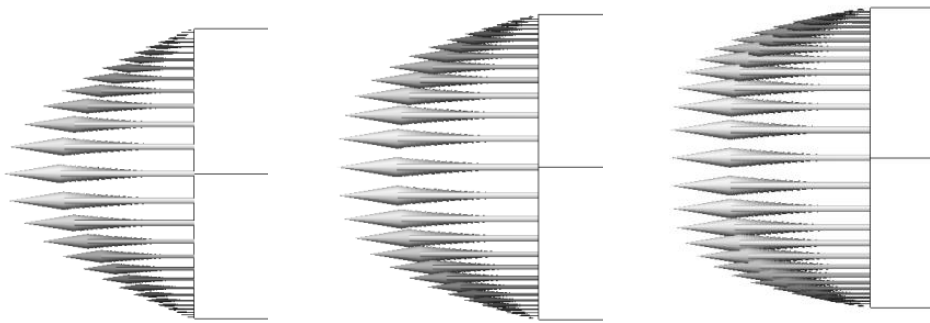
Figure 5-3, velocity *w* profile for fully developed power law fluid at outlet

(Left to right: *n*=1.0, *n*=0.5, *n*=0.3)

CFD simulation of forced convection heat transfer of laminar phase-change non-Newtonian fluids in rectangular straight micro-channels

It is possible to observe that the profile goes from a parabolic curve to a dull profile at the center as the power law index goes down. This is in good agreement with Figure 2-12 and it is possible to conclude that the power law models are developing as expected.

The next figures show the velocity plots in three dimensions. Only the Newtonian and the non-Newtonian $n = 0.3$ are presented. The velocity w is plotted as a dimensionless velocity calculated with w / V.
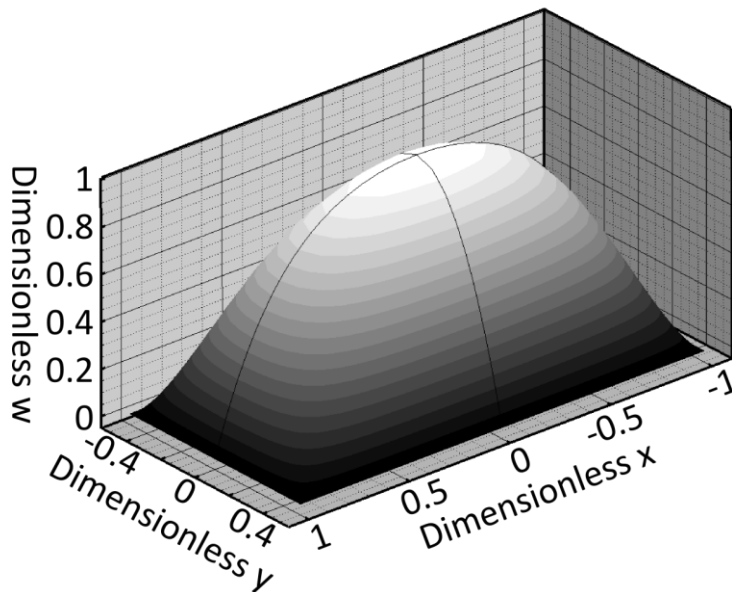
Figure 5-4, three dimensional plot of w for α=0.5, n=1.0
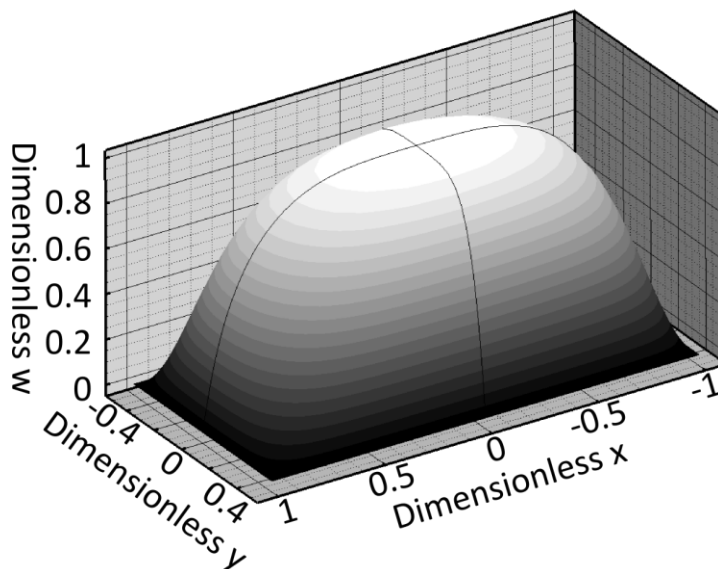
Figure 5-5, three dimensional plot of w for α=0.5, n=0.3

As in the two dimensional figure, it is possible to see how the profile for a Newtonian flow follows a parabolic path, while for the non-Newtonian fluid, the velocity at the center reaches the same maximum value in a larger area.

As a last verification, a dimensionless plot of the shear stress is presented. Recalling the equation for the shear stress for non-Newtonian flows:

$$\tau = K_c \left(\frac{\partial w}{\partial y}\right)^n \tag{5.1}$$

The curves that are expected to be obtained from the last equation is a straight line for $n = 1.0$ (11) and a curve of order n for $n \neq 1.0$. The results behave just as expected, as depicted in the next figure.
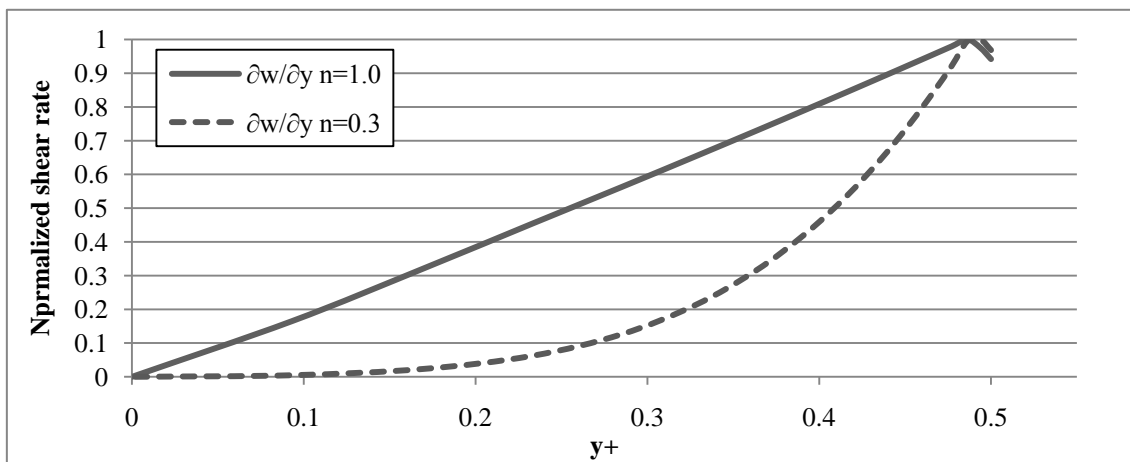
Figure 5-6, shear stress for Newtonian and non-Newtonian flow

The value $y^+ = 0$ is located at the center of the tube and it increases until it reaches the wall (at $y^+ = 0.5$). The values of this plot are normalized, and are not at the same scale. The numerical results for the non-Newtonian flow are a lot smaller than for the Newtonian, but they are adjusted for the sake of the comparison.

Figure 5-6 presents a small deviation at the end of the curves that are due numerical error, but the tendency in the plot is evident.

The next graph depicts the comparison on a normalized rheogram of the Newtonian and the non-Newtonian flows.

CFD simulation of forced convection heat transfer of laminar phase-change non-Newtonian fluids in rectangular straight micro-channels
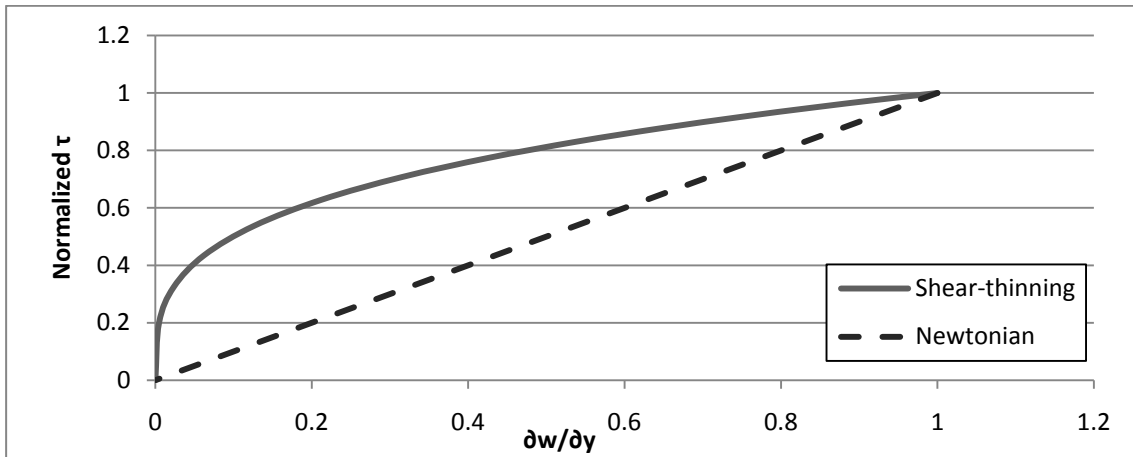
Figure 5-7, normalized rheogram for Newtonian and non-Newtonian flows

It is possible to see that the last figure presents a behavior that is in good agreement with Figure 2-11.

5.2.1.3   Non-Newtonian flow

For the non-Newtonian case, the next tables present the obtained results for both boundary conditions (H1 and CWT) and compare them with known values from other works. The circular pipe was not analyzed for these cases.

Table 5-3, local Nu with CWT for fully developed non-Newtonian fluid

(Literature values from (4), (5), (6), (7))

α	n=0.5 numerical	n=0.5 literature	n=0.3 numerical	n=0.3 literature
1.0	3.18	3.20	3.40	3.44
0.5	3.56	3.58	3.80	3.82
0.2	4.90	4.92	5.15	5.12

Table 5-4, local Nu with H1 for fully developed non-Newtonian fluid

(Literature values from (4), (5), (6), (7))

α	n=0.5 numerical	n=0.5 literature	n=0.3 numerical	n=0.3 literature
1.0	3.87	3.89	4.18	4.22
0.5	4.36	4.40	4.66	4.71
0.2	5.94	5.98	6.22	6.28

It is possible to see that the values are in good agreement with the theoretical values, then, it is safe to conclude that the rheological properties of the flow are correctly selected and that the power law model is working with good results for values of *n*=0.3, 0.5.

5.2.1.4 Comparison between single phase fluids

The following plots depict a comparison of Nu for the different power law index and with the same aspect ratio, under one of the boundary conditions H1 (constant heat flux and constant peripheral temperature) and CWT (constant wall temperature).
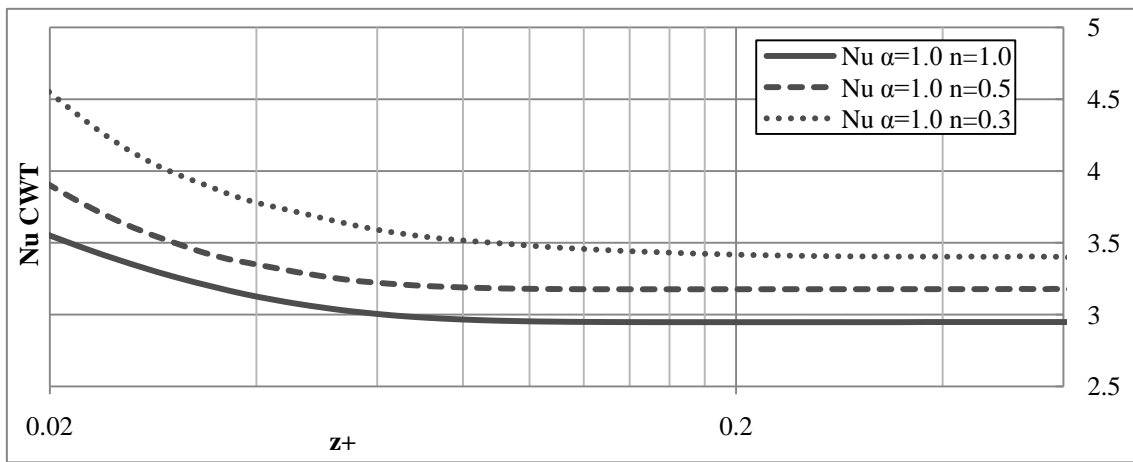
Figure 5-8, Nu for α=1.0 CWT BC
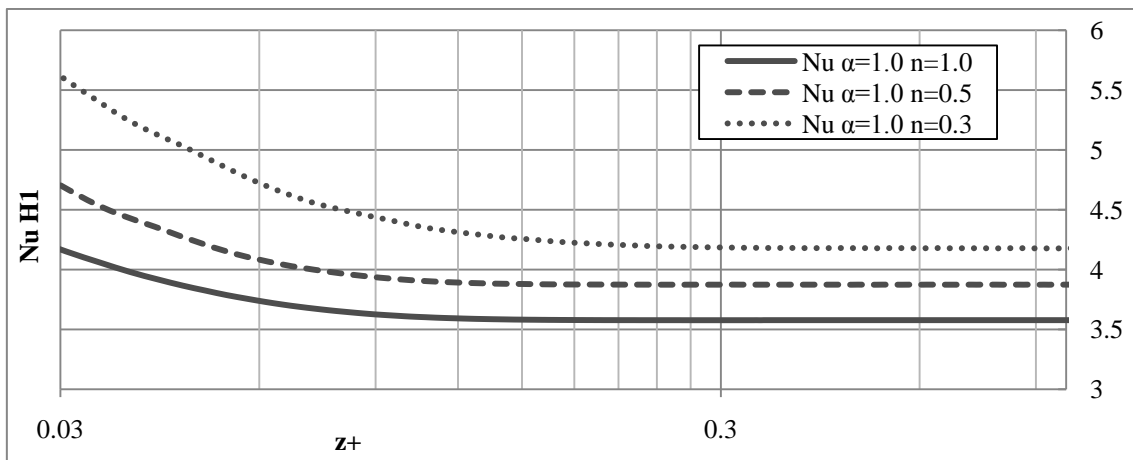
Figure 5-9, Nu for α=1.0 H1 BC

CFD simulation of forced convection heat transfer of laminar phase-change non-Newtonian fluids in rectangular straight micro-channels
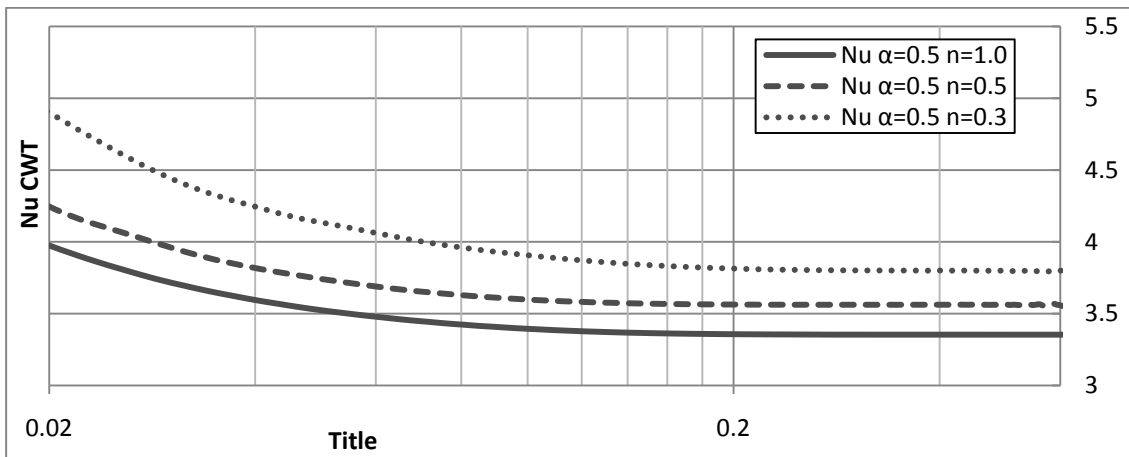
Figure 5-10, Nu for α=0.5 CWT BC
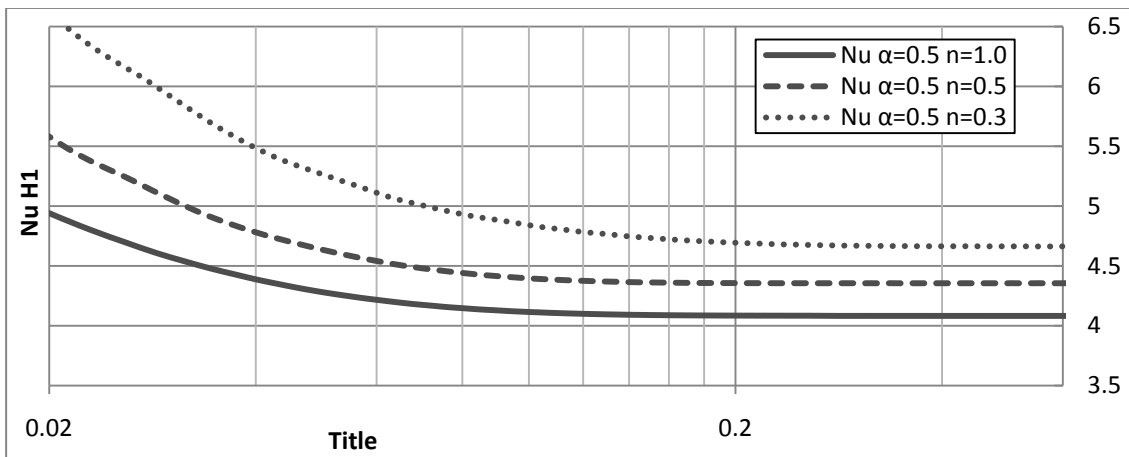
Figure 5-11, Nu for α=0.5 H1 BC
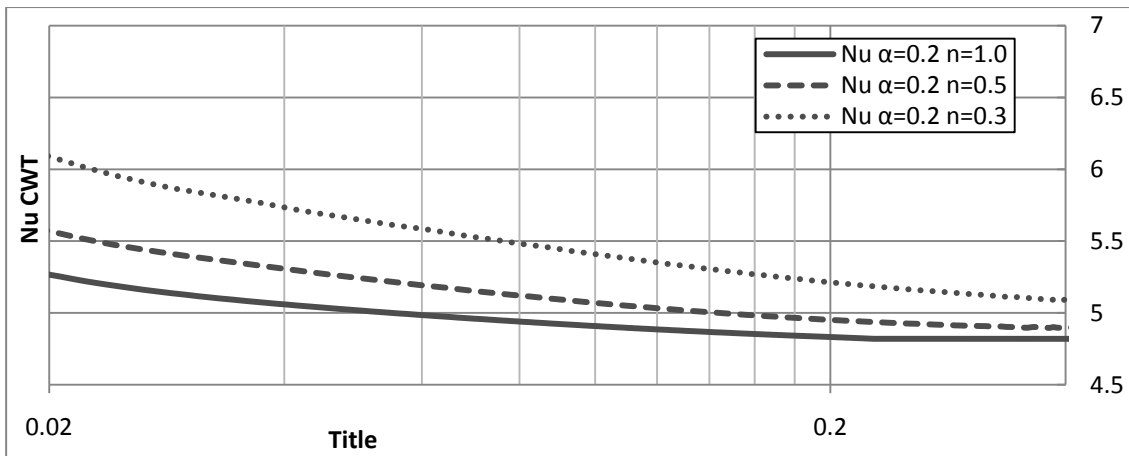
Figure 5-12, Nu for α=0.2 CWT BC
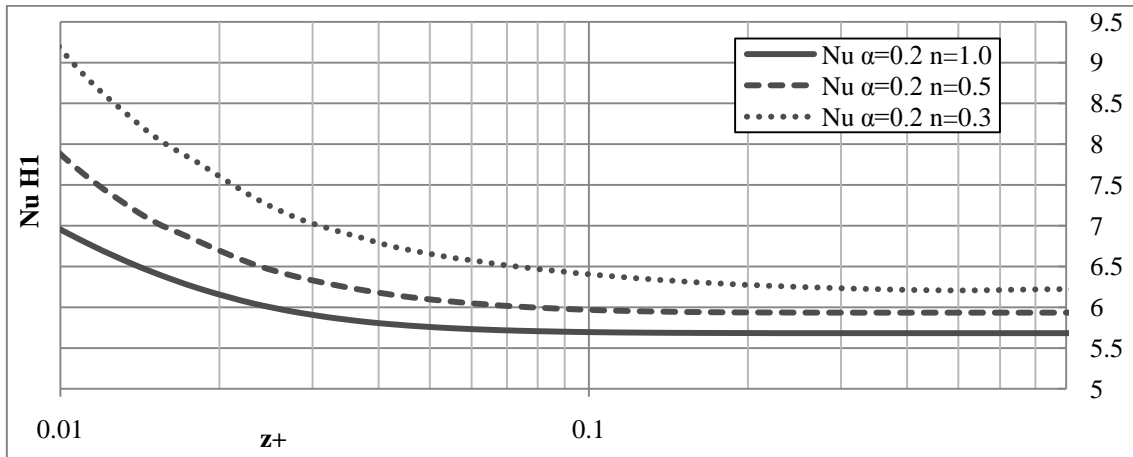
Figure 5-13, Nu for α=0.2 H1 BC

From the last figures it is possible to observe that lower power law index *n* have better heat transfer properties for both H1 and CWT BC's, confirming that the non-Newtonian fluids have a better heat exchange performance.

For *α*=0.2 CWT BC (Figure 5-12), it was not possible to get a thermally fully developed fluid before the center, bulk and wall temperature get the same value. Several parameters were modified to analyze the impact in the results, but no satisfactory solution was found. Because of that, the value of Nu never reaches a constant value but keeps decreasing slightly. This result is consistent to the behavior found by Chung (5) as it is depicted in the next figure.
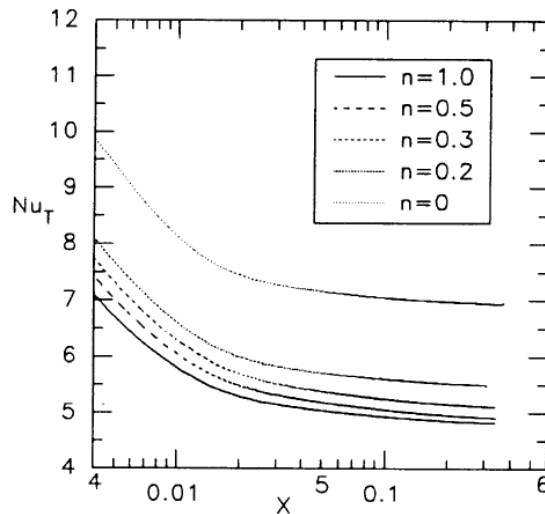
Figure 5-14, thermally developing Nu under CWT BC *α*=0.2

(Reproduced under "fair use" from (5))

CFD simulation of forced convection heat transfer of laminar phase-change non-Newtonian fluids in rectangular straight micro-channels

As the local values at the end of the curves are in good agreement with the values reported in the literature, the results are granted as good for this work, but the refinement and analysis of this case is left as future work.

The difference between H1 and CWT BC's is meaningless because as these are boundary conditions, it is not possible to conclude that one condition is better than the other. However, the difference between aspect ratios is important.

In these cases, the plots are using the value of z instead of z^+ because the value of the dimensionless length does not allow comparing the curves in an easy way for different aspect ratios in the same chart, as depicted in the next figure.
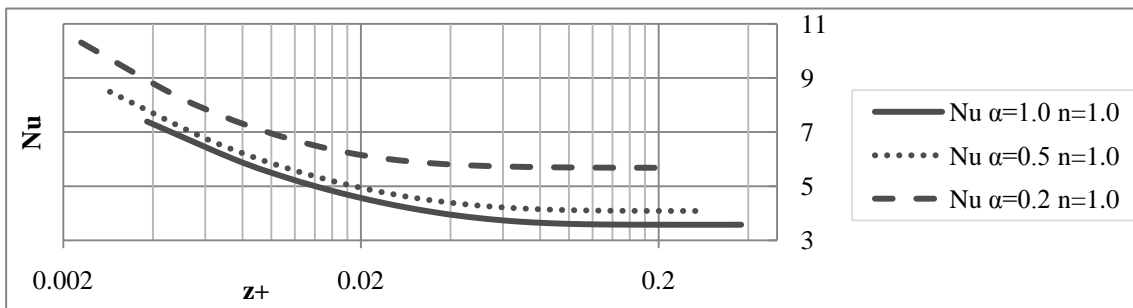
Figure 5-15, different aspect ratio curves plotted against z^+

This is because the dimensionless length is a function of the Peclet number and the hydraulic diameter as defined in equation 4.1. The hydraulic diameter varies for the different cross sectional areas, thus, the dimensionless is no constant between them. For the same aspect ratio, the Peclet number varies between the power law indexes, but as Pe is a function of V, the bulk velocity of the fluid compensates the differences, allowing plotting the curves in the same chart.

If it is needed that the curves keeps the same points over the dimensionless length, the Pe must be kept as a constant and the start point must be controlled with V, but this will cause a variation in Re across the aspect ratios.

This phenomenon is more notorious for the PCM materials. The next plot will be discussed in detail in next sections, but it is presented here as an example of the variation of the dimensionless length between aspect ratios.

86
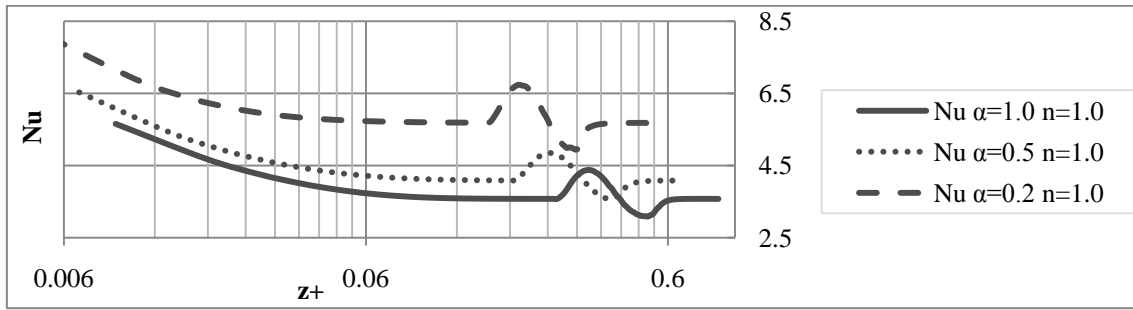
Figure 5-16, different aspect ratio curves plotted against z^+ (PCM)

The charts to compare the different aspect ratios follow this paragraph. It is possible to observe that there is an improvement in the heat transfer as α gets smaller, being the cross-section area of $\alpha = 0.2$ a better choice to enhance the heat transfer compared to the others cross sections analyzed in this work as depicted in the next figures.
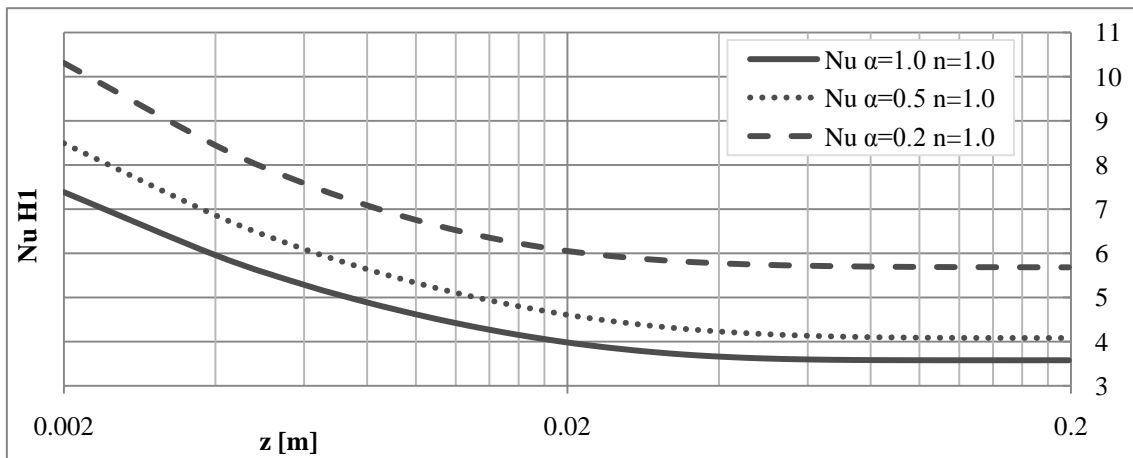
Figure 5-17, Nu for various aspect ratios under H1 BC and n=1.0
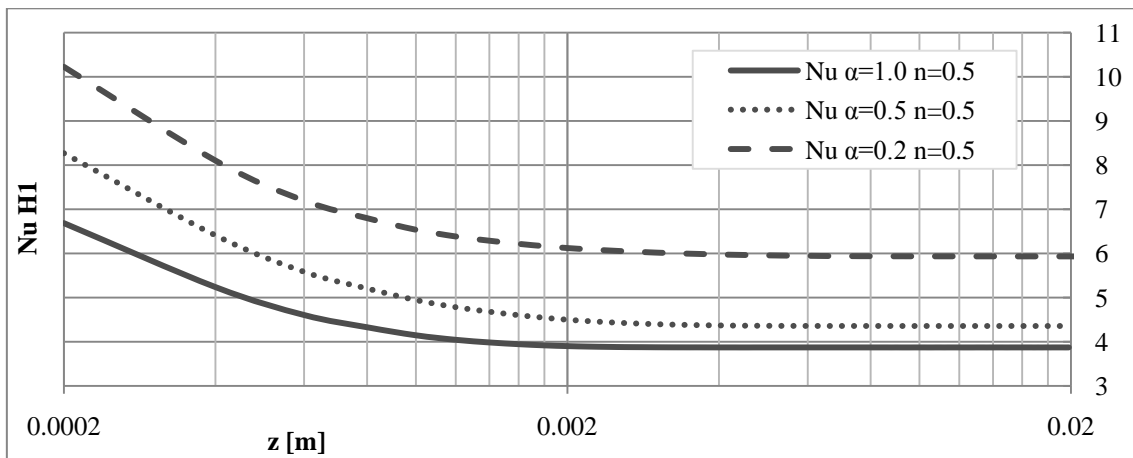
Figure 5-18, Nu for various aspect ratios under H1 BC and n=0.5

CFD simulation of forced convection heat transfer of laminar phase-change non-Newtonian fluids in rectangular straight micro-channels
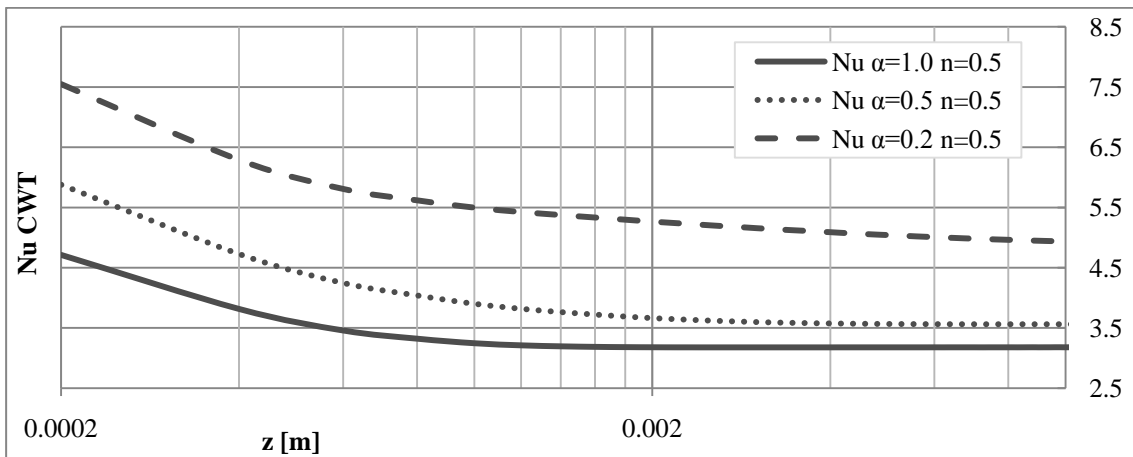
Figure 5-19, Nu for various aspect ratios under CWT BC and n=0.5

Although only some plots are presented, the same behavior remains for all the cases, under CWT and H1 BC's.

5.2.1.5   Conclusions for the section

Single phase Newtonian and non-Newtonian fluids behave as expected considering that the results are in good agreement with the documented data ((4), (5), (6) …). The Nusselt numbers values are under the 5% of deviation against the theoretical values, thus, the models can be granted as good and can be used as reference fluids when evaluating the non-Newtonian with PCM thermal performance.

5.2.2   Phase change material

This section presents the results for a PCM fluid. Results are divided in Newtonian (*n*=1) and non-Newtonian flow (*n*=0.3, 0.5). Only rectangular sections with different aspect ratios were analyzed.

The phase change region is depicted in the next figure. It is possible to see a surface limiting the temperature to the inferior melting point (lighter surface), and a second one to indicate where the temperature reaches the upper limit and where the liquid region starts (darker surface).
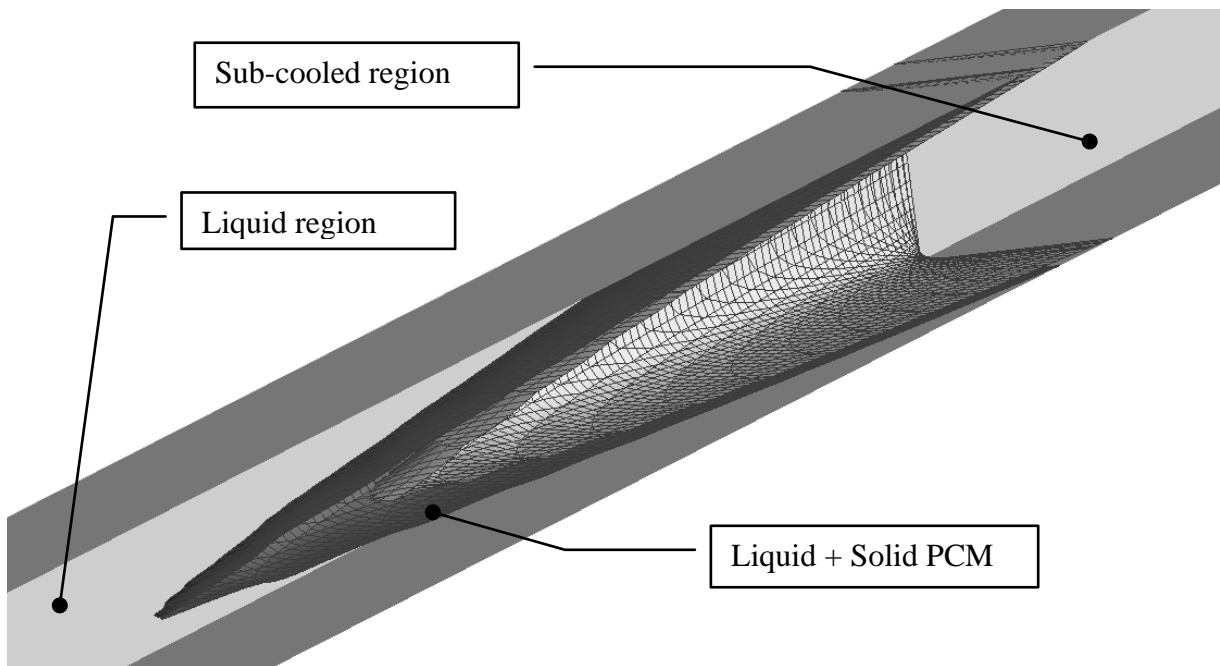
Figure 5-20, Cut of the rectangular cross sectional pipe showing the phase change region

It is possible to observe how the temperature at the wall and in the phase change region does not have the same values at the same time. This will be important in the next section when the value of the Nusselt number will be evaluated.

Another point to remember is that the melting point of a solid is given at a single temperature and not during an interval as it was modeled. The melting point of the N-Eicosane is 310 [K] but using only this point could lead to instabilities in the simulation (9).

The temperature profiles before, during and after the phase change region is depicted in the next figure.

CFD simulation of forced convection heat transfer of laminar phase-change non-Newtonian fluids in rectangular straight micro-channels
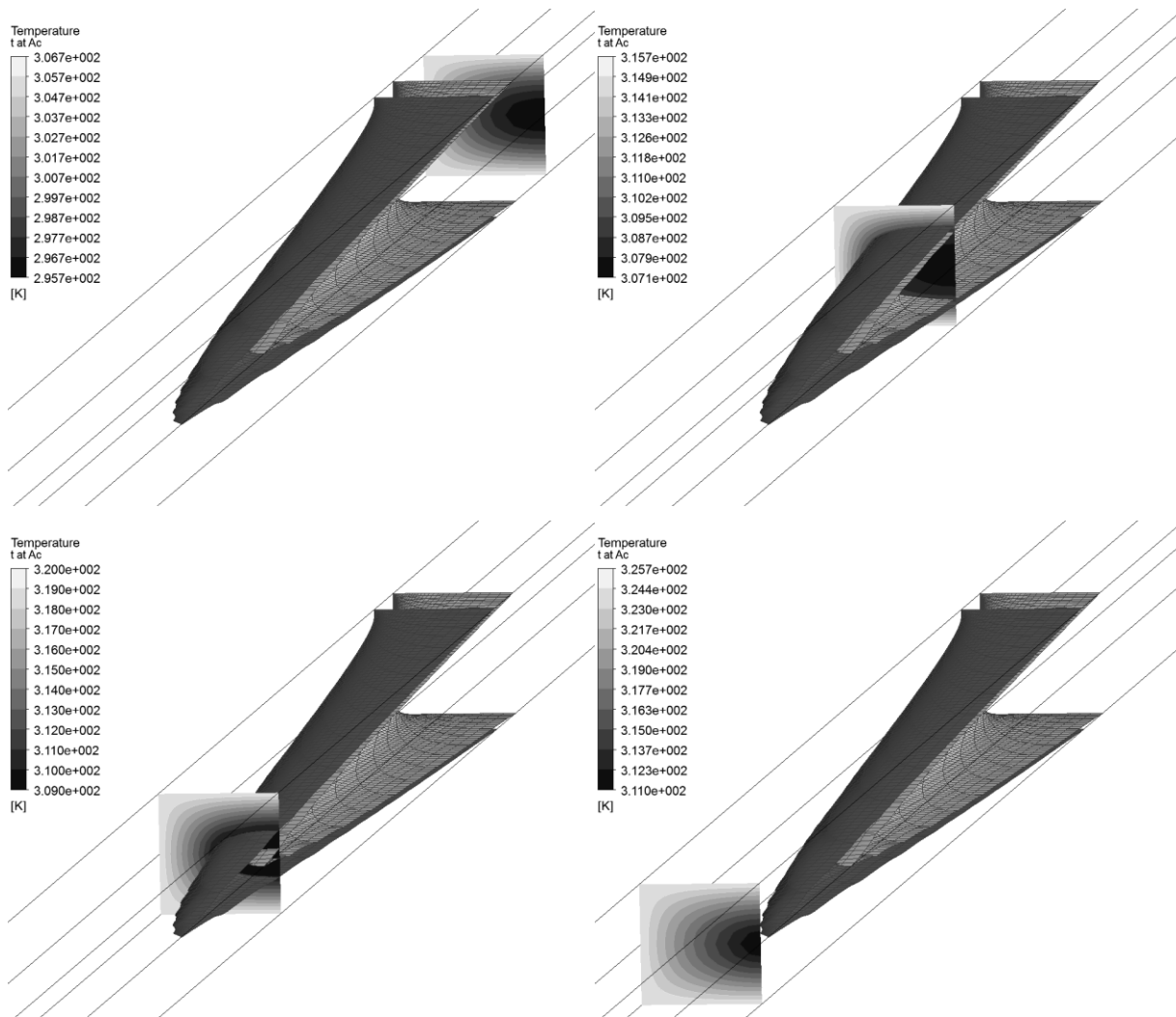
Figure 5-21, temperature profile near the phase change region

In the last figure it is possible to observe how the temperature at the center of the pipe, during the phase change, keeps a near constant temperature of approximately the temperature of the melting point. Before and after the phase change region the temperature is distributed more uniformly from the center to the wall.

The difference in the temperature distribution can be easily observed in the next figure.
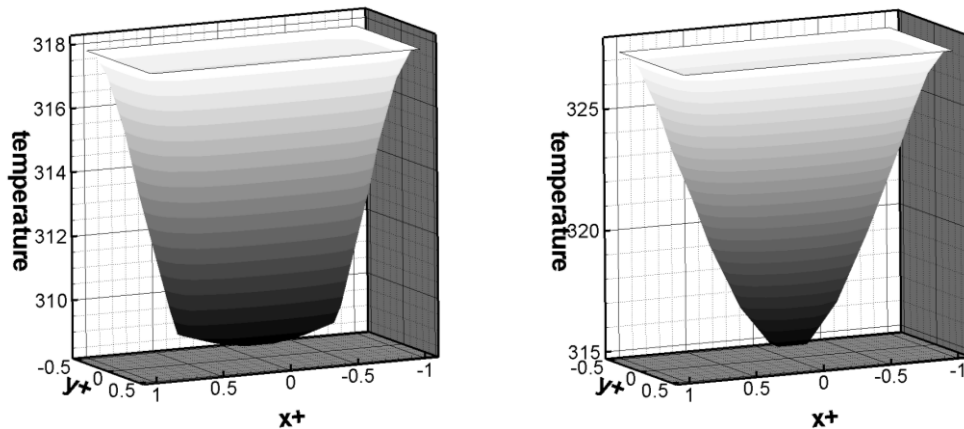
Figure 5-22, temperature profile during the phase change and in the liquid region

α=0.5, n=0.5 H1 PCM (Left and right respectively, temperature in [K])

In the figure at the left it is possible to observe the near constant value at approximately the melting point temperature (309-310 [K] in this case) while in the figure at the right it is possible to appreciate a more uniform gradient in all the cross section area.

5.2.2.1   Newtonian Flow (*n* = 1.0)

For the PCM simulations and Newtonian fluids, the results were compared with those obtained by Kondle (9). However, the cited author worked with ratios of 0.5, 0.25 and 0.125, thus, only the case for *n*=1.0 and *α*=0.5 can be used for validation.

It is important to remember that Kondle used a constant dynamic viscosity for his work, while in the models generated this work uses a power law model. This is a substantial difference between both analyses, but as it will be seen, the results of this investigation are in good agreement with the results presented by Kondle, accomplishing the objective of this section in validating the power law model and its parameters for PCM fluids.

CFD simulation of forced convection heat transfer of laminar phase-change non-Newtonian fluids in rectangular straight micro-channels
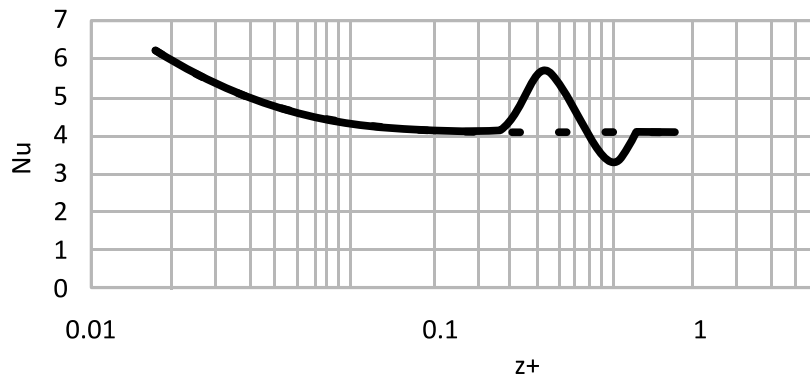
Figure 5-23, Nu for α=0.5 under H1, Newtonian fluid. Numerical results by Kondle (9).

(Continuous line: PCM; Dashed line: single phase)

From the results by Kondle, it is possible to observe that the value of Nu have an increment in the phase change region, as expected, and dropped when the phase change is near completion.

The results obtained in the present work are depicted in the next figure. The solid line represents the PCM simulation, while the dashed line is the value for Nu obtained from the single phase fluid simulation.
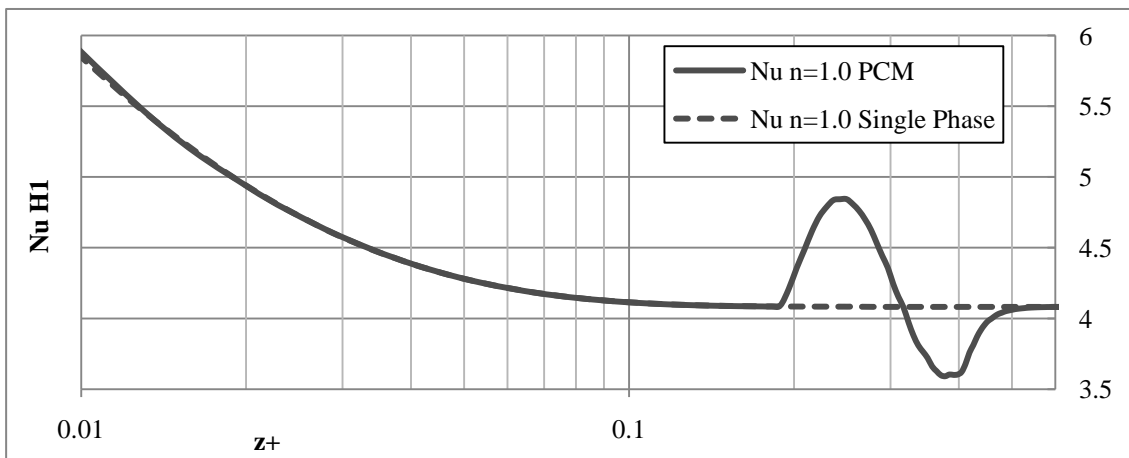
Figure 5-24, Nu for α=0.5 under H1, Newtonian fluid

At a first glance, the values for Nu in the phase change area are not the same as the reported by Kondle, but further analyses reveals that for PCM, the maximum value of Nu reached by the fluid, is a function of the heat flux applied to the wall, as depicted in the next figure.
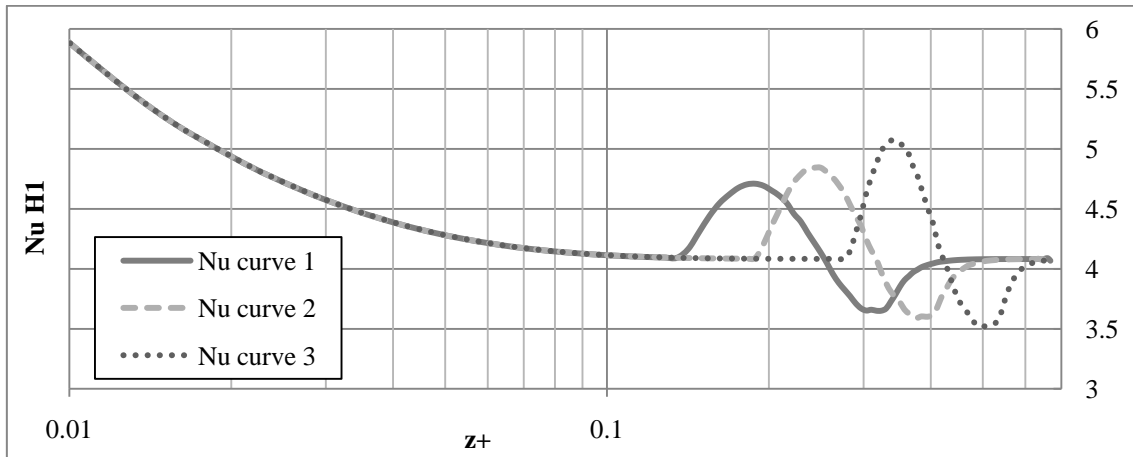
Figure 5-25, Nu variation due different heat flux under H1 BC

(curve 1: higher q", curve 3: lower q")

The last figure depict the curve for Nu for the same rectangular section (α=0.5) and same power law index (n=1.0). The only difference between the curves is the value of the constant heat flux applied as boundary condition at the wall. Curve 3 has the lowest value while curve 1 has the higher heat flux, thus, it starts its phase change earlier. It is possible to observe that as the phase change begins later, the peak value of Nu increments.

The bulk temperature can be obtained from the next equation:

$$q" = \dot{m}c_p(t_m - t_i)$$

5.2

If the mass flux and the specific heat are considered as constants, it's possible to observe that with higher heat flux, the difference between the bulk fluid and the inlet temperature will be higher for a given position of the tube. The mass flux is a function of the velocity V of the fluid, then for the same value of V, more heat will flow from the wall to the fluid if there is a higher $q"$ applied to the wall at that given position. The temperature at the inlet is also constant, then, it is possible to deduce that with higher heat flux, the bulk temperature of the fluid will be higher than for the other cases. As the bulk temperature increases faster, it will reach the phase change region at a shorter length z. The same behavior can be achieved by modifying the inlet velocity of the fluid; smaller values of V causes that the phase change starts earlier.

CFD simulation of forced convection heat transfer of laminar phase-change non-Newtonian fluids in rectangular straight micro-channels

In the next figure, the phase change temperature for this work is represented by 309 [K] – 280 [K] = 29 [K]. It is possible to observe that the curve for a higher heat flux reaches this point before the other two cases.
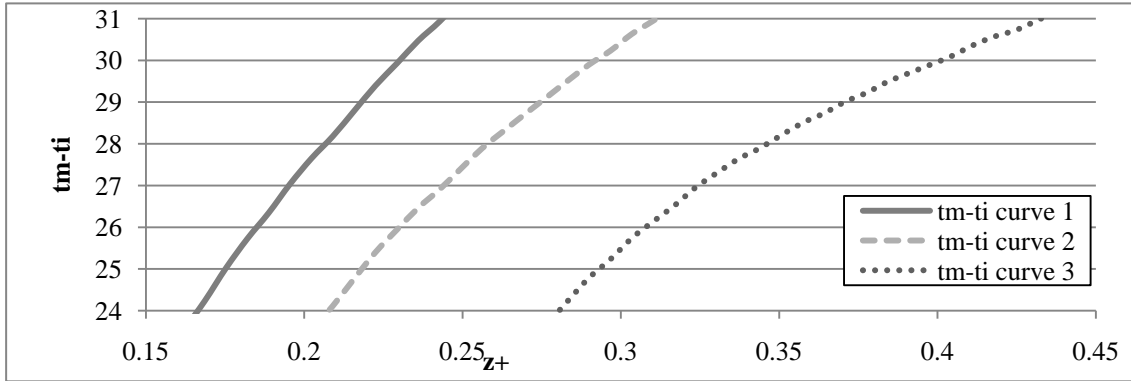
Figure 5-26, temperature difference t_m - t_i between the bulk fluid and the inlet

(curve 1: higher q", curve 3: lower q". Inlet temperature = 280 [K])

Once the phase change has begun, the value of the heat flux will increase due the increment in the specific heat model used in this work, and the value of Nu will also increase.

Recalling the equation for Nu

$$Nu = \frac{hD_h}{k}$$

5.3

It is possible to observe that the only difference between a fluid with higher and lower q'' applied must come from h, as the hydraulic diameter and k remains constant.

The convective coefficient is defined as

$$h = \frac{q''}{(t_w - t_m)}$$

5.4

As the value of the heat flux applied over an area is constant by definition, due the H1 BC, the only variable left is the difference of temperatures.

With a higher heat flux applied as boundary condition given a value of z^+, the $t_w - t_m$ value is also higher than for the other cases. This can be observed in the next figure.

94
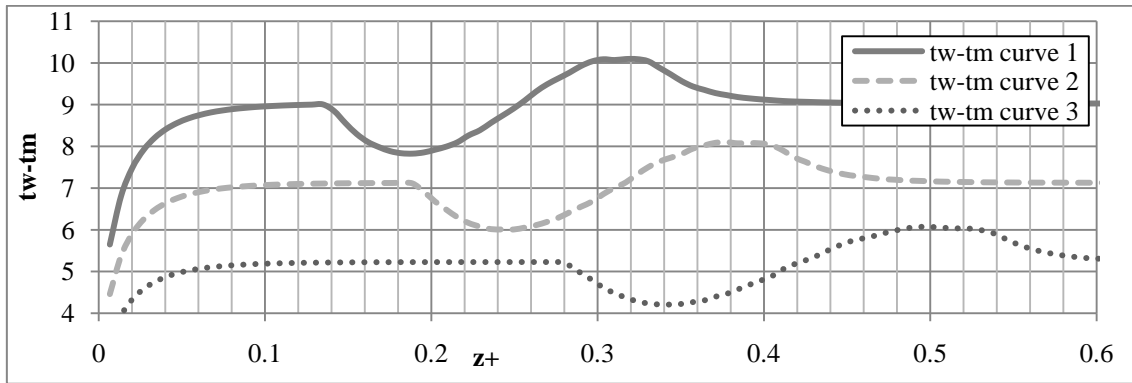
Figure 5-27, temperature difference between the wall and the bulk fluid

(curve 1: higher q", curve 3: lower q")

Then, with higher q'', the fluid needs a shorter distance z^+ to reach the melting point and with that higher value of the heat flux, a higher difference $t_w - t_m$ is also expected, thus, a lower value of h and a lower value of Nu will be developed. This explains the differences in the values between the plot by Kondle and the results of this work.

The drop in the value of Nu at the end of the phase change is because, at that point, the phase change is occurring only at the center of the cross section, keeping this area at nearly constant temperature, while the temperature of the wall keeps increasing, as depicted in Figure 5-21. As the difference between the wall and bulk temperature increases, the value of the convective coefficient h decreases and it also does it the value of Nu.
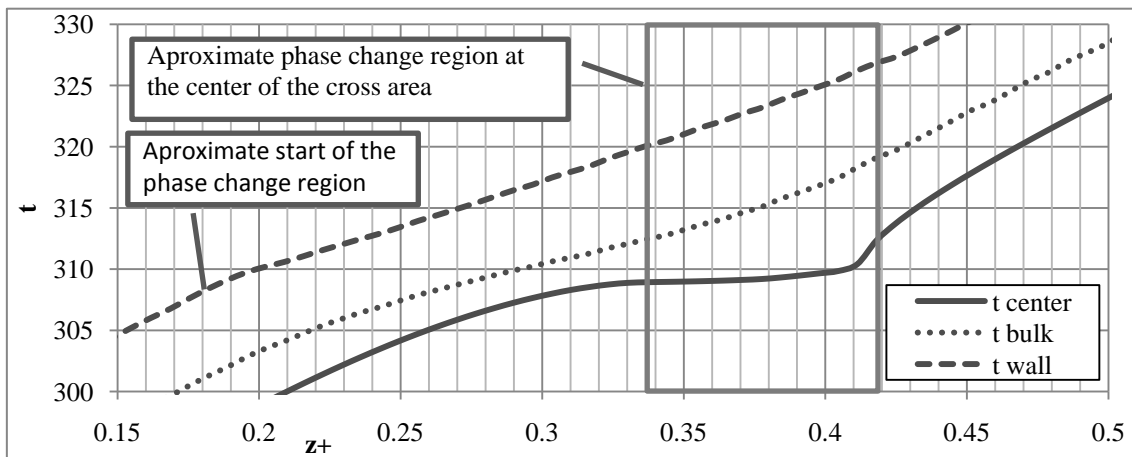
Figure 5-28, temperature difference between the wall and the center (H1, $\alpha=0.5$, $n=1$)

CFD simulation of forced convection heat transfer of laminar phase-change non-Newtonian fluids in rectangular straight micro-channels
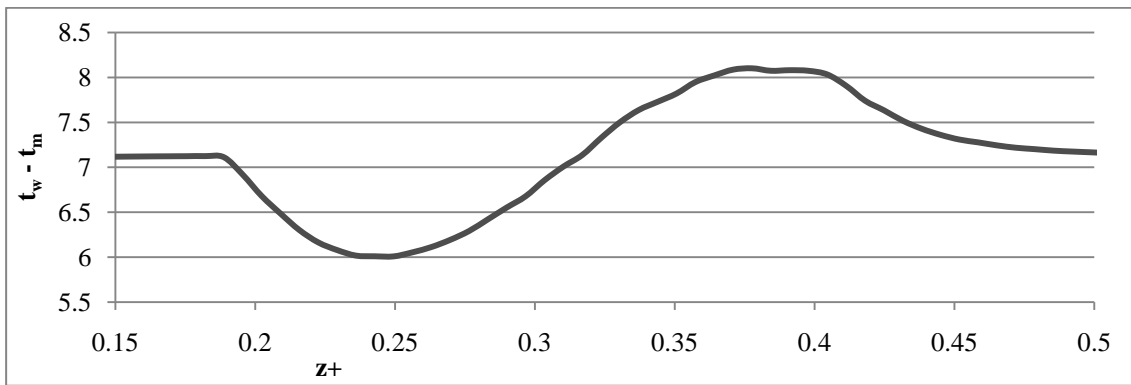
Figure 5-29, t_w - t_m for the phase change region (H1, α=0.5, n=1)

For the rest of the aspect ratios, it is possible to observe that the value of Nu for the fully developed region converges to the same value as for the single phase fluid as it was depicted for α=0.5 in Figure 5-24.
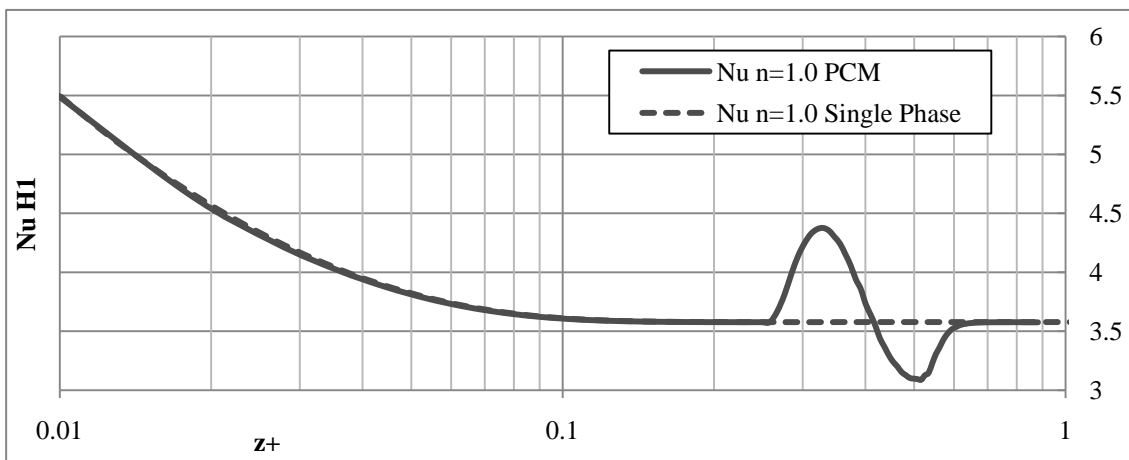
Figure 5-30, Nu for α=1.0 under H1, Newtonian fluid
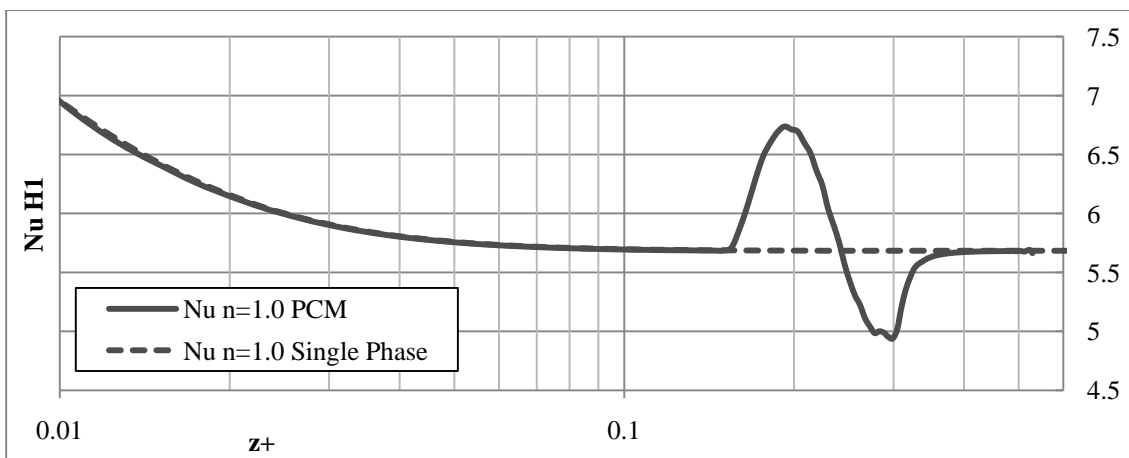
Figure 5-31, Nu for α=0.2 under H1, Newtonian fluid

96

The results for all the rectangular channels with $n=1.0$ and H1 BC are depicted in the next figure.
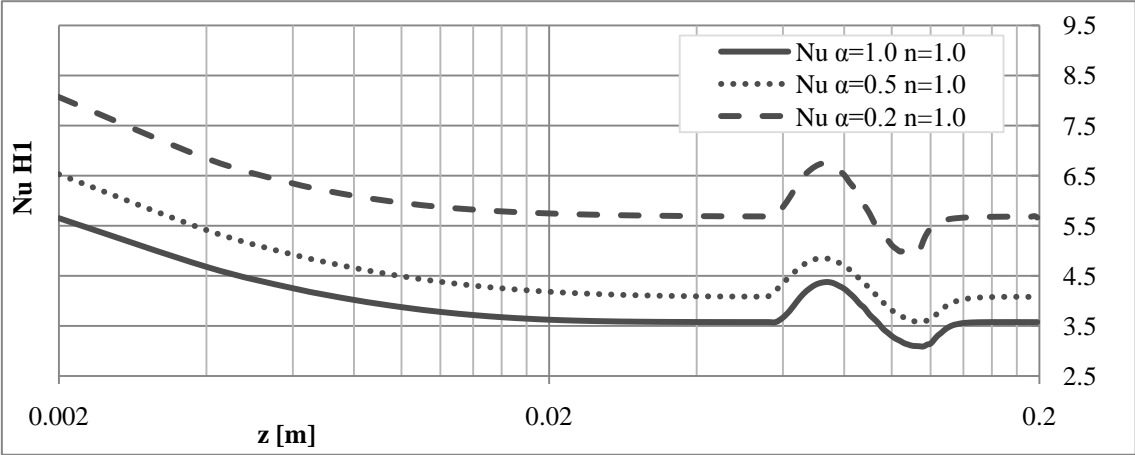
Figure 5-32, Nu for various aspect ratios under H1 BC and n=1.0

The behavior of the PCM is as expected considering the tendency reported by the results of the verification section and literature; a higher value of Nu for lower α and an increment in the value when the phase change begins.

For the CWT BC, the wall temperature is already over the melting point of the PCM from the beginning of the tube, then, the phase change starts almost immediately. The results from Kondle (9) can be observed from the next figure.
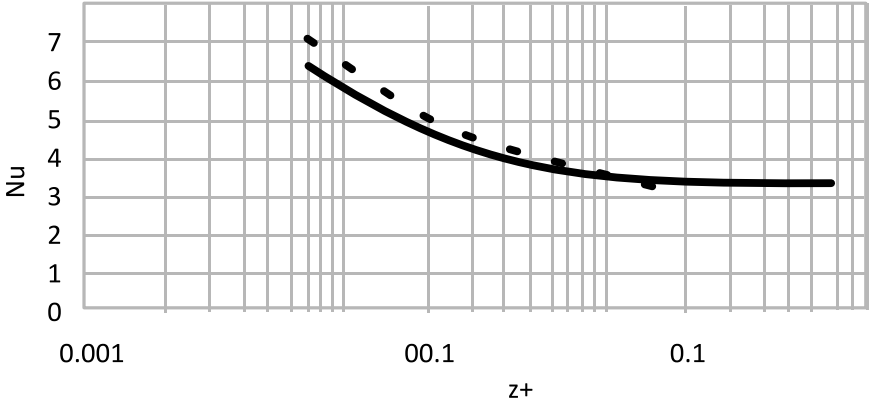
Figure 5-33, Nu for $\alpha=0.5$ under CWT, Newtonian fluid. Numerical results by Kondle (9).

(Continuous line: PCM; Dashed line: single phase)

The results of the present work for the same case are depicted in the next figure.

CFD simulation of forced convection heat transfer of laminar phase-change non-Newtonian fluids in rectangular straight micro-channels
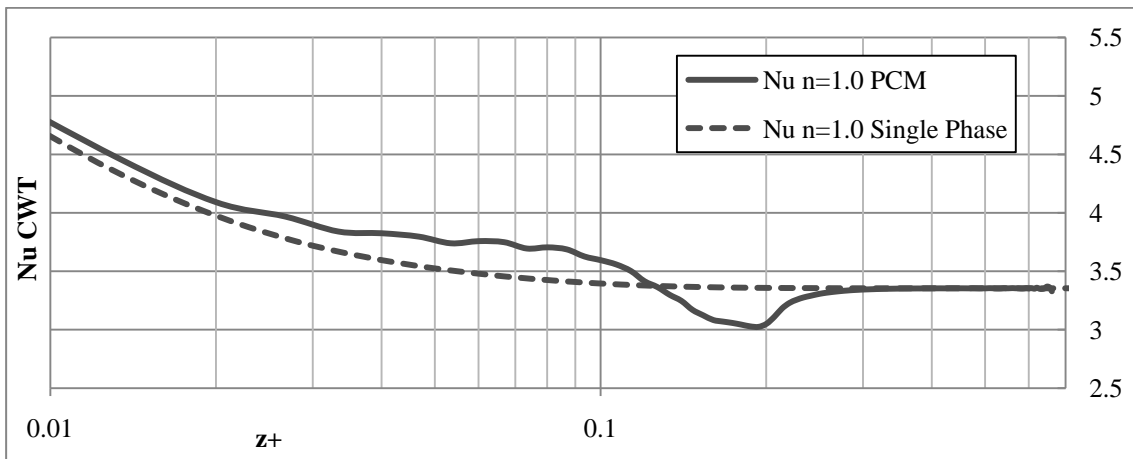
Figure 5-34, Nu for α=0.5 under CWT BC, Newtonian fluid

There is no peak increment in Nu, but it presents a raise of the value in the entry region of the fluid. In the fully developed region, the values of both fluids converge to the same value.

It is possible to observe that Figure 5-33 has no oscillations in the entry region and do not present a drop in the value of the Nusselt number in contrast with the results presented in this work. As the entry section was not fully investigated and it is not know if that data obtained by Kondle was treated in a particular way before its presentation, it is hard to conclude the reason why his results present no oscillations. With respect of the drop, it is unknown if the cited figure reports all the values or just a portion of the curve, but following the same considerations as for the H1 boundary condition, in which the drop in the value is cause by the difference in temperatures between the central region of the flow and the wall, it is safe to assume that it should be present in the CWT case as well.

It is possible to force the behavior of the flow, to approximate the reaction to a H1 BC, but this imply artificially modify the inlet characteristics of the fluid. By dropping the inlet temperature to 180 [K], it is possible to obtain the next figure.
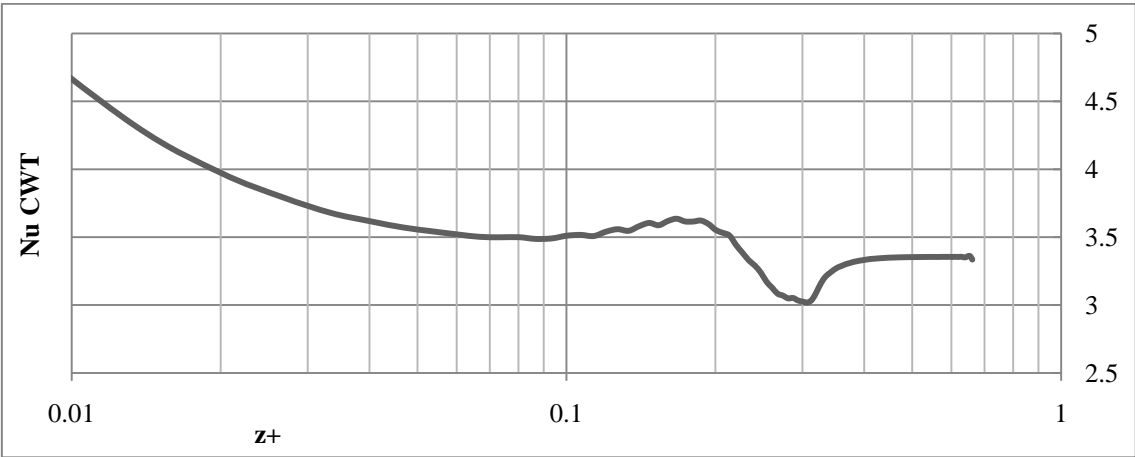
Figure 5-35, Nu for *α*=0.5 under CWT BC, Newtonian fluid with t_i = 180 [K], t_w = 320 [K]

For this case, it is possible to observe a small increment in Nu before the dropping region, but as it has been said, this implies to have a very large temperature difference between the inlet fluid temperature and the wall temperature BC.

The results for the other two aspects ratios are presented in the next figures.
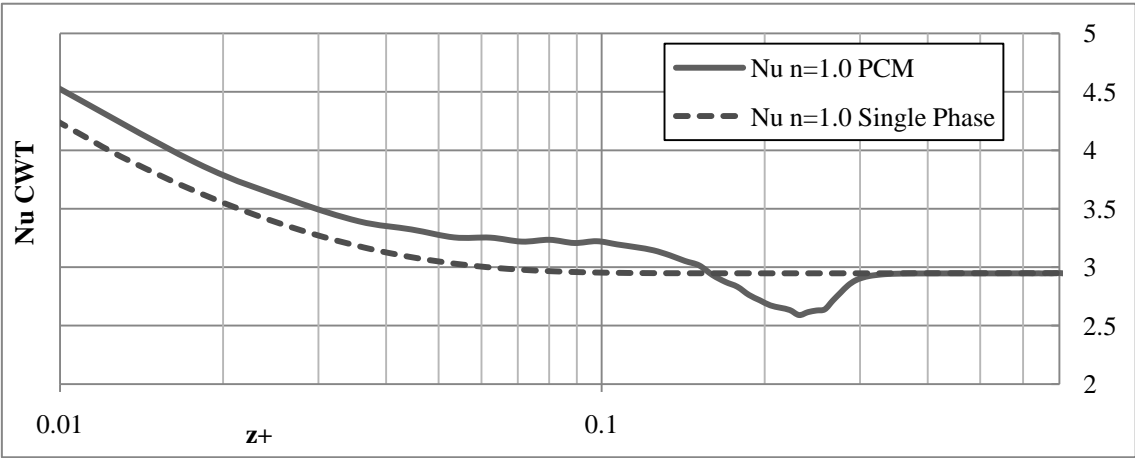
Figure 5-36, Nu for *α*=1.0 under CWT BC, Newtonian fluid

CFD simulation of forced convection heat transfer of laminar phase-change non-Newtonian fluids in rectangular straight micro-channels
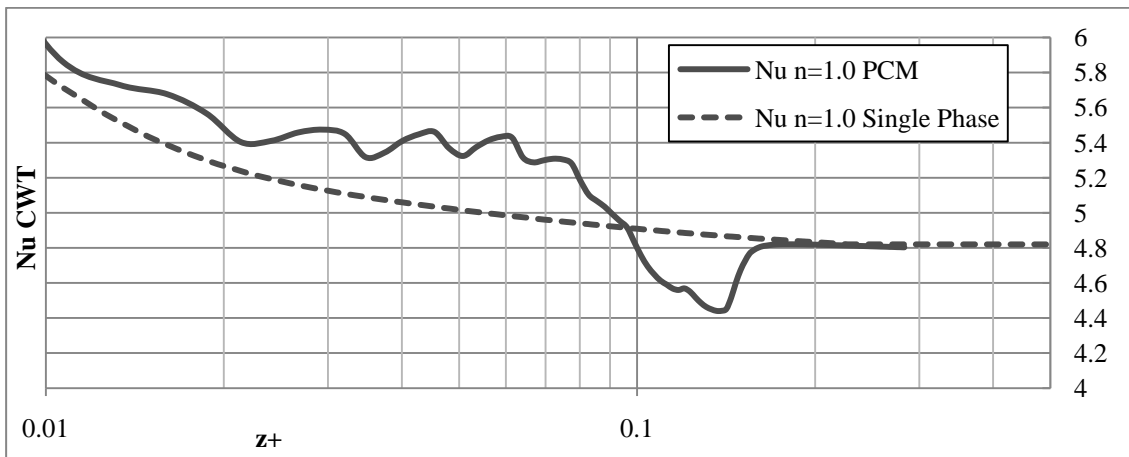
Figure 5-37, Nu for $\alpha=0.2$ under CWT BC, Newtonian fluid

Although all the cases present small oscillations of the values for this region, it is only in this case where the variations are really severe. As for the single phase fluids, it was not possible to obtain a fully developed flow for the tube with $\alpha = 0.2$. This could cause the variations observed in the entry region of Figure 5-37, but it is not confirmed. Further analyses are recommended to understand this behavior.

For the three aspect ratios, the obtained values are presented in the next figure.
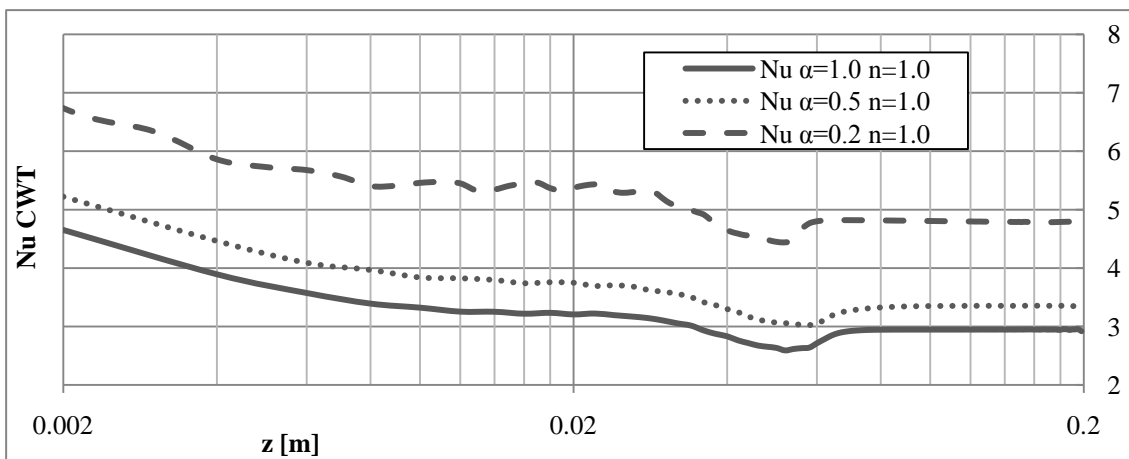
Figure 5-38, Nu for different aspect ratios, Newtonian flow

5.2.2.2 Conclusions for the section

The results obtained in this section are in good agreement with those in the reference work, thus, it can be conclude that the PCM Newtonian model is working as expected. The results

100

presented in the next section are derived from the same model, thus, it is safe to conclude that the results will reflex the physical phenomena in a reliable way.

5.3 Contribution: PCM and Non-Newtonian fluid slurry

This section presents the contribution that this work does to known new properties of the PCM non-Newtonian fluids. No data was found about these numerical simulations on the literature but due the results of previous sections seem to properly agree with other works, it can be inferred that this numerical simulations are reliable as well; nevertheless caution in their use is advised.

For PCM flow with $n = 0.5$, 0.3 fluids under the H1 boundary condition, the results of the analyses can be observed from the next figures.
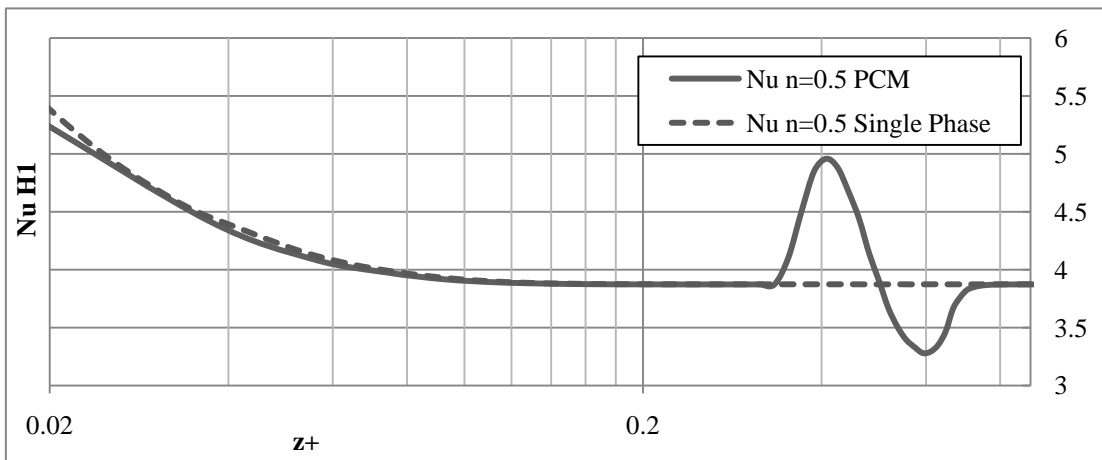
Figure 5-39, Nu for α=1.0 under H1, $n = 0.5$
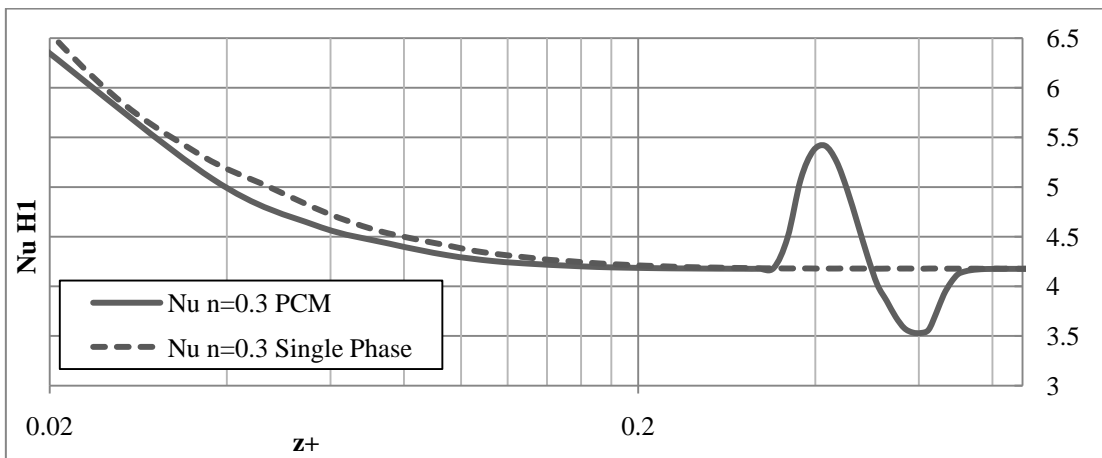
Figure 5-40, Nu for α=1.0 under H1, $n = 0.3$

CFD simulation of forced convection heat transfer of laminar phase-change non-Newtonian fluids in rectangular straight micro-channels
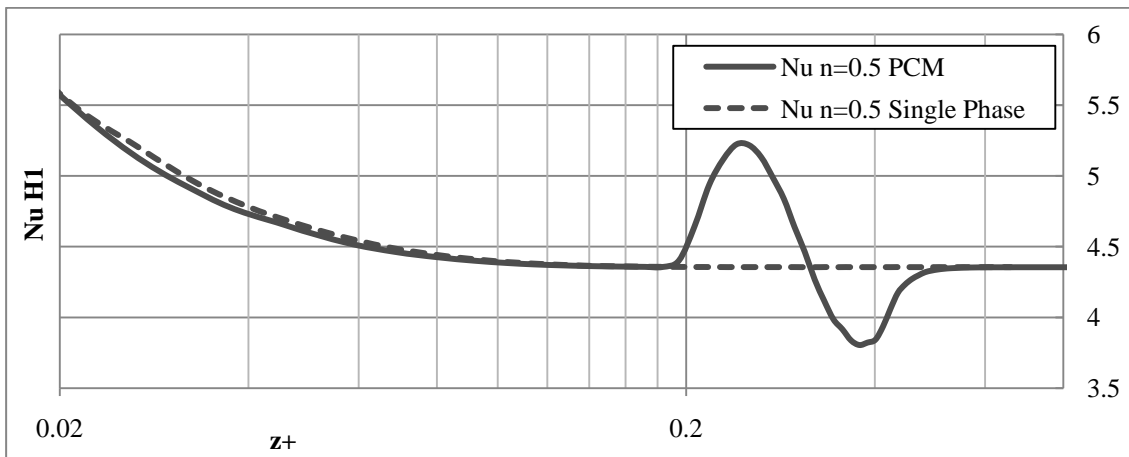
Figure 5-41, Nu for α=0.5 under H1, n = 0.5
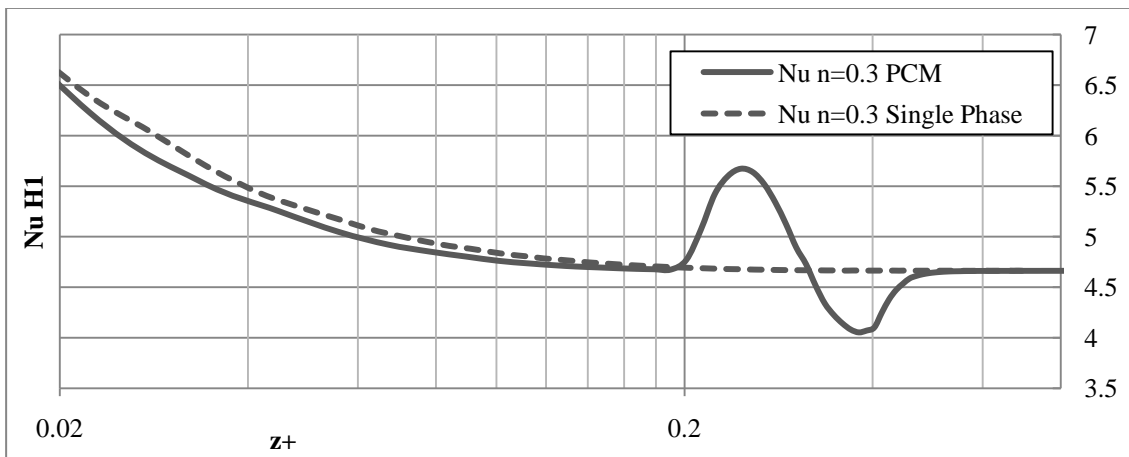
Figure 5-42, Nu for α=0.5 under H1, n = 0.3
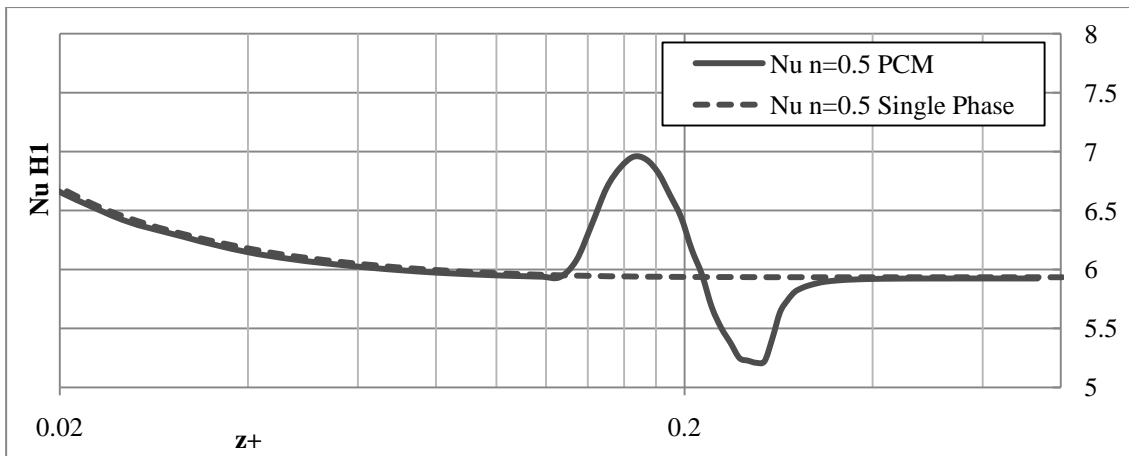
Figure 5-43, Nu for α=0.2 under H1, n = 0.5
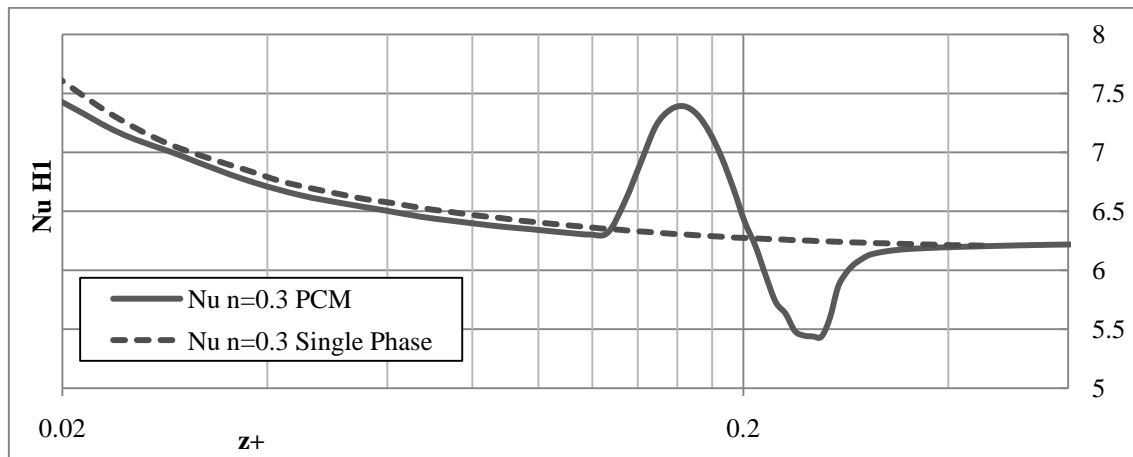
Figure 5-44, Nu for *α=0.2* under H1, *n = 0.3*

From the last figures, it is possible to observe that the PCM materials follow the same behavior of the single phase, with the corresponding raise in the value of Nu when the phase change starts. It can be concluded that as the results behave as expected, by converging with the single phase fluid curve in the sub-cooled and liquid regions, the simulations are accurate and the results can be trusted.

It is interesting to note that for the phase change to start at the same point of the tube in *z* length, the simulations require a displacement in z^+; for a lower aspect ratio, it needs to start before. This can be explained with the definition of heat transfer, which is a function of the cross sectional area. With a higher area, the fluid needs a higher heat flux to reach the melting temperature, but as it has been said, with higher heat flux, the phase change starts earlier in the dimensionless distance z^+.

The differences in the entry region in the last images are due numerical errors, and can be minimized by selecting a larger number of sampling points at that region. This work keeps a reasonable low number of sampling points in order to maintain the calculations no so computing expensive.

The results for the different aspect ratios and non-Newtonian power law indexes for the CWT BC are presented in the next figures.

CFD simulation of forced convection heat transfer of laminar phase-change non-Newtonian fluids in rectangular straight micro-channels
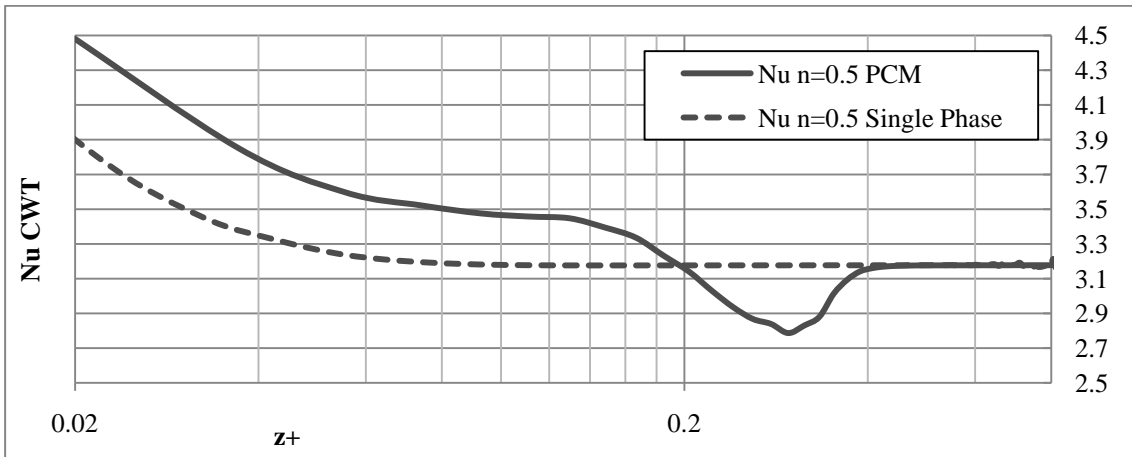
Figure 5-45, Nu for α=1.0 under CWT, *n* = 0.5
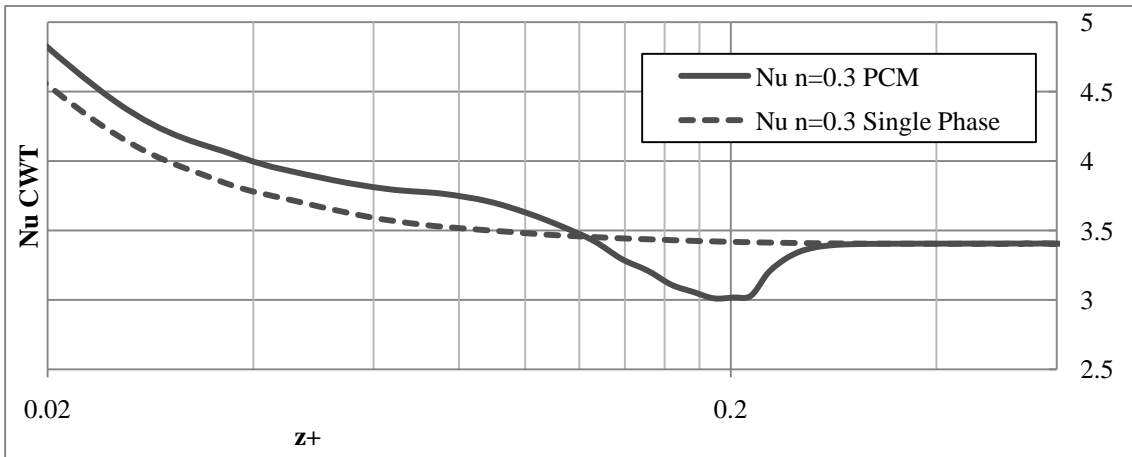
Figure 5-46, Nu for α=1.0 under CWT, *n* = 0.3
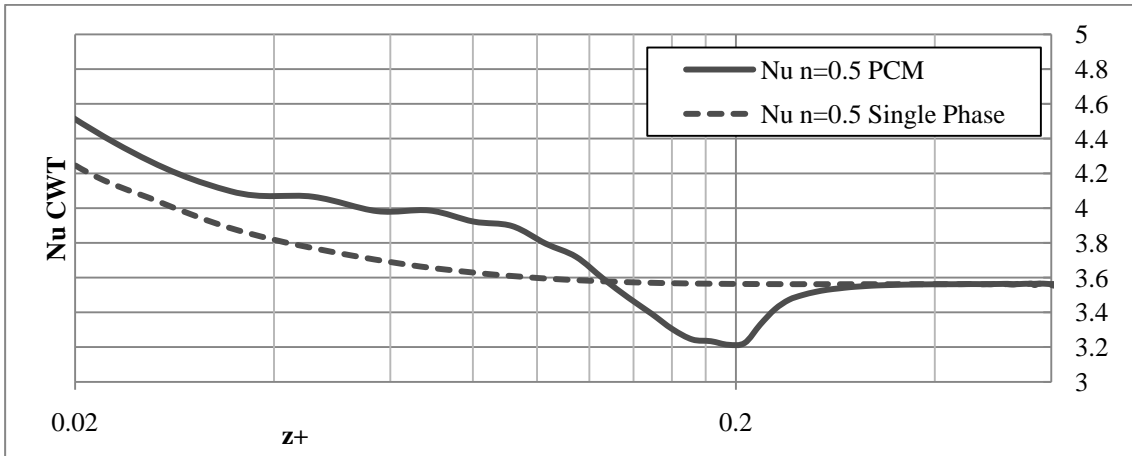
Figure 5-47, Nu for α=0.5 under CWT, *n* = 0.5
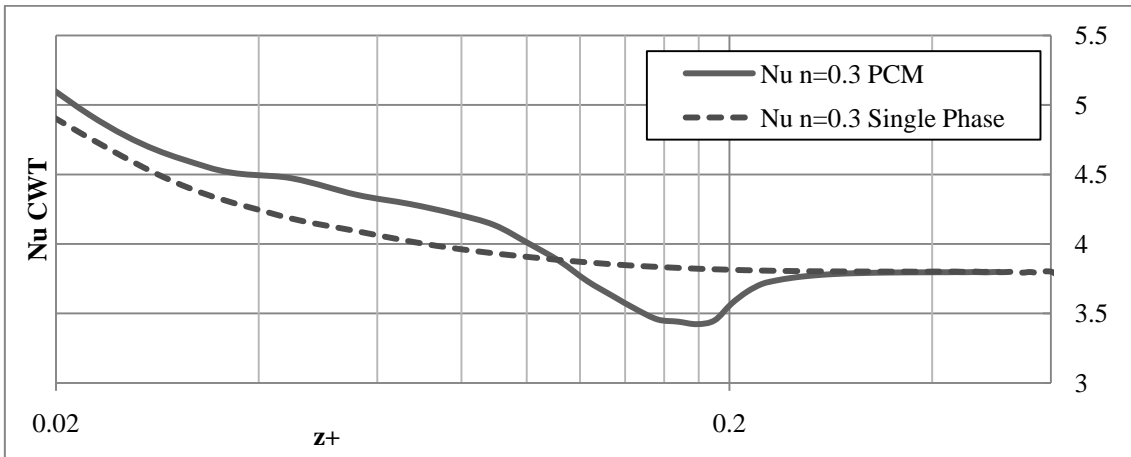
Figure 5-48, Nu for α=0.5 under CWT, *n* = 0.3
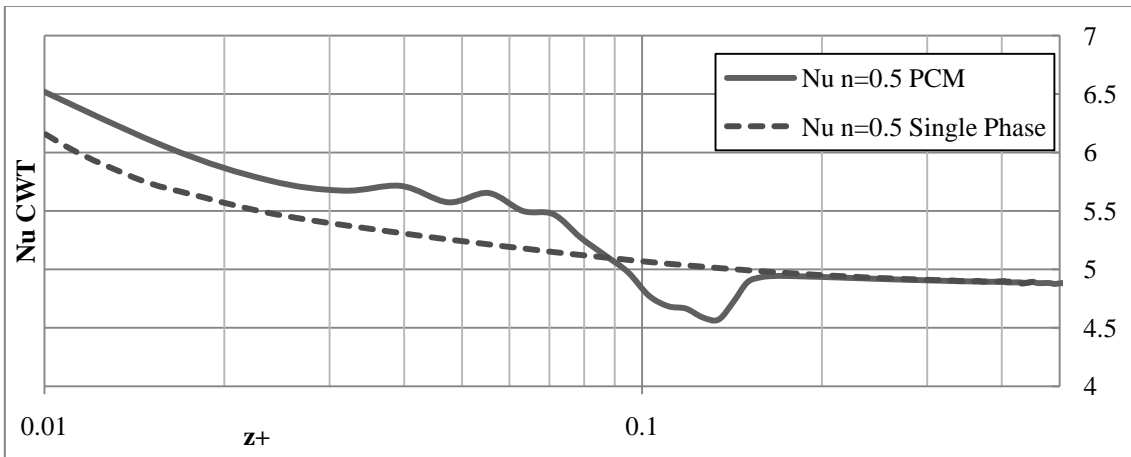
Figure 5-49, Nu for α=0.2 under CWT, *n* = 0.5
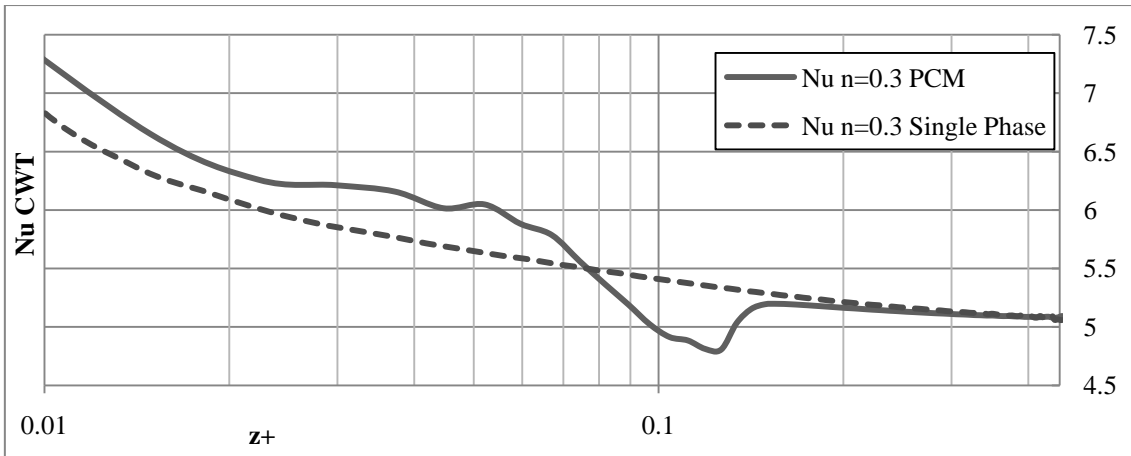
Figure 5-50, Nu for α=0.2 under CWT, *n* = 0.3

From the last figures it is possible to observe that lower power law index *n* represent a higher value of Nu. This behavior is as expected considering the results reported on the literature.

CFD simulation of forced convection heat transfer of laminar phase-change non-Newtonian fluids in rectangular straight micro-channels

The behavior of the rectangular tube with $\alpha=0.2$ CWT BC (Figure 5-12), maintains the same behavior as for single phase and PCM Newtonian were an asymptotic curve is not reached, showing that the simulations are, at least, accurate in reproduce the problem.

For the CWT case, it is possible to observe the same displacement in de dimensionless length as for the H1 case, with the phase change starting earlier for the lower aspect ratio.

5.3.1 Comparison between PCM fluids

The PCM non-Newtonian flows behave as expected, having the fluid with lower power law index, the higher Nu. Some results are depicted in the next images.
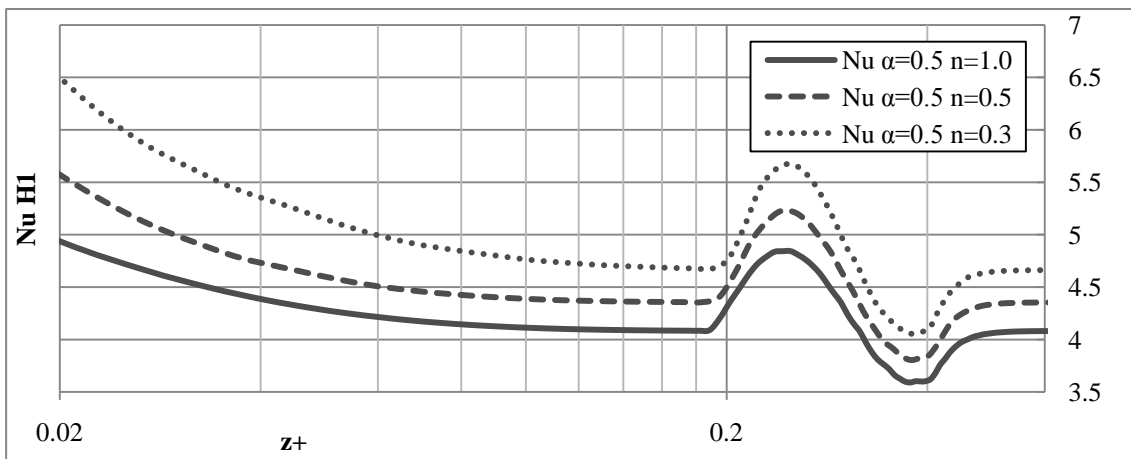
Figure 5-51, Nu for $\alpha=0.5$ under H1 with different power law indexes
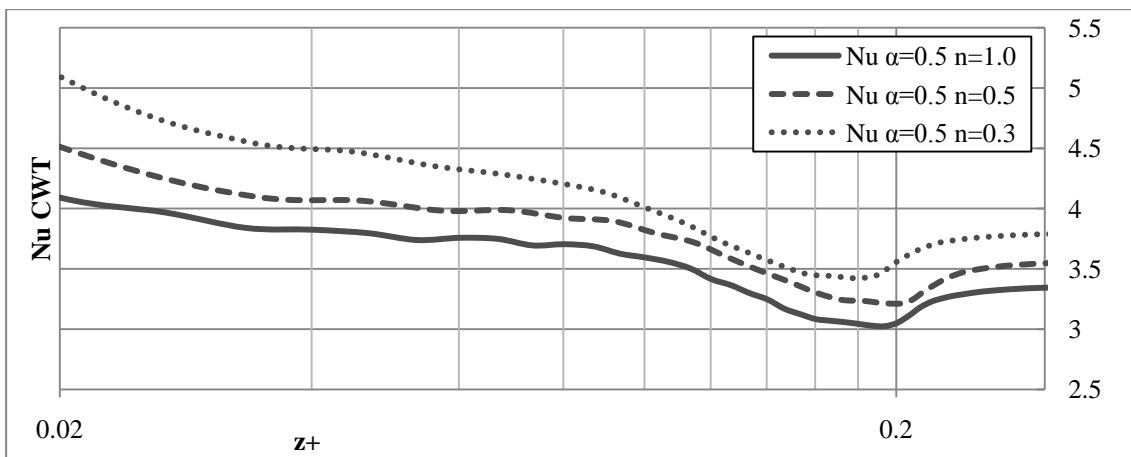
Figure 5-52, Nu for $\alpha=0.5$ under CWT with different power law indexes

The next figures depict a comparison between different aspect ratios for PCM non-Newtonian fluids.

106
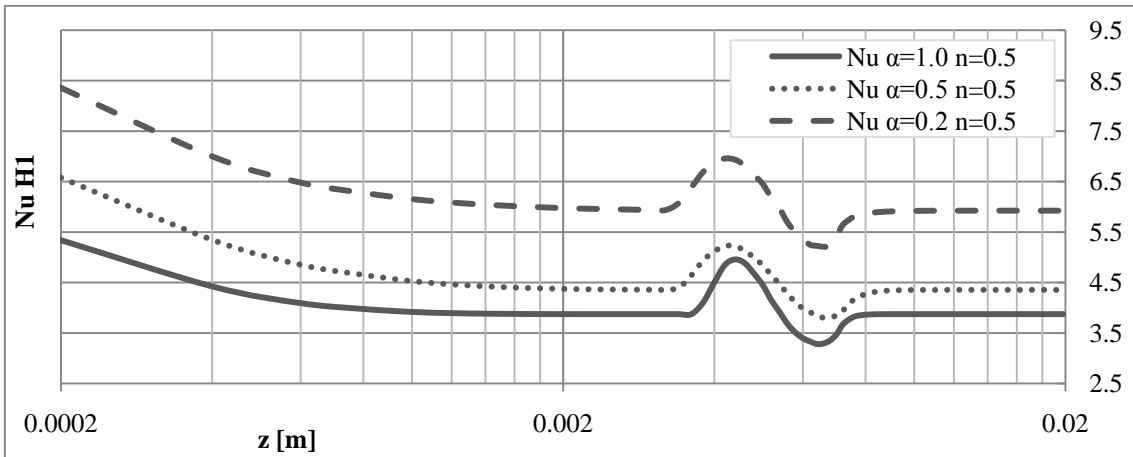
Figure 5-53, Nu for different aspect ratios for *n*=0.5 fluids under H1 BC
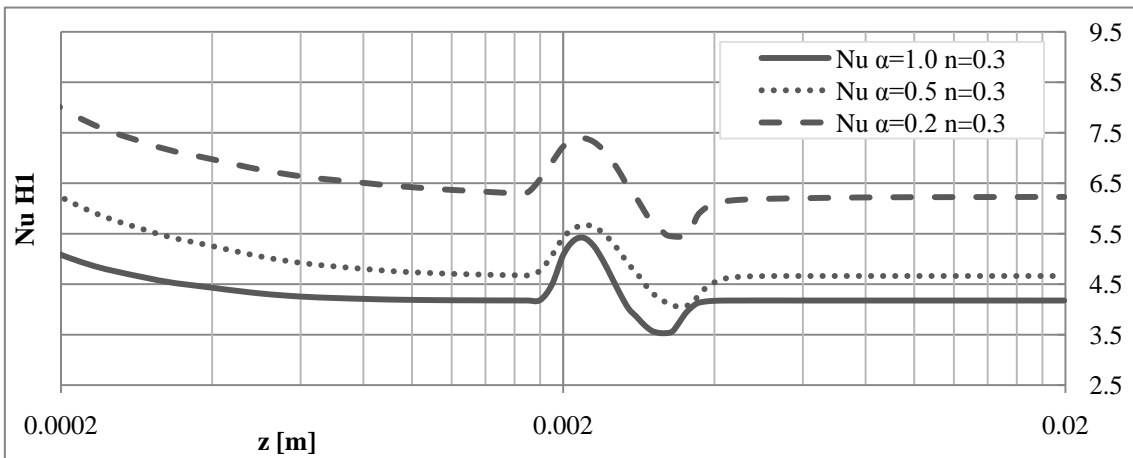
Figure 5-54, Nu for different aspect ratios for *n*=0.3 fluids under H1 BC
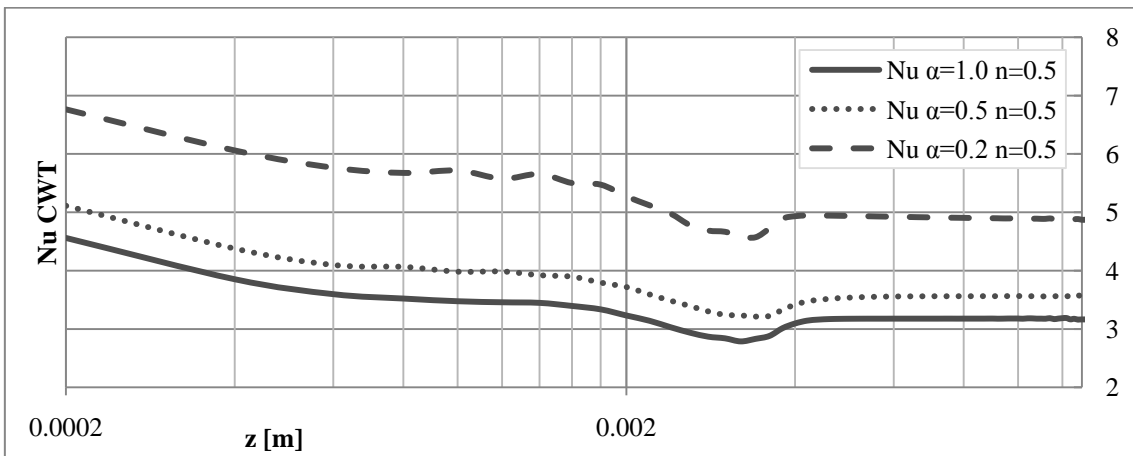
Figure 5-55, Nu for different aspect ratios for *n*=0.5 fluids under CWT BC

It can be observed from the last figures that, as for the single phase fluids, the heat transfer performance increments when the value of the aspect ratio α decreases.

CFD simulation of forced convection heat transfer of laminar phase-change non-Newtonian fluids in rectangular straight micro-channels

5.3.2 Conclusions for the section

Except for the case of aspect ratio of 0.2 under CWT (constant wall temperature) boundary condition, all the results present data that is in good agreement with the results obtained in the verification section, with a rise in the value of the Nusselt number (Nu) during the phase change region and a drop of the value near the end of the melting region for the H1 (constant heat flux and constant peripheral temperature) BC, and an increment of the value during the entry region of the fluid for the CWT BC. All the cases (including $\alpha = 0.2$, CWT) behaves with consistency with the previous results in this work.

As it has been said, there is no data to compare against the results obtained in this work, but as the behavior is consistent with the other simulations, and the values of Nu for the fully developed region are in good agreement with the results obtained for the single phase fluids, it is safe to conclude that the results represent closely the physics of the phenomenon.

5.4 Thermal efficiency factor of non-Newtonian with PCM fluids

Although several comparisons could be drawn from the data presented in the last sections, the objective of this work is to test the thermal efficiency of PCM fluids, thus, the computing of the thermal performance will be focused only on those cases.

The thermal performance factor is calculated with

$$\eta_p = \frac{Nu/Nu_{reference}}{\left(f\,Re_{NN}/f\,Re_{NN\,reference} \right)^{1/3}}$$

5.5

The thermal performance values reported in the following figures compares the efficiency in which two different fluids transfer the heat separately. A value over 1 represent an increment in percentage of the efficiency of the tested fluid when compared with the reference fluid (e.g. 1.5 can be read as a 50% of increment in the performance); a value of 1 represents equal performance. A value less than 1 represent a decrement in performance.

The reference fluids used in the last equation are those obtained from the verification section, as they used the same power law model, but for a single phase fluid. The reference fluid for evaluating the non-Newtonian fluids was the Newtonian with PCM fluid resented in the last section.

To calculate the thermal performance factor, it is necessary to obtain first the Fanning friction factor with equation 4.12, and for that purpose, it is necessary to obtain the pressure drop in the tube. That pressure drop is obtained directly from the postprocessor by comparing the pressure at the inlet and at the outflow of the tube.

Table 5-5, pressure drop for all the cases (all values in [Pa])

α	n	CWT Single P.	H1 Single P.	CWT PCM	H1 PCM
1.0	1.0	8.36×10^6	8.48×10^6	3.39×10^6	3.36×10^6
0.5	1.0	3.87×10^6	3.87×10^6	1.39×10^6	1.55×10^6
0.2	1.0	2.43×10^6	2.43×10^6	978333	969004
1.0	0.5	4282.44	4282.44	3720.6	3155.75
0.5	0.5	2781.08	2781.07	2046.66	2046.66
0.2	0.5	2171.88	2164.64	1597.64	1597.64
1.0	0.3	608.432	608.418	516.884	516.884
0.5	0.3	425.109	424.791	361.294	361.304
0.2	0.3	342.658	342.658	291.367	291.539

The f Re factor is presented in the next table.

Table 5-6, f Re$_{NN}$ factor for all cases

α	n	f Re$_{NN}$ CWT Single P.	f Re$_{NN}$ H1 Single P.	f Re$_{NN}$ CWT PCM	f Re$_{NN}$ H1 PCM
1.0	1.0	14.08211	14.28424	14.1647	14.03935
0.5	1.0	15.45214	15.45214	15.55048	15.35167
0.2	1.0	18.9502	18.9502	18.9252	18.74474
1.0	0.5	5.708639	5.708639	5.749822	5.694548
0.5	0.5	5.988058	5.988037	5.965318	5.965318
0.2	0.5	6.78305	6.760439	6.75435	6.75435

CFD simulation of forced convection heat transfer of laminar phase-change non-Newtonian fluids in rectangular straight micro-channels

α	n	$f\,\mathrm{Re_{NN}}$ CWT Single P.	$f\,\mathrm{Re_{NN}}$ H1 Single P.	$f\,\mathrm{Re_{NN}}$ CWT PCM	$f\,\mathrm{Re_{NN}}$ H1 PCM
1.0	0.3	3.899645	3.899555	3.888946	3.888946
0.5	0.3	4.02113	4.018122	4.011755	4.011866
0.2	0.3	4.383512	4.383512	4.375498	4.378081

5.4.1 Newtonian PCM fluid

The next charts show the thermal performance of the Newtonian fluids with different aspect ratios with both BC's, using the single phase fluid as reference.
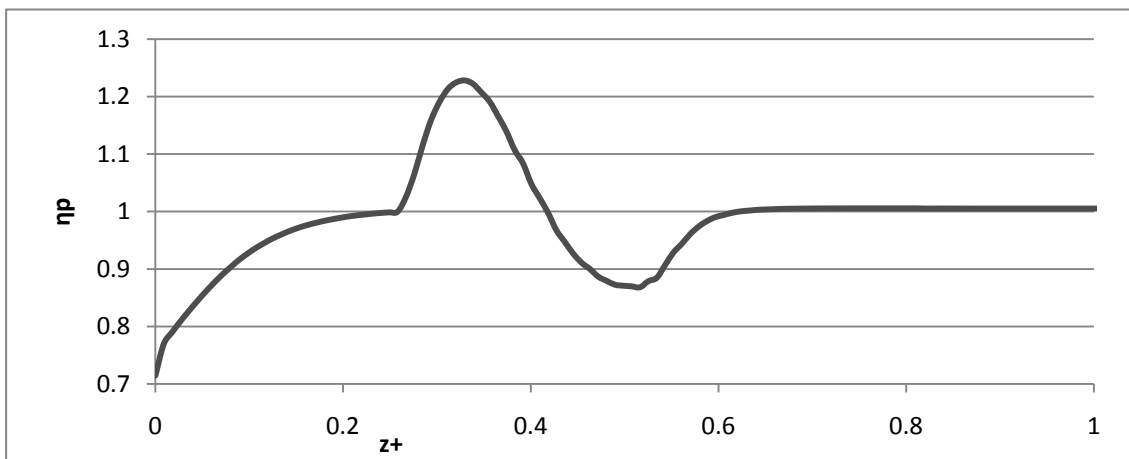
Figure 5-56, thermal performance for α=1.0, n = 1.0, H1
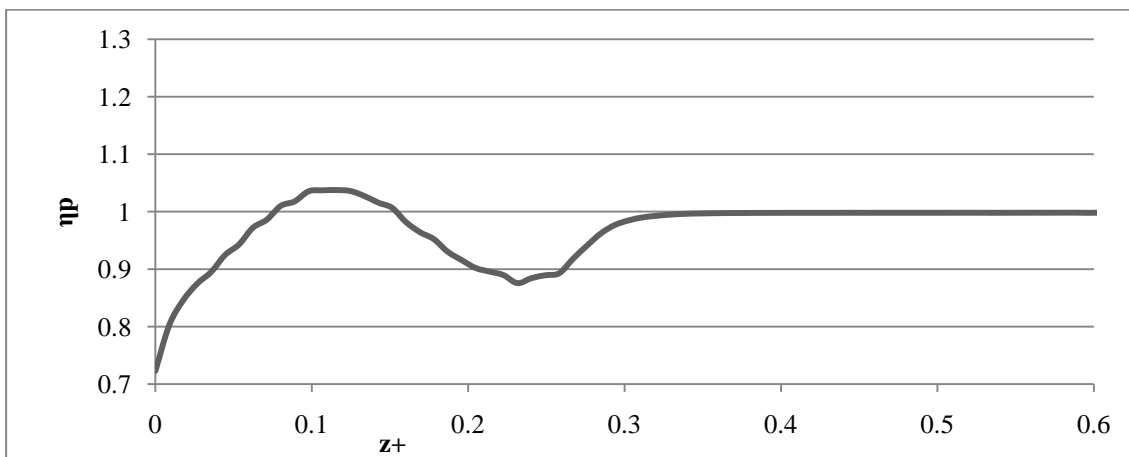
Figure 5-57, thermal performance for α=1.0, n = 1.0, CWT
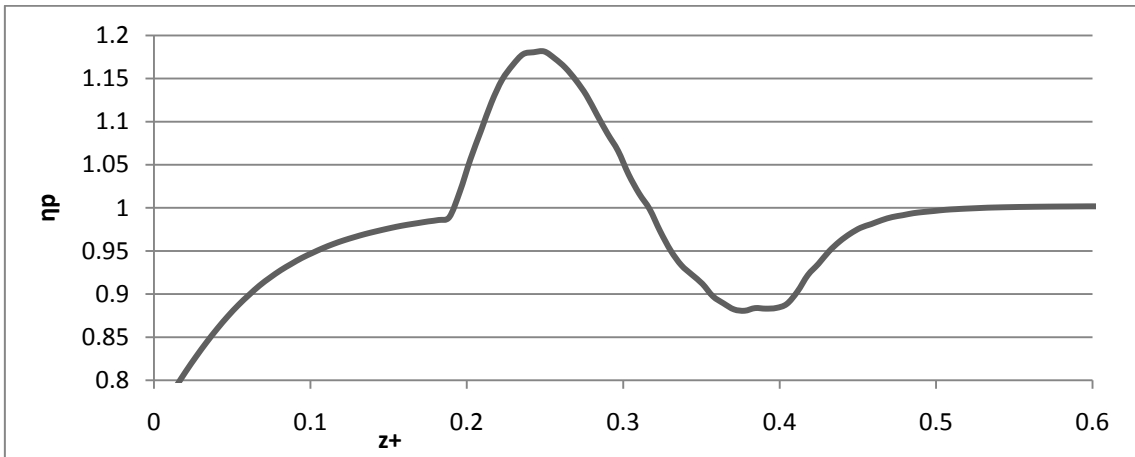
Figure 5-58, thermal performance for *α*=0.5, *n* = 1.0, H1
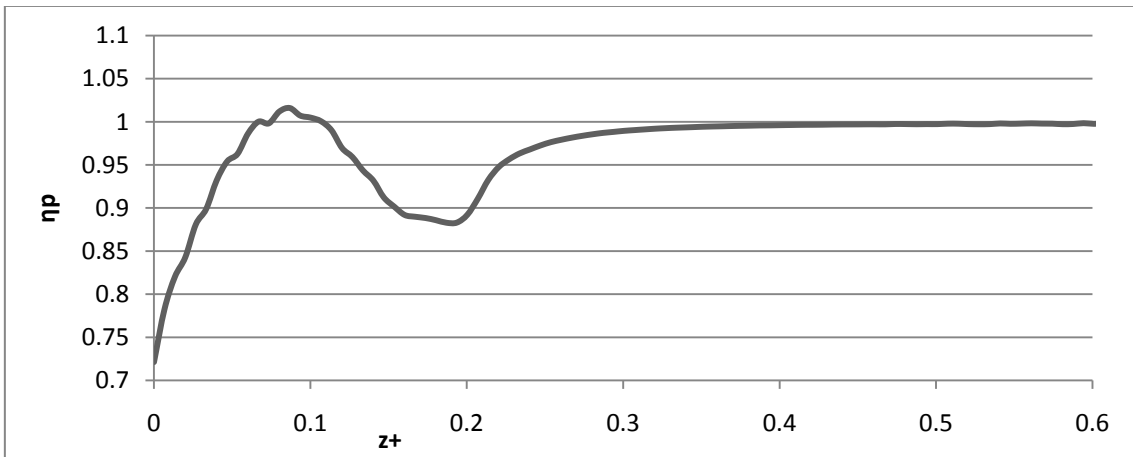
Figure 5-59, thermal performance for *α*=0.5, *n* = 1.0, CT
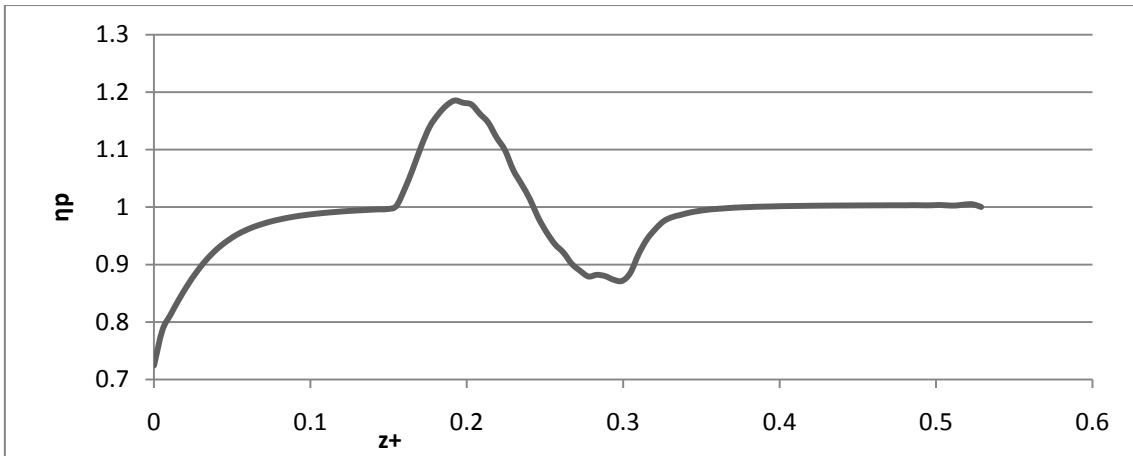
Figure 5-60, thermal performance for *α*=0.2, *n* = 1.0, H1

CFD simulation of forced convection heat transfer of laminar phase-change non-Newtonian fluids in rectangular straight micro-channels
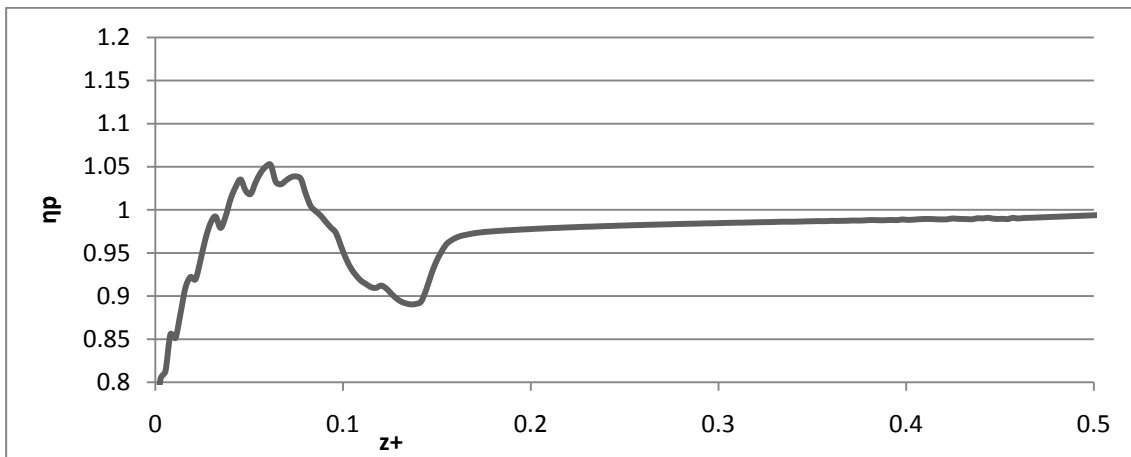
Figure 5-61, thermal performance for $\alpha=0.2$, $n = 1.0$, CWT

The last figure in particular present oscillations in the entry region as the values for Nu do not have an exact correspondence between the curves. This situation has been present for some of the cases with $\alpha=0.2$ CWT.

From the previous figures, it is evident that the H1 boundary condition has a better thermal performance than the CWT BC, with some cases around with an increment of 20% when compared with the single phase fluid. The drop in performance after the phase change region is around 10%. The increment in performance of the CWT BC does not reach the 10%, but the drop is around the same value as for the H1 BC.

5.4.2   Non-Newtonian PCM fluid

This section presents the charts that depict the thermal performance of the PCM non-Newtonian flows when compare with single phase non-Newtonian fluids.

112
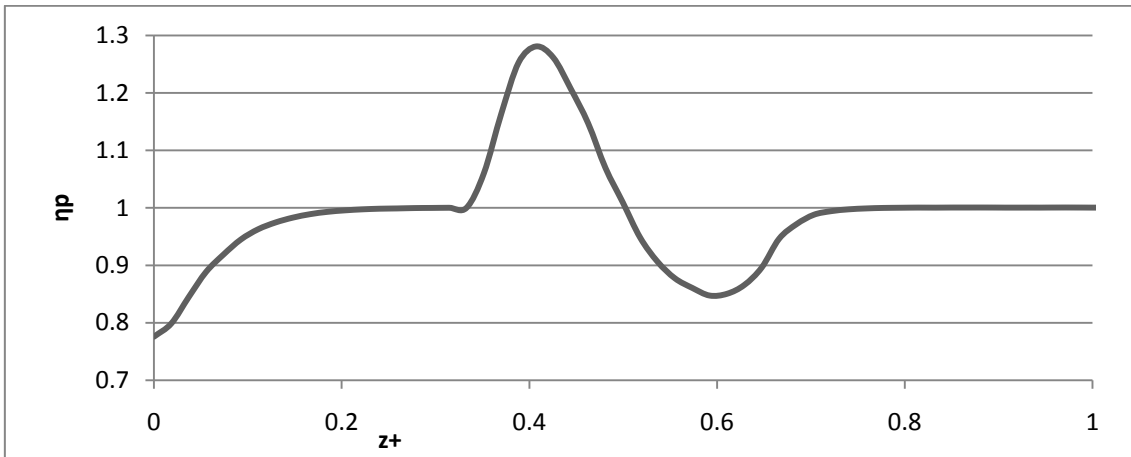
Figure 5-62, thermal performance for α=1.0, n = 0.5, H1
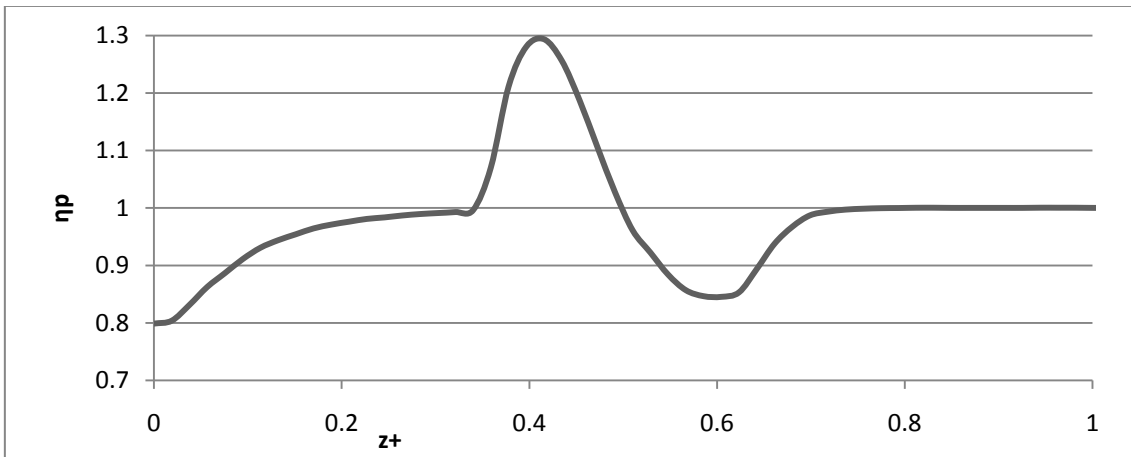
Figure 5-63, thermal performance for α=1.0, n = 0.3, H1

From the last two figures it is possible to observe that as the power law index decreases, the thermal efficiency have an increment, until almost 30% for the n = 0.3 case. However, as it has been said, the maximum value of Nu is not constant for the same case, then, the increment of the performance with lower power law cannot be considered as a rule as shown in the next figures.

CFD simulation of forced convection heat transfer of laminar phase-change non-Newtonian fluids in rectangular straight micro-channels
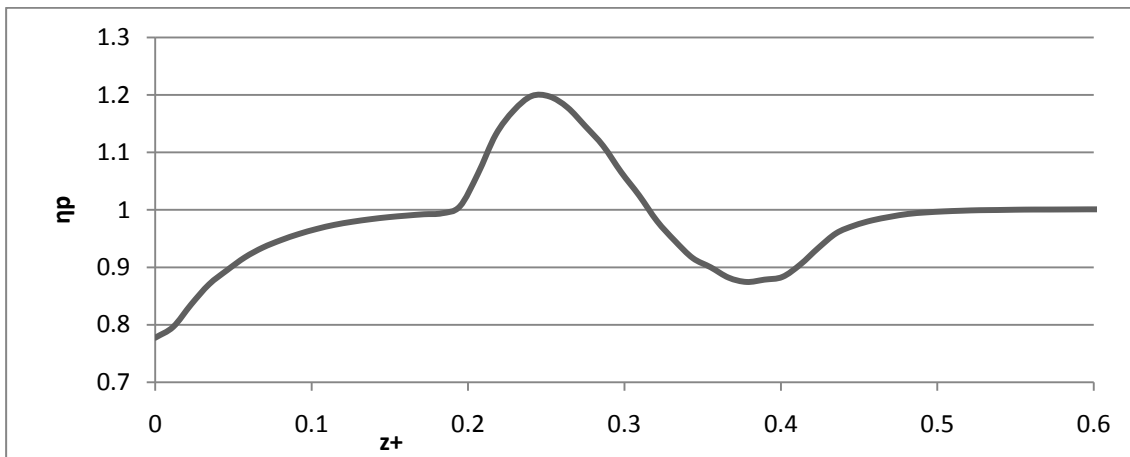
Figure 5-64, thermal performance for α=0.5, n = 0.5, H1
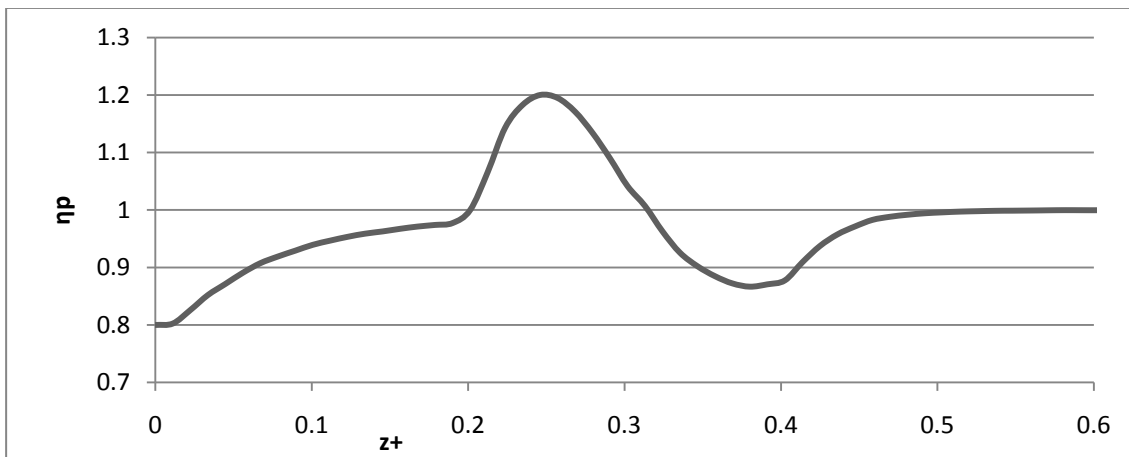
Figure 5-65, thermal performance for α=0.5, n = 0.3, H1

For the last two figures, the thermal performance increment is almost the same, although the value of the power law index is different, confirming that the performance is, as Nu, a function of the heat flux applied at the wall.
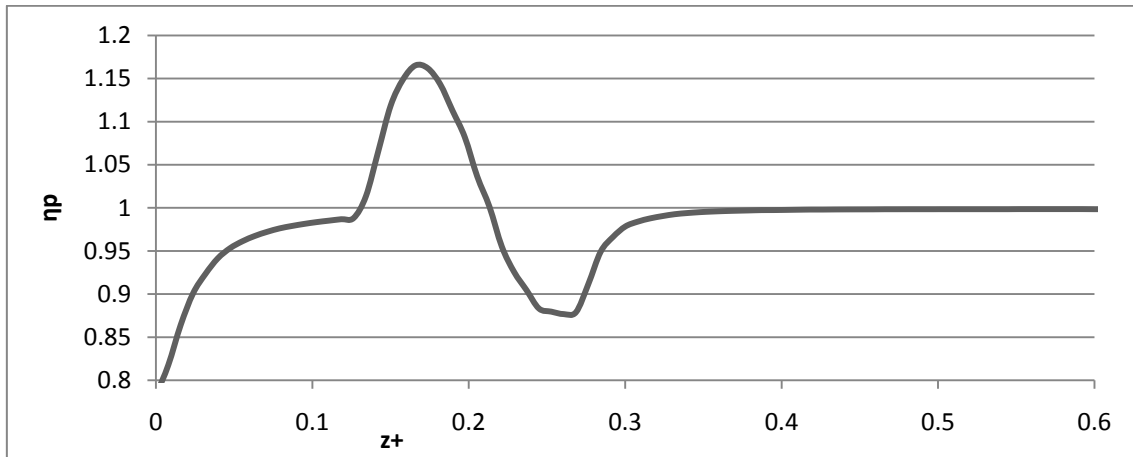
Figure 5-66, thermal performance for *α*=0.2, *n* = 0.5, H1
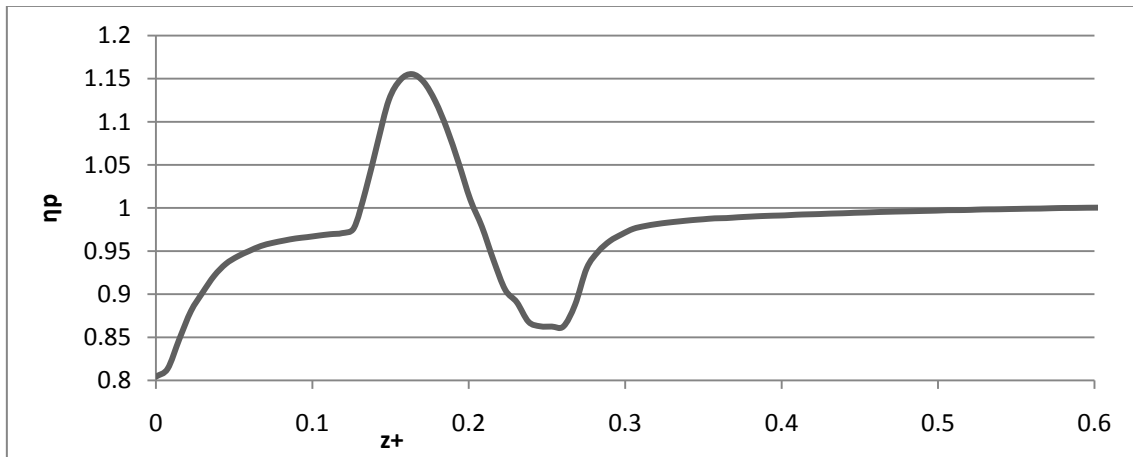
Figure 5-67, thermal performance for *α*=0.2, *n* = 0.3, H1

The last figures show a smaller increment in the performance for the smaller aspect ratio, contrary of what is expected, but this is only because for those cases a higher heat flux was used as a boundary condition, then, the phase change starts earlier in z^+. In the next section the thermal performance of the different aspect ratios will be presented, where it could be compared directly the effects of the geometry in the thermal performance.

The cases with CWT maintain a similar behavior than for the Newtonian flow, thus, only two representative plots will be presented.

CFD simulation of forced convection heat transfer of laminar phase-change non-Newtonian fluids in rectangular straight micro-channels
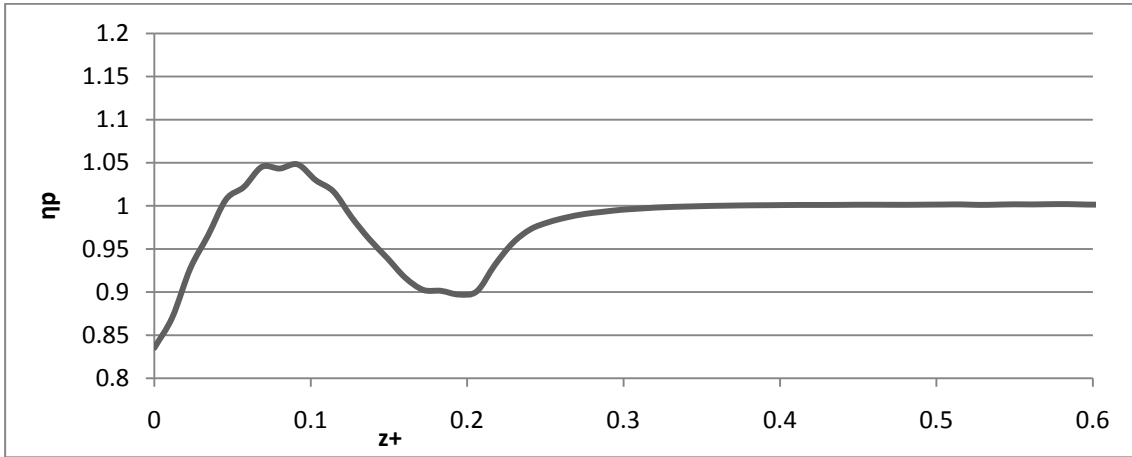
Figure 5-68, thermal performance for α=0.5, n = 0.5, CWT
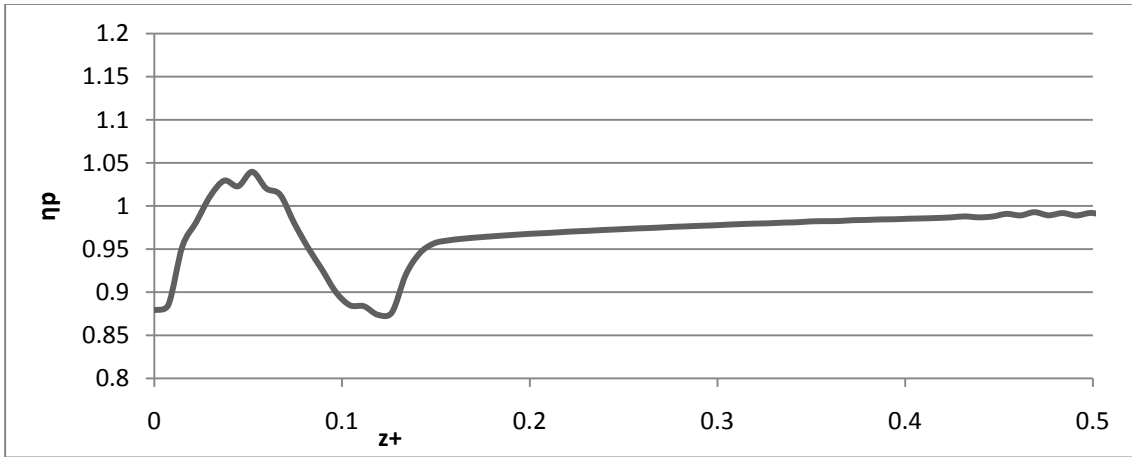
Figure 5-69, thermal performance for α=0.2, n = 0.3, CWT

As it can be seen in the last two figures, the increment of the thermal performance of the CWT cases are still very low compared with the H1 case, but the decrement after the phase change region maintains almost the same value for both conditions.

5.4.3   Different aspect ratio and PCM thermal performance

For this comparison, the reference tube is the one with $\alpha = 1.0$. The fluids presented is one Newtonian and one non-Newtonian for the H1 BC, as they show the most interesting variations in the values.
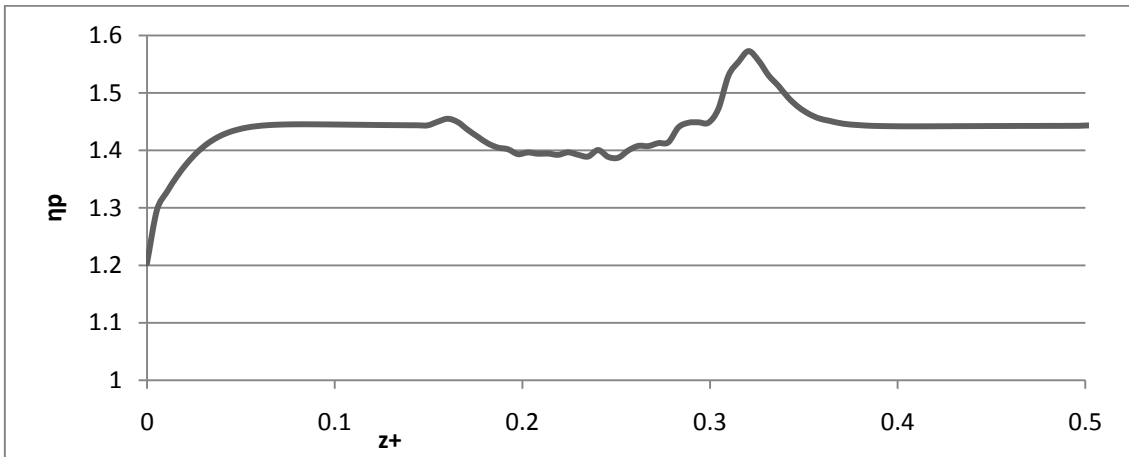
Figure 5-70, thermal performance for α=0.2, n = 1.0, H1

From the last figure, it is interesting to notice that the overall performance is far higher than for the case with $\alpha = 1.0$. However, there is a drop in the value for the phase change region. The plot is comparing the values point to point, and for that region, the lower aspect ratio is given with a higher heat flux as boundary condition, thus, the peak value of the phase change is relatively lower as can be observed in the figure. But even with the drop in performance, the lower aspect ratio has a better thermal performance than the higher one.
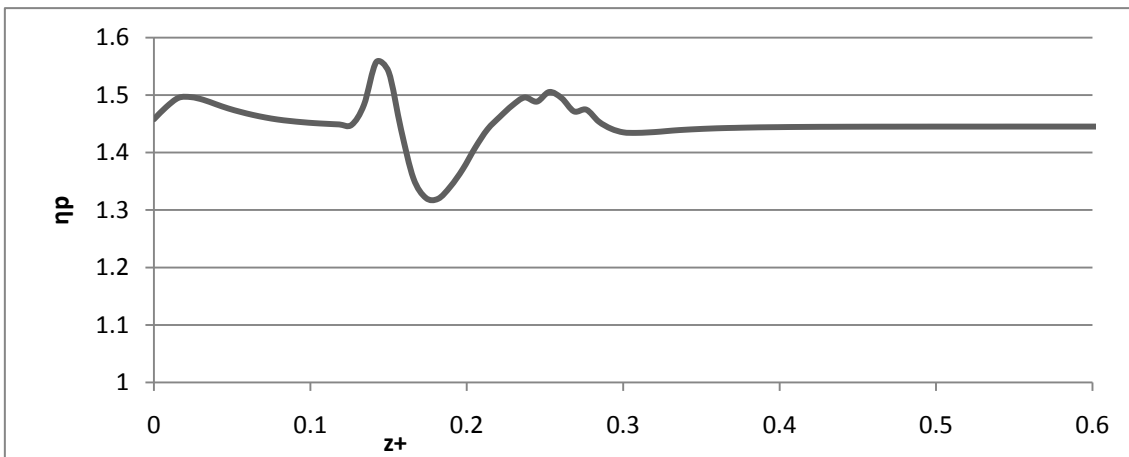
Figure 5-71, thermal performance for α=0.2, n = 0.5, H1

For the non-Newtonian case, the variation in the performance during the phase change is more evident, as it can be observed from the last figure. The overall performance is higher as well, with almost the same increment as for the Newtonian flow.

It is then clear that lower aspect ratio causes an increment in the thermal performance of the fluid.

CFD simulation of forced convection heat transfer of laminar phase-change non-Newtonian fluids in rectangular straight micro-channels

5.4.4   Different power law index and PCM thermal performance

For this comparison, the reference fluid is the Newtonian with $n = 1.0$. The fluid is compared with the other cases for the same aspect ratio and only for the H1 BC as in the last section.
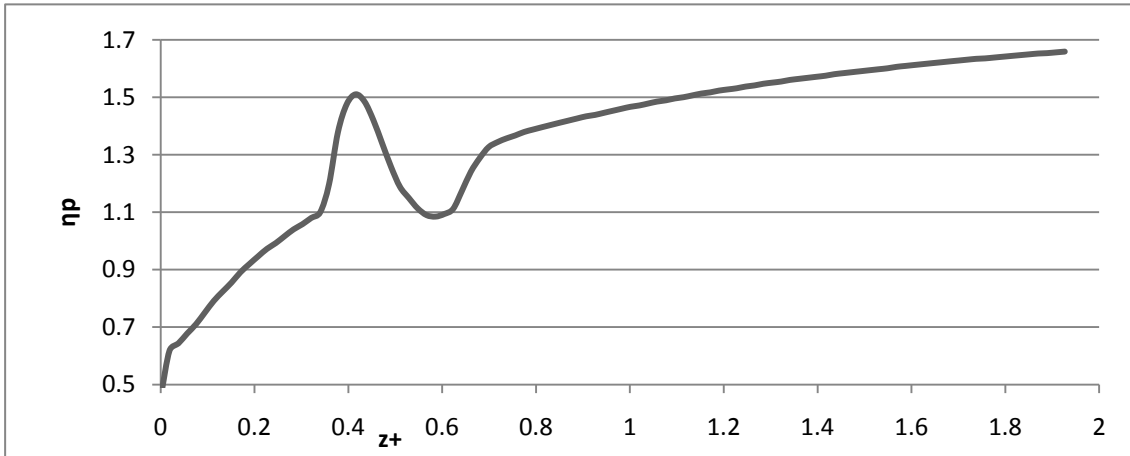
Figure 5-72, thermal performance for α=1.0, $n = 0.3$, H1

In the last figure it is not possible to observe the asymptotic part of the curve because of the difference in the entry length between the flows with different power law index. As lower power law fluids had a very short entry length, when compared with the Newtonian flow, the number of points to sample will be very large to obtain a good resolution of the curve; but it is possible to observe the tendency and the increment in the performance when compared with the Newtonian fluid.

The same tendency can be observed in the next figure, for a different aspect ratio.
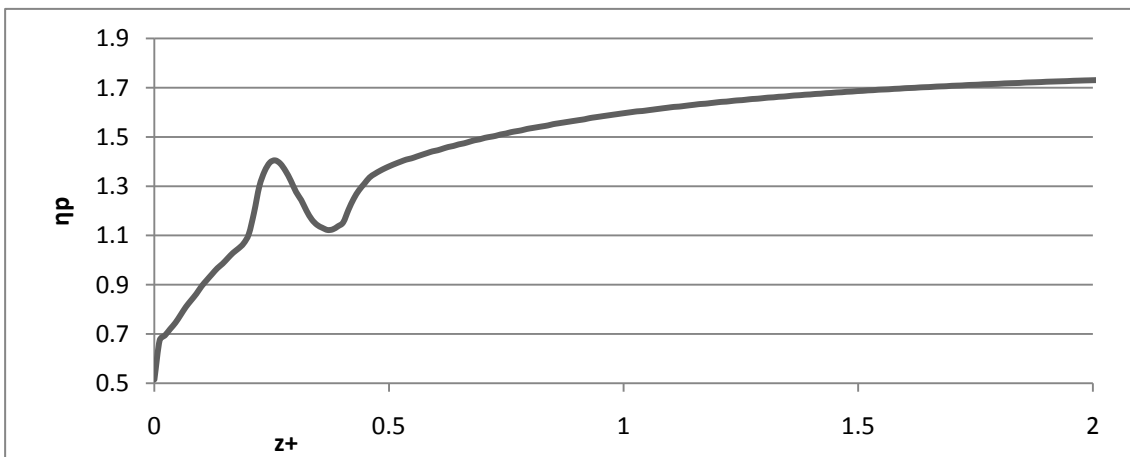
Figure 5-73, thermal performance for α=0.5, $n = 0.3$, H1

118

It is possible to observe that the increment in thermal performance due to the power law index is larger than in the other cases. Although there is not a constant value due the difference in the entry length, the tendency is clearly represented by the last two figures.

5.4.5 Conclusions for the section

The cases working with PCM (phase change material) and the H1 (constant heat and constant peripheral temperature at the wall) boundary condition have a clear advantage when compared with the single phase fluids, but only during the phase change region. Depending on the initial parameters, the increment in performance could be of around 30%, as shown in Figure 5-63, but it could be higher or lower, as it has been said, because the maximum value of Nu is not constant along all the length of the tube.

The CWT (constant wall temperature) cases present a very low increment in performance, but the drop in the efficiency to transfer heat at the end of the phase change is almost the same as for the case H1. The increment in performance for this boundary condition does not go beyond 10% when compared with single phase fluids.

However, the higher increment in the performance is given when comparing two different power law indexes with the same aspect ratio. The lower power law index represents an important gain of performance when compared with a Newtonian flow.

Page intentionally
left blank

CHAPTER 6   Discussion of the results

The results showed in the last chapter show many interesting aspects that are worth discussing in this section.

The increment in performance due the aspect ratio of the tubes was expected, as it is a well documented property of the fluids in micro-channels, i.e., the work by Erdogan (27) that has demonstrate the relation between the aspect ratio of the tube and Nu.

In the same way, the increment in performance due to the low power law index has been documented, i.e. by Chung (5), who demonstrates this characteristic of the power law fluids. This work just confirms the findings reported on those other works and verify that the results obtained here can be used with confidence as reference fluids for evaluating the thermal performance of the non-Newtonian with PCM fluids.

For the PCM Newtonian flows, the work of Kondle (9) has shown the behavior that the fluid presents when it enters in the phase change region, and how the values of Nu converge to the single phase fluids in the sub-cooled and liquid regions. This work found the same behavior for this case.

For non-Newtonian PCM fluids, the contribution of this work in the form of the new data generated can be granted as good as they present several characteristics that point to that conclusion:

- The fluid outside the phase change region converges to the single phase values of Nu.
- Lower aspect ratios deliver an overall higher thermal performance, but it is important to remember that the peak value of Nu during the phase change region is not a constant value as it is a function of the heat flux applied as a BC and the mean velocity of the flow.
- The lower power law indexes deliver better performance than higher n.

CFD simulation of forced convection heat transfer of laminar phase-change non-Newtonian fluids in rectangular straight micro-channels

After observing these characteristics, it is hard to think that the results couldn´t be reliable enough, because there are many convergence points with other works that demonstrate that the simulations are working as expected and delivering the right results for the documented cases.

In general, it is possible to say that the PCM fluids have indeed a higher thermal performance than the single phase fluids.

The increment in the performance of the PCM slurry comes from a combination of factors; the aspect ratio is an important one that has already been demonstrated by Erdogan (27), who presented the next figure, plotting the relation between the aspect ratio and Nu.
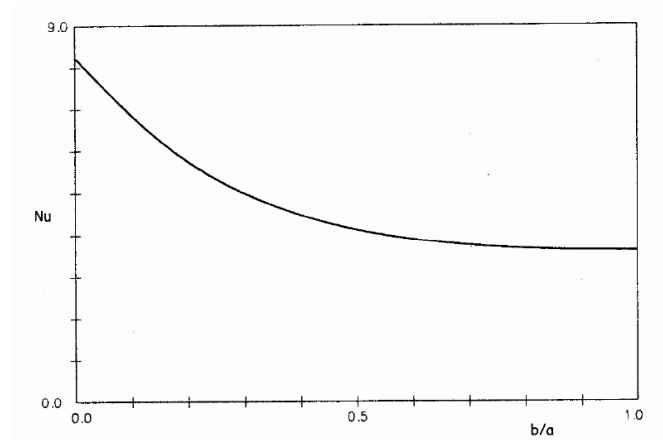
Figure 6-1, Variation of Nu for channels of different aspect ratio
(Reproduced under "fair use" from (27))

Other factor is the power law index, which has been tested by a number of authors like Chung (5) and Syrjälä (6) among others. Their works demonstrate that the value of Nu is higher for fluids with lower power law index, and thus, the results obtained for this work in that respect was as expected.

122
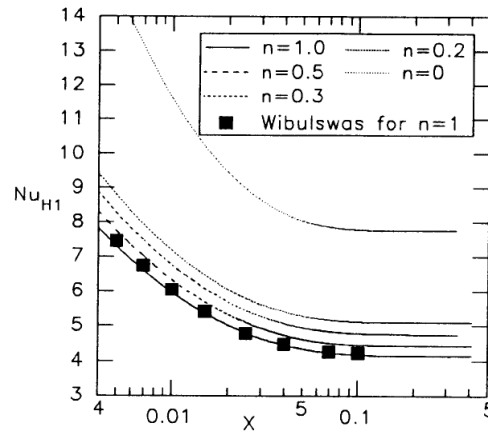
Figure 6-2, Variation of Nu for fluids with different power law index (α=0.5, H1 BC)

(Reproduced under "fair use" from (5))

For the difference in performance between the single phase fluids and the PCM, the increment is notorious only during the phase change of the material, as for the sub-cooled and liquid regions the value converge to the values obtained for a single phase fluid. This characteristic was already presented by Kondle (9) for Newtonian flows.
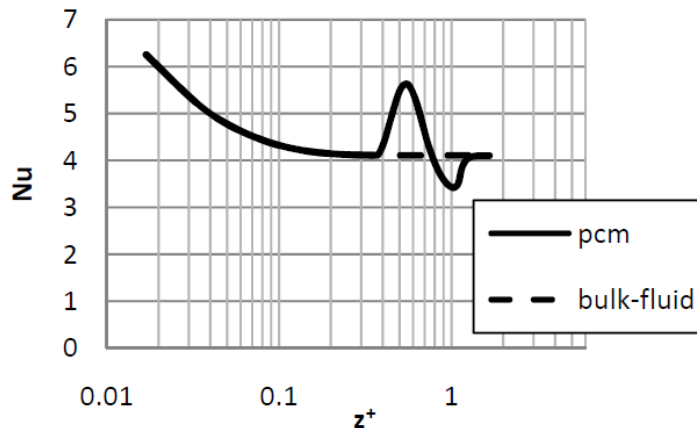
Figure 6-3, Variation of Nu for single phase and PCM Newtonian fluids (α=0.5, H1 BC)

(Reproduced under "fair use" from (9))

As for the non-Newtonian PCM fluids, this work demonstrated that under the right selection of the parameters they can result in an important increment of the thermal performance, when compared with the single phase fluids. The cause of this increment in the performance is due the increment in the amount of heat flowing from the walls to the fluid during the phase change. The model used in this work simulates the phase change with an increment in the

specific heat, and with this model, it is evident how the heat flux is affected when the phase change starts by remembering the definition of heat flux:

$$q'' = \dot{m}c_p(t_m - t_i)$$ **6.1**

The combination of a phase change material and a non-Newtonian flow causes an acceptable increment in the performance of the fluid. Although it has been already said, it is important to remember that the increment due the PCM is given only when the fluid is in the phase change region; after and before that, the values converge to the ones obtained for a single phase fluid.

CHAPTER 7   Conclusions

Thos work can be split in two parts: one directed to verifications and comparison of already known data, such the analyses realized for single phase Newtonian fluids (section 5.2.1.1), single phase non-Newtonian fluids (section 5.2.1.3) and PCM (phase change material) and Newtonian fluid slurry (section 5.2.2.1). The second one is the contribution section in which PCM and non-Newtonian fluid slurries were analyzed (section 5.3) and their thermal performance evaluated (section 5.4). For these last sections, no previous works were found, and because of that, the verification work was an important part to ensure the reliability of the new data generated. The evaluation of the thermal performance of the non-Newtonian fluids with PCM used the results of the verification section as a reference. It is important to notice that the verification work that was done to replicate other investigations used the power law model and gives an excellent appreciation of the phenomenon and the role of their parameters.

Various cases with three different aspect ratios (α = 1.0, 0.5 and 0.2) of rectangular pipes under two boundary conditions (H1 and CWT) were modeled in this work. Three power law indexes were used for the fluids, going from Newtonian (n = 1.0) to shear-thinning non-Newtonian (with n = 0.3 and 0.5) for a single phase fluid. For PCM (phase change material), the same three rectangular cases were analyzed, with the same power law indexes and ratios as for single phase. All the cases were analyzed under the laminar regime. Several conclusions can be drawn from this work:

7.1   Verification section

- CFD demonstrate to be a very efficient tool to solve fluid and heat transfer problems, but it is necessary to have an accurate method for validation, as the software will return some results most of the time without failing in the attempt, but that does not mean that the results are correct.
- The simulations are in good agreement with the known values and behavior that other investigators has presented, thus, it is safe to conclude that the numerical models

presented in this work are reliable, with the exceptions mentioned along this work (i.e. $\alpha = 0.2$ in CWT BC).

- About the aspect ratios of the tubes, this works demonstrate that lower values represent an increment in the values of the Nusselt number, that represents the ratio of the heat transfer by convection and conduction, where a higher number represent a better performance.

- Non-Newtonian power law fluids with power law indexes less than one (shear-thinning fluids) present an increment in the value of Nu when compared with power law Newtonian fluids ($n = 1$) in the same aspect ratio tubes.

- Lower power law indexes present a higher value for Nu for the same aspect ratios.

- Fluids with PCM present a local increment in the values of Nu when compared with single phase fluids, independently of the power law indexes. The increment in the value is given only during the phase change region and it converges to the single phase fluids in the sub-cooled and liquid region.

- PCM fluids, however, present a lower value of Nu when compared to single phase at the end of the phase change region. This is due the difference in temperatures between the wall and the bulk fluid.

- The highest value of Nu reached by PCM fluids in H1 BC is a function of the applied heat flux and the inlet velocity. The value will be higher with lower value of heat flux or higher value of velocity. It can be said that the fluid will reach a higher value when the phase change starts farther in the axial length tube. Because of this, it is not possible to assign a constant value for Nu during the phase change of the PCM.

- PCM working with H1 condition present a notorious increment of Nu during the phase change region. On the other hand, CWT condition is not as notorious as the phase change region starts from the beginning of the tube and present just a raise in the value of Nu during the combined entry length.

7.2 Contribution section

- Following the conclusions of the verifications, it is safe to conclude that the results of the PCM non-Newtonian slurry analyses can be deemed as reliable under the conditions used for this work.

- It is possible to simulate phase change materials and non-Newtonian fluid slurries with fluent, obtaining results that are coherent with the results obtained for their single phase counterparts.

- The best heat transfer performance is obtained in the phase change region with a PCM and as a carrier a power law non-Newtonian fluid with a low power law index in a tube with a low aspect ratio α with H1 BC.

- The value of Nu is function of the traveled length inside the tube; it is possible that the same values could be reach with different fluid or aspect ratio traveling farther in the tube.

- The new data generated can be taken by other investigators as an entry point for further works such as fluids in geometries other than rectangular or the analyses of the entry region of the tube. The models used demonstrate to behave in good agreement when compared with the counterpart single phase models.

- During the realization of this work, it was found that an incorrect selection of the rheological properties of the fluids could cause the solutions to diverge or to be wrong.

Page intentionally
left blank

CHAPTER 8   Future work and recommendations

Because this study was conducted within a highly bounded schedule and given the high extension of the area added to the lack of equipment, this work has left many interesting phenomena and secondary analysis for further investigations.

As it has been stated many times along this work, all the presented results are approximations. It would be very important to verify their accuracy not only comparing them with documented results, but with experimental data as well. The numerical results are good when compared with other sources of equally numerical outcomes, but if it were possible to access to experimental data, the simulations could be fine-tuned to set them as close as possible to the experimental results, obtaining in this way, a very reliable model that could be used then with full confidence.

The problems presented for the tube with aspect ratio of 0.2 under the CWT BC requires a deeper analysis of the particular case study. The present work leaves it as a demonstration, but the results are not reliable. It would be a good idea to test larger tubes, but this implies a large number of control volumes and, therefore, a more powerful workstation.

Only some power law indexes and rectangular channels were tested. A recommendation is to analysis different cross section geometries and it could be of interest to perform a study for shear-thickening power law indexes ($n > 1$). Testing channels with crossed pins or with fins could lead to interesting results as well.

The entry region presents interesting aspects that were omitted from this work. A full investigation of this region is recommended to understand how the flow develops under different conditions and how could it affect the performance of the fluid.

On this work, the Reynolds number was kept constant for the flows, and thus, the direct comparison between different aspect ratios is not possible under the dimensionless length. It could be interesting to keep the Peclet number constant, varying Re, to allow a direct comparison over z^+.

CFD simulation of forced convection heat transfer of laminar phase-change non-Newtonian fluids in rectangular straight micro-channels

This works focuses in boundary conditions, H1 and CWT dealing with H2 only briefly. It will be important to consider H2 BC for further analyses, to have the full range of conditions that could be present in a system.

Another interesting aspect to investigate is the factors that affect the length of the phase change region. This would lead to a longer region and thus, an extra increment of the thermal performance of the fluid.

CHAPTER 9 Appendixes

APPENDIX A. Fluent parameters and settings

In this section there is presented a brief scope of the parameters and settings used in Fluent for the simulations. A complete description of the functionality and options of every parameter will be impractical for this work, due the amount of information required to explain every setting. For a detailed description of the functionality of Fluent, the ANSYS documentation, like (23) and (24), has exhaustive information about the subject.

The mentioned parameters are turned on. If a parameter is not mentioned, then is turned off. Only the most relevant parameters are enlisted.

- Problem Setup
  - Solver
    - Type: Pressure-Based
    - Velocity formulation: Absolute
    - Time: Steady
  - Models
    - Energy: on
    - Viscous: Laminar
  - Materials:
    - Fluid: Water
      - Properties as described in section 4.5
      - Viscosity: non-newtonian-power-law
        - Parameters from section 4.5
        - T_alpha: 273
        - alpha: 0
    - Wall: Aluminum
      - Default properties
      - Conductivity: Orthotropic

CFD simulation of forced convection heat transfer of laminar phase-change non-Newtonian fluids in rectangular straight micro-channels

- o Direction 0: 1,0,0

- o Direction 1: 0,1,0

- o Conductivity 0 and 1: 100000

- o Conductivity 2: 0.0001

  - ▪ Slurry: PCM

    - • Properties as described in section 4.5

    - • Specific heat: Defined in terms of temperature

      - o Piecewise-linear

        - ▪ Six points with values as described in Figure 4-8

    - • Viscosity: non-newtonian-power-law

      - o Parameters from section 4.5

      - o T_alpha: 273

      - o alpha: 0

  - o Boundary conditions: As described in section 0

    - ▪ Fluid inlet temperature and velocity as described in section 4.5

    - ▪ Fluid Outlet: Outflow

    - ▪ At wall:

      - • Thermal Conditions

        - o Heat flux for H1

          - ▪ Shell conduction: on

          - ▪ Wall thickness: 1e-6

        - o Temperature for CWT: 320

    - ▪ Symmetries as described in section 4.1

  - o Reference values: default

- • Solution

  - o Solution Methods

    - ▪ Scheme: Simple

    - ▪ Spatial discretization

      - • Gradient: Green-Gauss Cell Based

      - • Pressure: Second Order

- Momentum: Second Order Upwind

- Energy: Second Order Upwind

o Solution Controls

- Under-Relaxation Factors: Default

o Monitors

- Equations: All residuals convergence absolute criteria: 1e-06

o Solution Initialization

- Reference frame: Relative to cell zone

- Initial values: Calculated from inlet parameters

o Calculation

- Generally 1000 iterations, unless the simulation requires a different number for convergence

Page intentionally
left blank

APPENDIX B.   Macro for Nu calculation

#PERL

```
# Macro GUI begin
#
# macro name = Nusselt Number
# macro subroutine = Nusselt_Num
# macro report file = Nusselt_Num.html
#
# macro parameter = separator
#  type = Separator
#
# macro parameter = comment
#  type = Comment
#  default = Nusselt number for tubes. The tube must start at 0,0,0 and be parallel to one axis
(inlet must be in the x, y or z plane). Length of the pipe is the % to analyze (99 =100%,
50=50%, 0=1%)
#
# macro parameter = separator
#  type = Separator
#
# macro parameter = k
#  type = real
#  default = 0.6
#
# macro parameter = Flow Direction
#  type = Combo
#  list = x, y, z
#  default = z
#
# macro parameter = Number of points
#  type = real
#  default = 100
#
# macro parameter = Length of the pipe
#  type = integer
#  default = 101
#
# macro parameter = Wall Boundary
#  type = Location
#  location type = Boundary
#
#
```

CFD simulation of forced convection heat transfer of laminar phase-change non-Newtonian fluids in rectangular straight micro-channels

Macro GUI end

macro parameter = File Name
type = string
default = Nusselt_Num
$filen


```
!sub Nusselt_Num {

! ($k, $axis, $numsteps, $pipep, $wall_v)=@_;

!  if ($axis eq "X") {
!      $axisSpec = "1,0,0";
!  } elsif ($axis eq "Y") {
!      $axisSpec = "0,1,0";
!  } else {
!      $axisSpec = "0,0,1";
!  }#end if

  PLANE: Plane_Cross_Sec
    Option = Point and Normal
    Point = 0,0,0
    Normal = $axisSpec
  END

  USER SURFACE: Wall_Surface
    Option = Boundary Intersection
    Boundary List = $wall_v
    Location = /PLANE:Plane_Cross_Sec
  END

  POLYLINE: PL_Perimeter
    Option = Boundary Intersection
    Boundary List = $wall_v
    Location = /PLANE:Plane_Cross_Sec
  END

! ($peri, $lunits)=evaluate("length()\@PL_Perimeter" );
! ($Ac, $aunits)=evaluate("area()\@Plane_Cross_Sec");
! $Dh=(4*$Ac)/$peri;
! $Dh1=sprintf("%.6f", $Dh);
!
! open(OFH,">Nusselt_Num.html");
! print OFH "<!doctype html public \"-//w3c//dtd html 4.0 transitional//en\">\n";
```

136

```
! print OFH "<html>\n";
! print OFH "<head>\n";
! print OFH "    <meta http-equiv=\"Content-Type\" content=\"text/html; charset=iso-8859-1\">\n";
! print OFH "    <meta name=\"Adi Corrales\" content=\"CFD-Post\">\n";
! print OFH "    <meta name=\"GENERATOR\" content=\"CFD-Post\">\n";
! print OFH "    <title>Nusselt Number</title>\n";
! print OFH "</head>\n";
! print OFH "<body>\n";
! print OFH "<b><i><font color=\"#000099\"><font size=+4>Nusselt Number</font></font></b></i>\n";
! print OFH "<hr NOSHADE WIDTH=\"100%\">\n";
! $fileName = getValue("DATA READER","Current Results File");
! $date = scalar(localtime);
! print OFH "<p>Generated by CFD-Post from results file <i>$fileName</i> at <i>$date</i>\n";
! print OFH "<p>Macro by Adi Corrales \n";
! print OFH "<p><b><font size=+2>Data</font></b>\n";
! print OFH "<p>Hydraulic Diameter: $Dh1" ;
! print OFH "<table BORDER CELLPADDING=2 >\n";

! print OFH "<tr><td>Loc</td>" ;
! print OFH "<td>u,v,w max</td>";
! print OFH "<td>tm</td>";
! print OFH "<td>tw</td>";
! print OFH "<td>t</td>";
! print OFH "<td>tw-tm</td>";
! print OFH "<td>(tw-t)/(tw-tm)</td>";
! print OFH "<td>h</td>";
! print OFH "<td>Nu</td></tr> \n";

! if ($pipep == 99){$pipep=100}
! if ($pipep == 0){$pipep=1}
! $pipe_length=maxVal($axis,"$wall_v")*(($pipep)/100);
!
! for ($i=0; $i < $numsteps; $i++) {
!    $pos=(($pipe_length)/($numsteps))*$i;

!    $axis = substr(uc($axis),0,1);

!    if ($axis eq "X") {
!       $axisSpec = "1,0,0";
!       $posSpec = "$pos,0,0";
!    } elsif ($axis eq "Y") {
!       $axisSpec = "0,1,0";
!       $posSpec = "0,$pos,0";
```

CFD simulation of forced convection heat transfer of laminar phase-change non-Newtonian fluids in rectangular straight micro-channels

```
!   } else {
!      $axisSpec = "0,0,1";
!      $posSpec = "0,0,$pos";
!   }#end if


 PLANE: Plane_Cross_Sec
   Option = Point and Normal
   Point = $posSpec
   Normal = $axisSpec
 END

 POINT:Point_Central
        Option = XYZ
         Point = $posSpec
       END

 USER SURFACE: Wall_Surface
   Option = Boundary Intersection
   Boundary List = $wall_v
   Location = /PLANE:Plane_Cross_Sec
 END

! ($heatf, $hunits)=evaluate("areaAve(Wall Heat Flux)\@Wall_Surface");
! ($vel, $vunits)=evaluate("ave(Velocity)\@Point_Central");
! ($tm, $tunits)=evaluate("massFlowAve(Temperature)\@Plane_Cross_Sec");
! ($tw, $tunits)=evaluate("areaAve(Temperature)\@Wall_Surface");
! ($t, $tunits)=evaluate("ave(Temperature)\@Point_Central");
! if ($tw-$tm<=0){
!   print OFH "</table>\n";
!   print OFH "<p>Macro Interrupted! \n";
!   print OFH "<p>Bulk Temperature = Wall Temperature \n";
!   last;
! }
! $add_temp=($tw-$t)/($tw-$tm);
! $Deltm=$tw-$tm;
! $h=$heatf/$Deltm;
! $Nu=($h*$Dh)/$k;

! $pos=sprintf("%.6f", $pos);
! $vel=sprintf("%.6f", $vel);
! $tm=sprintf("%.6f", $tm);
! $tw=sprintf("%.6f", $tw);
! $t=sprintf("%.6f", $t);
! $Deltm=sprintf("%.6f", $Deltm);
! $add_temp=sprintf("%.6f", $add_temp);
```

138

```
! $h=sprintf("%.6f", $h);
! $Nu=sprintf("%.6f", $Nu);

! print OFH "<tr><td>$pos</td>" ;
! print OFH "<td>$vel</td>";
! print OFH "<td>$tm</td>" ;
! print OFH "<td>$tw</td>";
! print OFH "<td>$t</td>";
! print OFH "<td>$Deltm</td>";
! print OFH "<td>$add_temp</td>";
! print OFH "<td>$h</td>";
! print OFH "<td>$Nu</td></tr> \n";

! } #end for
! print OFH "</table>\n";
! print OFH "</body>\n";
! print OFH "</html>\n";
! close(OFH);
!} #end sub
```

Page intentionally
left blank

Bibliography

1. **Chhabra, R.P. and Richardson, J.F.** *Non-Newtonian Flow in the process industries.* Oxford : Butterworth Heineman, 1999. 0 7506 3770 6.

2. **Graebel, W. P.** *Advanced Fluid Mechanics.* New York : Elsevier, 2007. 978-0-12-370885-4.

3. **Incropera, Frank P. and DeWitt, David P.** *Fundamentals of heat and mass transfer.* New York : John Wiley, 2007. 0471457280.

4. *laminar forced convection heat transfer of a non-Newtonian fluid in a square duct.* **Chandrupatla, A. R.** Madras : International journal of heat and mass transfer, 1977, Vol. 20.

5. *Heat transfer for thermally developing flow of non-Newtonian fluids in rectangular ducts.* **Chung, B.T.F and Zhang, Z.J.** Akron : Witpress, 1994, Vol. 5. 1743-3533.

6. *Further finite element analyses of fully developed laminar flow of power-law non-Newtonian fluid in rectangular ducts: Heat transfer predictions.* **Syrjälä, Seppo.** 6, Tampere, Finland : Pergamon, 1996, Vol. 23. S0735-1933(96)00063-2.

7. *Thermally developing flow and heat transfer in rectangular microchannels of diferent aspect ratios.* **Garimella, S.** 49, West Lafayette : International Journal of Heat and Mass Transfer, 2006. 3060-3067.

8. *Laminar non-Newtonian fluid flow in non-circular ducts and microchannles.* **Muzychka, Y.S.** St. John's, NF. Canada : ASME, 2008, Vol. 130. 10.1115/1.2979005.

9. *Laminar flow forced convection heat transfer behavior of a phase change material fluid in microchannels.* **Kondle, S.** College Station, TX : ASME, 2009.

10. *Characteristics of microencapsulated PCM slurry as a Heat Transfer fluid.* **Yamagishi, Y.** 4, Osaka : AIChE Journal, 1999, Vol. 45.

CFD simulation of forced convection heat transfer of laminar phase-change non-Newtonian fluids in rectangular straight micro-channels

11. **Kays, W. M.** *Convective heat and mass transfer.* New York : McGraw-Hill, 1966.

12. **Chin, W.C.** *Computational rheology for pipeline and annular flow.* Boston : Gulf Professional Publishing, 2001. 0-88515-320-7.

13. **Liu, H.** *Pipeline Engineering.* New York : Lewis Publisher, 2005. 0-203-59487-8.

14. **Jahns, E.** *Microencapsulated phase change materials.* [Document] Ludwigshafen : BASf AG, Kunstsofflaboratorium.

15. *Nanofluids with enhanced thermal transport properties.* **Han, Z.** College Park : University of Maryland, 2008.

16. *Forced convection heat transfer in microencapsulated phase change material slurries: Flow in circular ducts.* **Charunyakorn, P.** 3, Miami : Int. J. Heat Mass Transfer, 1989, Vol. 34. 0017-9319/91.

17. *Laminar forced convection heat transfer with phase change material emulsions.* **Avanic, B.L.** 5, USA : Int. Comm. Heat Mass Transfer, 1997, Vol. 24. 0735-1933/97.

18. *Forced convection heat transfer with phase-change-material slurries: turbulent flow in a circular tube.* **Choi, E.** 2, Philadelphia : Int. J. Heat Mass Transfer, 1993, Vol. 37. 0017-9310/94.

19. **Anderson, John.** *Computational Fluid Dynamics.* New York : McGraw-Hill Science/Engineering/Math, 1995. 0-07-001685-2.

20. **Zienkiewics, O.C.** *The finite element method Volume 3: Fluid Dynamics.* Oxford : McGraw-Hill, 2000. 0 7506 5050 8.

21. **Bhaskaran, R. and Collins, L.** Introduction to CFD Basics. *FLUENT TUTORIALS - Cornell University.* [Online] 2002. [Cited: July 8, 2010.] http://courses.cit.cornell.edu/fluent/cfd/index.htm.

22. **Raatschen, H.J.** *Simulation of structures, fields and flow.* Aachen : s.n., 2009.

23. **ANSYS, Inc.** *ANSYS FLUENT 12.0 Theory guide.* s.l. : ANSYS, Inc., 2009.

24. —. *ANSYS FLUENT 12.0 User's Guide.* s.l. : ANSYS, Inc., 2009.

25. **Slater, John W.** Uncertainty and Error in CFD Simulations. *NPARC Verfication and Validation Web site Home Page.* [Online] July 17, 2008. [Cited: July 7, 2010.] http://www.grc.nasa.gov/WWW/wind/valid/tutorial/errors.html.

26. **University of Waterloo.** Fluid Properties Calculator. *Microelectronics Heat Transfer Laboratory.* [Online] Microelectronics Heat Transfer Laboratory, 1997. [Cited: May 26, 2010.] http://www.mhtl.uwaterloo.ca/old/onlinetools/airprop/airprop.html.

27. *The effects of duct shape on the Nusselt number.* **Erdogan, M.E.** 1, Gumussuyu : Mathematical and Computational Applications, 2005, Vol. 10.